STRUCTURAL AND FUNCTIONAL IMAGING OF TAUOPATHIES

by

Jenna Rae Smith-Forrester

BSc, Dalhousie University, 2010

A THESIS SUBMITTED IN PARTIAL FULFILLMENT OF

THE REQUIREMENTS FOR THE DEGREE OF

MASTER OF SCIENCE

in

THE FACULTY OF GRADUATE AND POSTDOCTORAL STUDIES

(Neuroscience)

THE UNIVERSITY OF BRITISH COLUMBIA

(Vancouver)

July 2015

Abstract

Repetitive head trauma is a known cause of tau protein accumulation and the leading cause of chronic traumatic encephalopathy (CTE). Currently, no robust method for in vivo detection of CTE exists and definitive diagnosis can only be made post-mortem. This thesis aimed to address two gaps in the literature surrounding head injury and tau accumulation. First, we sought to evaluate the effects of concussion on adolescent brain structure using mathematical modeling applied to diffusion tensor imaging (DTI). In our study, 12 adolescent athletes completed DTI in the sub-acute phase of recovery from concussion. The primary outcome measures included Complex Network Analysis metrics related to efficiency, nodal clustering, and fibre tract length. These measures were applied to diffusivity output (FA, MD, and number of tracts) in subnetworks of vulnerability, with specific focus on the Default Mode Network (DMN). Here we found microstructural changes in the DMN of concussed athletes with increased clustering and shorter path lengths, indicating increased local efficiency. A corresponding decrease in global efficiency and alterations in core hubs may underlie the clinical profile, suggesting concussion results in large-scale network disconnection. Longitudinal studies with network analysis may serve as a marker of collective injury and provide early detection of pathological structural organization. Second, we established the baseline measures of a novel positron emission tomography (PET) radioligand, ^{11}C-PBB3, which is specific for hyperphosphorylated tau protein. We collected data on healthy, elderly individuals (n = 8), and tested the tracer in a probable (n = 1) and severe (n = 1) case of Progressive Supranuclear Palsy (PSP), a known tauopathy. We found that tracer circulated in the venous sinuses in our healthy controls with little to no deposition in brain tissue. We also present preliminary findings of tracer accumulation in the basal ganglia and thalamus in the PSP cases. These results suggest ^{11}C-PBB3 is a viable

tracer for use in other tauopathies, including CTE. Longitudinal studies with combined DTI and PET are necessary to elucidate the potentially synergistic interactions between damage to white matter tracts, tau accumulation, inflammation, and the initiation of processes leading to CTE and other tauopathies.

Preface

Overview of my contribution to this thesis:

The work I describe in this thesis was made possible through collaborations with my primary research supervisor (Dr. A. Jon Stoessl), co-supervisor (Dr. Naznin Virji-Babul), supervisory committee (Dr. Jacqueline Pettersen, Dr. William Panenka, and Dr. Vesna Sossi), as well as my many mentors and colleagues at the Pacific Parkinson's Research Centre, the Perception Action Lab, the Movement Disorders Clinic, TRIUMF, the UBC PET Program, and the UBC MRI Research Centre. I have made a concentrated effort to acknowledge those who have contributed to my work through shared authorship in posters, publications, presentations, and in the Acknowledgements section of this thesis. I have written 100% of this thesis, and incorporated feedback and revisions from my supervisors and colleagues. Below is a comprehensive description of my roles and responsibilities in each project, as well as the team members who helped make this work possible.

Contributions to Chapter 2:

This chapter is based on secondary data analysis using DTI data collected from adolescent athletes during the summer of 2012. A subset of these diffusivity metrics have previously been published by Michael Borich; however, I advanced our understanding of post-concussive changes in neural network structures by employing a new analytic technique derived from the principles of Graph Theory. I completed 100% of the secondary investigation, and used a custom script based on measures from the Brain Connectivity Toolbox that was written by a collaborator, Colin J. Brown, at Simon Fraser University. Critical review of methodology and statistics were provided by Colin and Dr. Ghassan Hamarneh. Study design, methodology, analysis, and manuscript preparation was overseen by Dr. Naznin Virji-Babul, who offered feedback, revisions, and support throughout.

Contributions to Chapter 3 and 4:

The projects described in Chapters 3 and 4 required UBC's Clinical Research Ethics Board (CREB) approval. In Chapter 3, baseline investigations in healthy, elderly individuals were completed under the "Imaging Tau Accumulation with PBB3 in Healthy Controls" protocol

(Certificate Number: H14-02375). In Chapter 4, the tracer was used in a clinical population diagnosed with Progressive Supranuclear Palsy. A UBC CREB Certificate of Approval was issued under the "Tau and Neuroinflammation Imaging in Parkinson's Disease and Related Disorders" protocol (Certificate Number: H14-03268). This project is a component of the Pacific Parkinson's Research Centre's ongoing investigation into tau accumulation and inflammation in Atypical Parkinson's disease. In both studies Dr. Stoessl is the Principal Investigator, and Dr. Sossi the Co-Investigator.

The process of acquiring our new radioligand, ^{11}C-PBB3, was initiated in September 2013. For both studies, I wrote the protocols based on the vision, rigorous scientific inquiry, and constructive feedback provided by Dr. Stoessl and other members of the research team. I played a key administrative role in meeting regulatory requirements to ensure the tracer was approved for use at UBC by completing the online Researcher Information Services (RISe) applications, MRI and Hospital Applications, and Health Canada Application for Authorization and Attestation for Positron-Emitting Radiopharmaceuticals (PERs) Basic Clinical Research Study for use of ^{11}C-PBB3 in Healthy Controls (H14-02375) and in the Parkinsonian population (H14-03268). Each of the aforementioned documents were reviewed for accuracy and completeness by the PET Imaging Coordinators, Jessamyn McKenzie and Nicole Neilson. I completed a majority of the recruitment, screening, and scheduling for both the MRI and PET imaging for the healthy controls; attended all imaging sessions; and assisted with participant assessments of mood and cognition in the PET suite prior to their scans. The chart review and scheduling for the PSP patients and all motor assessments were completed by our registered nurses. PET data acquisition and re-alignment were completed by Carolyn English and Siobhan McCormick, while image reconstruction was facilitated by Nasim Vafai and Elham Shahinfard under the direction of Dr. Stoessl and Dr. Sossi. This work was funded by the Weston Brain Institute (Grant Number: F14-03750).

Table of Contents

List of Tables

List of Figures

List of Abbreviations

AAL	automated anatomic labeling
Aβ	amyloid-beta
ACC	anterior cingulate cortex
AD	Alzheimer's disease
AMPA	α-amino-3-hydroxy-5-methyl-4-isoxazolepropionic acid
ATP	adenosine triphosphate
BBB	blood brain barrier
BDI	BECK Depression Inventory
CBD	corticobasal degeneration
CM	connectivity matrices
CNA	complex network analysis
CT	computed tomography
CTE	Chronic Traumatic Encephalopathy
DAI	diffuse axonal injury
DLPFC	dorsolateral prefrontal cortex
DMN	Default Mode Network
DTBZ	Dihydrotetrabenazine
DTI	diffusion tensor imaging
DWI	diffusion weighted image
EEG	electroencephalography
FA	fractional anisotropy
^{18}F-FDG	^{18}F-Fluorodeoxyglucose

fMRI	functional Magnetic Resonance Imaging
FOV	field of view
HRRT	High Resolution Research Tomograph
ICA	independent component analysis
LOR	line of response
MCI	Mild Cognitive Impairment
MD	mean diffusivity
MRI	Magnetic Resonance Imaging
MSA	Multiple System Atrophy
mTBI	mild Traumatic Brain Injury
MoCA	Montreal Cognitive Assessment
NDMA	N-methyl-D-aspartate
NFL	National Football League
NFT	neurofibrillary tangles
NIfTI	Neuroimaging Informatics Technology Initiative
NIRS	National Institute of Radiological Science
^{11}C- PBB3	2-[4-(6-[11C]methylaminopyridinyl)-1,3-butadienyl]-benzothiazol-6-ol pyridinylbutadienyl-benzothiazole 3
^{11}C-PBR	[O-methyl-11C]N-acetyl-N-(2-methoxybenzyl)-2-phenoxy-5-pyridinamine Peripheral Benzodiazepine Receptor
p-tau	hyperphosphorylated tau
PCC	posterior cingulate cortex
PCS	post-concussion syndrome

PD	Parkinson’s disease
PET	Positron Emission Tomography
PFC	prefrontal cortex
PHF	paired helical filaments
PiB	Pittsburg Compound B
PPRC	Pacific Parkinson’s Research Centre
PSP	Progressive Supranuclear Palsy
PSP-P	Progressive Supranuclear Palsy - Parkinsonism
rs-fMRI	resting state functional Magnetic Resonance Imaging
ROI	region of interest
SD	standard deviation
SEM	standard error of the mean
SPM	statistical parametric mapping
SRC	sports-related concussion
SUV	standard uptake values
TAC	time activity curves
TBI	traumatic brain injury
TDP-43	43 kDa TAR DNA-binding protein
TE	echo time
TR	repetition time
UBC	University of British Columbia
UPDRS	Unified Parkinson’s Disease Rating Scale
WM	white matter

Acknowledgements

My first acknowledgement goes to my supervisor, Dr. A. Jon Stoessl. I whole-heartedly thank you for the opportunity to join your research team and the endless inspiration you have provided. Through your quick wit, wise words, and guidance as a clinician, a scientist, and an administrator, I feel my time at the Pacific Parkinson's Research Centre has both challenged and motivated me to set the bar ever higher, personally, professionally, and intellectually. I am excited to embrace the next step in my education, knowing I am better prepared after the privilege of your mentorship.

To my co-supervisor, Dr. Naznin Virji-Babul, thank you for your ongoing support and encouragement. You have opened the door to many rewarding leadership opportunities. I am grateful for your prompt replies and flexibility in accommodating unpredictable schedules inextricably linked to co-supervision. Thank you for making time to celebrate the milestones in your student's lives – there is always an excuse for streamers!

To my Supervisory Committee, Dr. Jacqueline Pettersen, Dr. William Panenka, and Dr. Vesna Sossi. I look to each of you in great admiration - thank you for your support from near and far, and sharing your expertise.

Next, I express my humble gratitude to the Canadian Institute for Health Research for the Frederick Banting and Charles Best Canada Graduate Scholarship Master's Award (#300911) that funded my first year of study, and the University of British Columbia Graduate Program in Neuroscience for welcoming me to their program with a lucrative Entrance Award. Lastly, I express my gratitude as recipient of a 2015 Mitacs Accelerate Internship.

To the wonderfully supportive teams at the Pacific Parkinson's Research Centre and those who make UBC's PET Program possible, your kindness has made our working arrangements feel more like family gatherings. My most sincere thanks to Jessamyn McKenzie and Nicole Neilson, you have truly brought this project to life! I turn to Dr. Appel-Cresswell's sentiment that this is "a team to be treasured".

To our research participants – I have been profoundly impacted by an extensive family history of neurodegenerative disease, experiencing first-hand the frustration, pain, and loss the shortcomings in our understanding and lack of treatment options or efficacy bring. Your selfless acts have made substantial contributions to my education, and validated the decisions of all who dedicate their careers to unravel the mystery of neurodegeneration. Without you, we could not pursue a cure.

To my colleagues - Naama Rotem-Kohavi, Courtney Hilderman, Shaun Porter, Najah Alhajri, and Danielle Murray, thank you for enriching my educational experience with intellectual discourse, coffee, and laughter. Matt Sacheli, the words “thank you” fall so incredibly short in expressing my gratitude for all you have contributed to my education and experience at UBC. Thank you for your sincerity in making time to answer my questions, offer genuine solutions, and always going out of your way to help a friend in need. I wish you a world of success in your future endeavours. You are, and always will be, one of the greats. Never change. It has been an utter privilege to work with all of you.

To my family - Thank you for an upbringing that fostered a willingness to try, the courage to fail, and the strength to carry on when life throws lemons. To my brothers, Justin, Dylan, and Tyler, each of you have brought such light to my life. Mom and Dad, I am humbled by your strength and dedication. Your love and support (and most of all, patience) have provided me with a personal resolve that has, and will continue to, contribute to my success. May I always make you proud.

To my husband, Alexander - Thank you for embracing my chaos and enriching my adventure. May we never lose our love of spontaneity and embarking on journeys down the road less traveled. We have conquered every challenge together, and this serves as another feather in our cap. I am forever grateful our worlds collided, and share this success with you.

This thesis is lovingly dedicated to those who have given me the world.

To my beautiful parents, Don and Lovanna,

Your immeasurable sacrifice has instilled the belief that life's true richness lies in three things:

family, education, and generosity.

&

To my husband, Alexander,

For graciously embracing each of my ambitious goals as if they were your own.

Chapter 1: Overview of Neurotrauma and Tau

1.1 General Introduction and Overview of Thesis

Mild traumatic brain injury (mTBI) remains one of the most highly prevalent neurological conditions, being described as a silent epidemic (CDC, 2010). Concussion, which has become synonymous with mTBI in the literature, is defined as 'a complex pathophysiological process affecting the brain, induced by biomechanical forces either by a direct or indirect blow resulting in an impulsive force transmitted to the head' (McCrory et al., 2013). Emerging evidence has contradicted the widespread notion that mTBI is a minor, independently dismissive injury, revealing profound deleterious long-term effects on brain function (Ling et al., 2015). By acknowledging that trauma initiates a pathological cascade that may be more damaging in the days and weeks following the immediate injury, the concept of mTBI has also shifted towards one of a process rather than a static injury.

In recent years, media attention has put a spotlight on the progressive neurological conditions, particularly Chronic Traumatic Encephalopathy (CTE), appearing in former professional athletes, military personnel, and others who experience numerous head injuries (McKee et al., 2009, Baugh et al., 2012, Kiernan et al., 2015). Repetitive neurotrauma in the form of concussive and subconcussive insult has long been associated with increased incidence of depression, progressive cognitive decline, and neuropsychiatric abnormalities (Parker, 1934, Courville, 1962). The resulting pathology may serve to predispose individuals to develop a pathologically distinct form of early onset tauopathy-related dementia and underlie changes in mood and motor function (Corsellis and Brierley, 1959). Despite serving as a significant risk factor for future neurodegenerative disorders including mild cognitive impairment, Alzheimer's disease (AD) and Parkinson's disease (PD), not all people who sustain mTBI go on to develop future long-term sequelae. It is therefore imperative to better understand the brain's response to mTBI, identify key biological markers of injury and recovery, and to identify those at risk of long-term consequences.

Concussive impacts elicit a pathophysiologic cascade that includes temporary neural dysfunction, disrupted connectivity, impaired axonal transport, and aberrant protein phosphorylation. While transient, trauma-induced alterations in neurometabolic processes are well characterized (Giza and Hovda, 2001), understanding the disruptions to white matter integrity and abnormal protein phosphorylation, particularly of a microtubule associated protein tau, are areas of active research. The overarching intent of this thesis is twofold:

1. To investigate the microstructural changes in white matter tracts following a single sports-related concussion in adolescent athletes using diffusion tensor imaging (DTI).
2. To establish a baseline for tau deposition in healthy, elderly individuals using a novel tau-specific radioligand, phenyl/pyridinyl-butadienyl-benzothiazoles/benzothiazoliums compound (^{11}C-PBB3) in high resolution positron emission tomography (PET).

Collectively, these efforts provide the groundwork for subsequent study of CTE and other related tauopathies, and provide insight into how a combination of imaging modalities and may serve as potential diagnostic biomarkers of trauma-induced neurodegeneration.

"***No head injury is too trivial to ignore***" ***(Hippocrates, 460-370 BC)***

1.2 History of CTE

Punch drunk syndrome, a condition prominent among prize fighters, was first described in 1928 by an American pathologist (Martland, 1928). Martland described the symptom onset as first evident in the extremities and accompanied by intermittent periods of slight mental confusion. The progressive nature of the disorder would evolve such that fighters would "develop a peculiar tilting of the head, a marked dragging of one or both legs, a staggering, propulsive gait with the facial characteristics of the Parkinsonian syndrome, or a backward swaying of the body, tremors, vertigo, or deafness … [and] marked mental deterioration" (Martland, 1928). Originally thought to be confined to boxers, the condition emerged among other professional athletes in high contact sports and war veterans exposed to frequent head injury. In 1937, the term "dementia pugilistica" was proposed to describe the devastating early onset of progressive cognitive decline; however, the condition was subsequently redefined as Chronic Traumatic

Encephalopathy in 1957. Neuropathological studies have since identified that the characteristic degeneration and neurobehavioural changes are associated with widespread and extensive deposition of the hyperphosphorylated protein, tau.

1.3 Clinical Presentation of Concussion and CTE

Clinical diagnosis of a concussion is primarily based on subjective symptom reporting and neuropsychological testing. A concussion is characterized as a mild TBI with an initial Glasgow Coma Scale of 13 - 15, post-traumatic anterograde amnesia (less than 24 hours), any alteration in mental state at the time of the accident, and may or may not be accompanied by a loss of consciousness of approximately 30 minutes or less ((ACRM), 1993). The signs and symptoms of concussion may be subtle and present hours or days after the initial injury. As a result, many symptoms often go unreported. While the clinical presentation varies between patients, commonly reported symptoms include headache, nausea, dizziness, difficulty concentrating, and sensitivity to light or noise. More severe concussions may result in temporarily impaired balance, visual and auditory disturbances, and emotional instability. Most symptoms resolve fully within 7 - 10 days; however, it is well documented that adolescents may experience delayed recovery and a greater window of vulnerability to secondary injury (Virji-Babul et al., 2013, Borich et al., 2015, Purcell et al., 2015). An initial 48 hours of cognitive and physical rest following injury is recommended, as an early return to activity may exacerbate symptoms and underlying pathology.

In approximately 10% of cases symptoms may persist for weeks to months post-injury; here the diagnosis transitions to ‘post-concussive syndrome’ (PCS) (Willer and Leddy, 2006). Irrespective of the initial combination of symptoms, longer term manifestations of concussion may result in disturbances in sleep or depression (Lynall et al., 2013, Noble and Hesdorffer, 2013). However, differentiating between prolonged PCS and the onset of a more devastating, irreversible illness can be challenging. Concussions do not cause gross structural abnormalities in brain tissue; hence conventional neuroimaging tests such as computed tomography (CT) or MRI are insensitive to the microstructural damage underlying post-injury structural and functional change.

Clinical manifestation of CTE is often insidious, with initial changes in mood such as increased feelings of anxiety, apathy, depression, and even suicidality; an increase in aggressive tendencies; deficits in cognition including memory loss and executive dysfunction; and occasionally motor disturbances in balance and gait. Initial presentation typically occurs around ages 35 – 45 years old (range 24 - 65 years) (McKee et al., 2013) and the progression is often slow, over decades. Characteristically, there is a long latent period (mean 8 years, range 0 – 37 years) between the last documented trauma and the onset or recognition of symptoms (McKee et al., 2009, Maroon et al., 2015). A recent study of a large cohort of pathologically confirmed CTE patients suggests clinical presentation may be divided into two distinct phenotypes, (i) predominantly mood and behavioural symptoms in younger individuals in their third decade; and (ii) predominantly cognitive impairment presenting in the fifth decade (Stern et al., 2013). Despite the well characterized presentation, a definitive diagnosis of CTE can only be made post-mortem, highlighting the need for reliable diagnostic biomarkers.

1.4 Pathophysiology of Concussion and Evolution of CTE

Concussion initiates a transient cascade of neurometabolic dysfunction, whereas repetitive and more severe injury can perpetuate symptoms through diffuse axonal injury and the deposition of aberrant tau protein. Early studies in subconcussive injury revealed that “permanent damage, in the form of microscopic destructive foci, can be inflicted on the brain by what are regarded as trivial head injuries” (Oppenheimer, 1968), thus reiterating that even subconcussive injury may result in functional disturbance and axonal injury.

The pathology of CTE is defined by a distinctive pattern of progressive brain atrophy and concomitant deposition of hyperphosphorylated tau. The formation of neurofibrillary and glial tangles, appearance of 43kDa TAR DNA-binding protein (TDP-43) neuronal and glial aggregates, microvascular pathology, neuroinflammation, and white matter degeneration are also features associated with CTE (Daneshvar et al., 2015). The pathological processes are described below.

1.4.1 Post-Concussive Cascade of Neural Dysfunction

The characteristic elements of post-traumatic neural dysfunction include global depolarization, excessive release of excitatory neurotransmitters, disturbances in ionic gradients, altered glucose metabolism and cerebral blood flow (see Figure 1.1), and impaired axonal function and transportation. These alterations are correlated with post-concussion vulnerability and neurobehavioural abnormalities (Giza and Hovda, 2001, Langlois et al., 2006, Prins et al., 2013, Giza and Hovda, 2014).

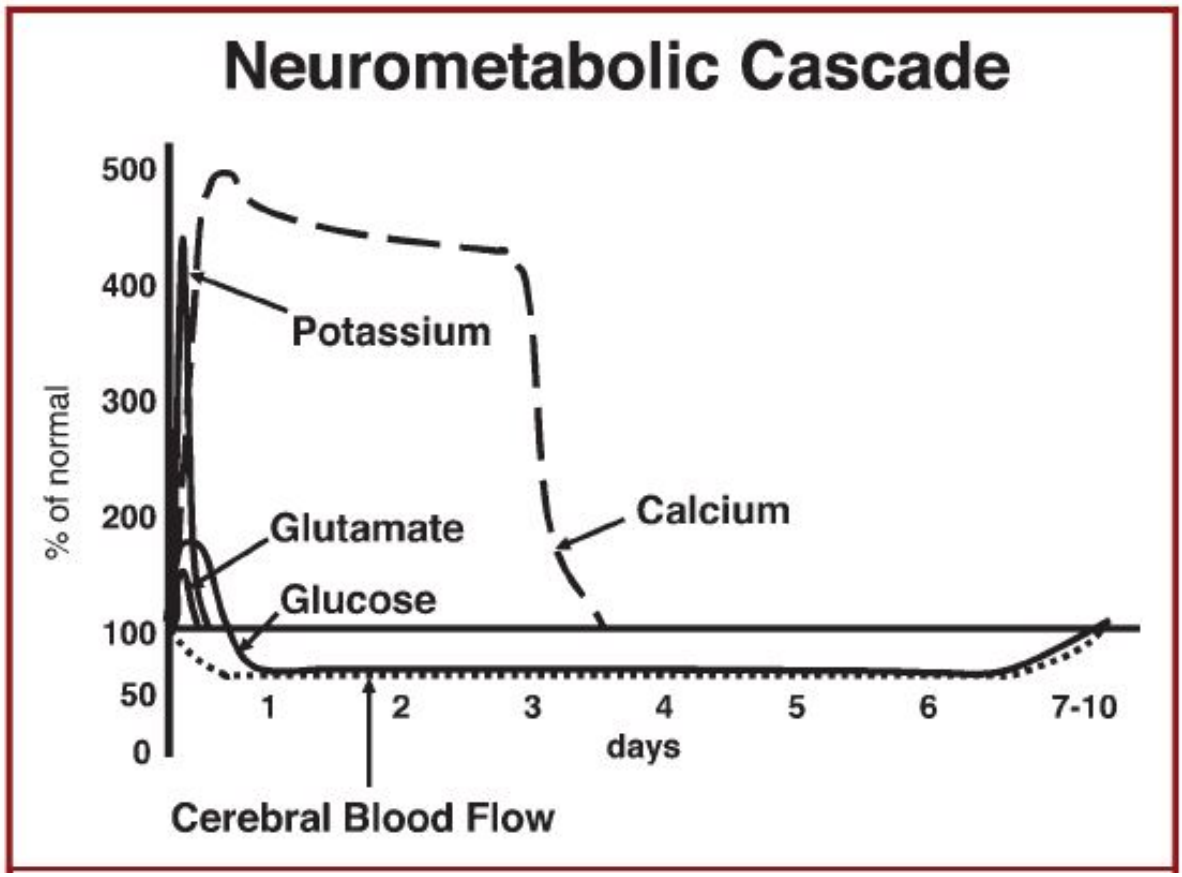

Figure 1.1 Time Course of Post-Concussive Neurometabolic Dysfunction

Concussions disrupt neural homeostasis. The immediate increases in glutamate and potassium tend to resolve within a few hours, while elevated calcium levels persist for several days. Decreases in cerebral blood flow and glucose metabolism may persist for up to 10 days post-injury. Figure reproduced with permissions (Giza and Hovda, 2014).

Glutamate and Potassium Release: Immediately following concussive injury there is an abrupt and widespread presynaptic release of glutamate. Activation of postsynaptic N-methyl-D-aspartate (NMDA) receptors propagates neuronal depolarization, facilitating potassium (K^+) efflux and increased intracellular calcium (Ca^{2+}) levels (Goldberg et al., 1987). Inward Ca^{2+} currents are enhanced by a swift recruitment of α-amino-3-hydroxy-5-methyl-4-isoxazolepropionic acid (AMPA) receptors to excitatory synapses (Brorson et al., 1994). Normally, AMPA receptors are Ca^{2+} impermeable; however, traumatic, hypoxic, or ischemic conditions evoke a switch in the subunit composition, leading to Ca^{2+} permeable GluR2-lacking receptors (Brorson et al., 1994). These ionic shifts incite acute changes in cellular physiology, reinforcing a positive feedback cycle that stimulates excitotoxicity (Faden and Simon, 1988).

***Hypermetabolism*:** Ionic perturbances are ordinarily rectified by sodium-potassium (Na^+-K^+ ATPase) pumps. However, the surge of intracellular Ca^{2+} following concussion overwhelms the capacity of these pumps, escalating the energy demands of the cell. Attempts to increase the production of adenosine triphosphate (ATP) trigger a dramatic rise in glucose metabolism, forcing the cell into a hypermetabolic state. This occurs amidst decreased cerebral blood flow, and the subsequent disparity between glucose supply and demand has been referred to as a "cellular energy crisis" (Yoshino et al., 1991). This is postulated as one of the mechanisms underlying post-concussive vulnerability, and may explain the diminished capacity for response to subsequent injury and prolonged deficits (Guskiewicz et al., 2003, McCrea et al., 2009). Vulnerability persists until glucose demand and blood flow return to pre-injury levels up to one week later in mice, and two weeks later in humans (Zemper, 2003). The effects of a second injury within this window are compounded, but the extent of irreparable damage remains unknown (Zemper, 2003, Guskiewicz et al., 2005).

Lactate Accumulation: Hyperglycolysis results in excess lactate production. Impaired mitochondrial function abolishes normal oxidative metabolism, further compounding lactate accumulation. These elevated levels can disrupt the intracellular pH leading to acidosis, altered blood brain barrier (BBB) permeability, membrane damage, and, ultimately, cerebral edema (Kawamata et al., 1995, Giza and Hovda, 2001).

Calcium Overload and Mitochondrial Dysfunction: Ca^{2+} build-up through both the NMDA and GluR2-lacking AMPA receptors is evident within hours of experimental concussion, and may persist for up to 10 days (Xiong et al., 1997). A drastic increase in Ca^{2+} influx during sequestration impairs mitochondrial function, altering the inner membrane permeability, uncoupling oxidative phosphorylation, and collapsing the electron transport chain with the end result of organelle swelling (Xiong et al., 1997, Nicholls and Budd, 1998). As dysfunctional mitochondria become the primary source of reactive oxygen species, oxidative stress ensues and free radicals may prompt lipid peroxidation, collectively worsening the energy crisis (Barkhoudarian et al., 2011). Unbridled calcium accumulation can trigger catabolic cascades, activate apoptotic pathways and further disrupt neurofilaments and microtubules, impairing connectivity (Giza and Hovda, 2001, Barkhoudarian et al., 2011).

Hypometabolism: Following hyperglycolysis, the brain enters a period of depressed metabolism. Clinical studies using ^{18}F-Fluorodeoxyglucose (^{18}F-FDG) PET show persistent depressed cerebral glucose utilization up to one month post-injury (Bergsneider et al., 2000). During the prolonged metabolic depression, neurons show impaired metabolic response to peripheral stimulation (Queen et al., 1997).

1.4.2 Diffuse Axonal Injury

Rapid linear or angular acceleration, deceleration or rotational forces cause momentary brain deformation as a result of a coup-contrecoup injury whereby the brain first collides with the skull at the site of impact and secondarily at the site directly opposite. As a result, delicate axons that traverse long distances from the neuronal cell bodies are susceptible to stretching. This may compromise structural integrity through excess shearing or tearing forces and lead to diffuse axonal injury (DAI). This is the primary mechanism by which concussion and subconcussion occur, and the underlying basis for persistent symptoms (Reeves et al., 2005, McKee et al., 2014).

Concussion-induced DAI tends to occur in regions of stiffer structural attachment between the brain and the skull, and the extent of the axonal injury reflects the severity of the TBI. Glial cells and microvasculature are also vulnerable to stretching as a result of concussive impact. Shearing injuries result when the differing densities of grey and white matter, at varied distances from the axis of rotation, slide over one another (Ng et al., 1994). Two-thirds of DAI lesions occur at junctions between grey and white matter; tearing of these subcortical white matter fibres is generally accompanied by a loss of consciousness (Hammoud and Wasserman, 2002).

Additionally, axonal stretching leads to transient alterations in membrane permeability, triggering a secondary biochemical cascade that is responsible for significant damage and cytoskeleton degradation in the days and weeks following injury. This microscopic destruction continues long after most of the cognitive symptoms have subsided (Pettus and Povlishock, 1996, Giza and Hovda, 2001, Tang-Schomer et al., 2012, Johnson et al., 2013b).

The degree of axonal injury after traumatic impact may also vary with the direction of the head impact rotation, as experimental studies in gyrencephalic piglets have found greater behavioral abnormalities and more persistent axonal injury in piglets exposed to sagittal versus axial rotational injury (Sullivan et al., 2013). It has been suggested that the rotational acceleration such as blows to the head by hook punches in boxing are more likely to result in concussion than the linear acceleration caused by straight head blows and head contacts such as in American football (Ohhashi et al., 2002). However, injury mechanisms and thresholds continue to be a source of vigorous debate.

Secondary Biochemical Cascade: Axonal stretching opens sodium channels in the axolemma, propagates depolarization and the opening of voltage-gated Ca^{2+} channels in presynaptic terminals, and sustains glutamate release. The enhanced Ca^{2+} current, both pre- and post-synaptically, initiates destruction of mitochondria and the cytoskeleton through degradation by phospholipases and proteolytic enzymes, and the activation of secondary messengers (Hammoud and Wasserman, 2002, McBride, 2012).

Neuroinflammation and Microvascular Consequence: Microhemorrhage, loss of microvascular integrity, and neuroinflammation may also occur after concussion. Neuroinflammation occurs with the activation of microglia and astroglia which lead to the expression of pro-inflammatory cytokines (such as Interleukin-1β and tumor necrosis factor alpha) and chemokines. The axonal injury produced by mTBI is multifocal, with a tendency to be most severe in the corpus callosum, fornix, parasagittal white matter and cerebellum, and within these areas, more pronounced around small blood vessels (Tang-Schomer et al., 2012, McKee et al., 2014). Pathological studies show that traumatically-induced vascular inflammation may facilitate breach of the blood brain barrier and release of normally excluded systemic proteins, such as perivascular hemosiderin, hematoidin-laden macrophages and pro-inflammatory cytokines (Oppenheimer, 1968, Blumbergs et al., 1994, McKee et al., 2014). Astrocytosis is most severe in the cerebral white matter and brainstem white matter tracts, and clusters of activated microglia are most prominent in the white matter around small vessels.

Cytoskeletal Disruption and Impaired Axonal Transport: Under normal conditions, axons exhibit mild elasticity; however, the rapid stretching forces of concussion may exceed their tensile capacity. Integrins connecting the extracellular matrix and cytoskeleton are thought to transmit the force of impact resulting in breaks or misalignment of actin filaments (Hemphill et al., 2011). Of particular interest, tau protein interacts with tubulin at the distal end of axons to stabilize microtubule structures, which may also have an elastic limit that is breached during concussion as microtubules are known to become unfastened (Buki and Povlishock, 2006). This compromise in the structural integrity of axons arrests intracellular transport at breaks in the cytoskeleton, leading to a buildup of transport products. The disruption of information flow contributes to local swelling, further weakening of actin networks, and eventual retraction into a characteristic retraction bulb (Hammoud and Wasserman, 2002). Axon remnants distal to a break undergo Wallerian degeneration, whereby the axolemma disintegrates, myelin breaks down and phagocytic cells are recruited. The pathological manifestation of injury-induced secondary axotomy, including deficits in axonal conductance and neurofilament dephosphorylation, is still evident 14 days after trauma; impaired retrograde transport can be visualized with Fluoro-Gold (Creed et al., 2011). In addition, a single head injury may promote increased deposition and

accumulation of amyloid-beta (Aβ), a protein aggregate linked to Alzheimer's disease, that further impedes axonal function (Washington et al., 2013). Collectively, these data suggest disruptions to the axonal cytoskeleton persist long after the recovery of acute cognitive deficits. A summary of acute and chronic neural dysfunction is provided in Figure 1.2. The long-term consequences of this underlying impairment are areas of active research. The thesis intends to explore cytoskeletal disruption through investigation of post-concussive white matter integrity.

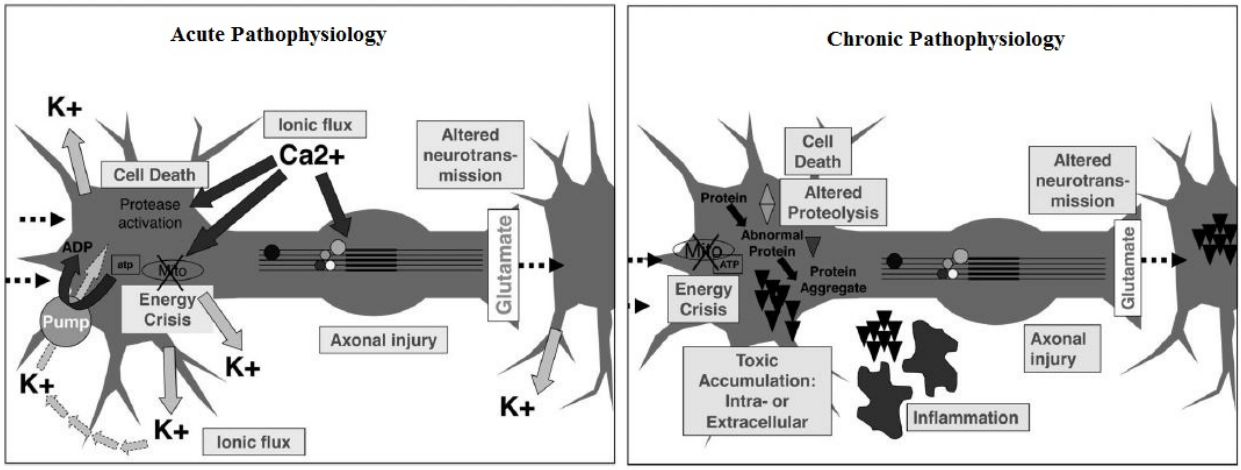

Figure 1.2 Acute and Chronic Phase Post-Concussive Neural Dysfunction
Figure reproduced and revised with permissions (Giza and Hovda, 2014).

1.4.3 Hyperphosphorylation of Tau

Acceleration–deceleration injuries also cause tau protein to become abnormally phosphorylated, leading to neurotoxic tau peptide fragments (Khlistunova et al., 2006, Liliang et al., 2010). When misfolded, this otherwise soluble protein forms extremely insoluble aggregates; assembling first as paired helical filaments and later forming intraneuronal deposits known as neurofibrillary tangles (NFTs).

Tau is a phosphoprotein with six known isoforms that result from the alternative splicing of exons 2, 3, and 10 within a single microtubule-associated protein tau (MAPT) gene located on chromosome 17. These isoforms are identified by the number and composition of their positively charged, carboxy-terminal binding domains; three isoforms have three binding domains, the rest have four binding domains. Tau proteins have up to 79 potential Serine and Threonine

phosphorylation sites; however, under normal conditions only around 30 of these sites are actively utilized (Billingsley and Kincaid, 1997). Phosphorylation is regulated by a number of kinases with the most prominent being the serine/threonine kinase, PKN (Taniguchi et al., 2001). Dysregulation of PKN can initiate abnormal and excessive phosphorylation of tau isoforms.

Following repetitive concussive injury, there is widespread deposition of all six abnormally phosphorylated isoforms resulting in NFTs throughout the brain (McKee et al., 2009, McKee et al., 2013). Although tau in CTE is composed of both 3- and 4- microtubule binding repeats, 4R predominates with a pattern of neuronal and astrocytic tau pathology distinct from deposition in normal aging and AD. Two additional features unique to tau in CTE are the perivascular presentation and the irregular distribution deep within cortical sulci (McKee et al., 2014). Focal perivascular accumulations of hyperphosphorylated tau (p-tau) and hyperphosphorylated TDP-43 (p-TDP43) occasionally occur after concussive injury. It has been suggested that dysregulation of TDP-43 may influence tau isoform expression and the development of tau pathology (Morales et al., 2009); however the potential synergistic link has been debated and requires further investigation (Wils et al., 2010, Zhou et al., 2010, Strong and Yang, 2011). The hyperphosphorylation of tau, and subsequently the development of intraneuronal NFTs constitute the proposed mechanism by which acute and/or repetitive mTBI may incite neurodegenerative processes associated with CTE.

1.4.4 Neuropathology of CTE

Neuropathological findings in CTE reveal a characteristic pattern of atrophy and concomitant deposition of p-tau. First, the stereotypical pattern of degeneration will be discussed. The staging patterns of abnormal tau accumulation in histological preparations will be described in the following section.

In the landmark study of 15 professional boxers, Corsellis proposed four major criteria for CTE (Corsellis et al., 1973):

1. Abnormalities of the septum pellucidum;
2. Cerebellar scarring on the inferior surface of the lateral lobes (especially the tonsillar regions);
3. Degeneration or pallor of the substantia nigra;
4. Widespread NFTs containing p-tau in the cerebral cortex and brainstem.

A characteristic sequence of atrophy has since been identified. First, diffuse atrophy of the frontal and temporal cortices and the medial temporal lobe, with ventricular dilation of the lateral ventricles and the third ventricle is evident. Unlike the early stages of AD, the hippocampus is spared in early phases of CTE. Subsequent atrophy is noted in the anterior cavum septi pellucidi and posterior fenestrations. As the disease progresses, the olfactory bulbs, thalamus, mammillary bodies, brainstem, and cerebellum begin to degenerate and depigmentation of the substantia nigra and locus coeruleus are notable. In its later stage, the hippocampus, entorhinal cortex, and amygdala also degenerate (Baugh et al., 2012, McKee et al., 2013, Kiernan et al., 2015).

1.4.5 Stages of CTE Defined by Tau Pathology

CTE has been described in four stages based upon the accumulation and distribution of p-tau deposition (McKee et al., 2013, McKee et al., 2015). These stages are described below and depicted in Figure 1.3.

Stage I: In Stage I CTE, tau is found in focal, perivascular clusters as NFTs and dystrophic neurites, often at the sulcal depths of frontal, septal, or temporal cortex. The surrounding cortex is typically unremarkable although rare NFTs may be found in the deep nuclei, such as the locus coeruleus.

Stage II: In Stage II CTE, multiple discrete clusters of perivascular p-tau NFTs are found in the sulcal depths, most commonly in frontal, temporal, parietal, insular, and septal cortices. NFTs are also found in the superficial layers of adjacent cortex surrounding the epicenters. The nucleus basalis of Meynert and locus coeruleus show NFTs as well. Rare NFTs may be found in entorhinal cortex, amygdala, hippocampus, thalamus, substantia nigra, and dorsal and median raphe nuclei of the midbrain.

Stage III: In Stage III CTE, the medial temporal lobe structures including the hippocampus, entorhinal cortex, and amygdala show neurofibrillary degeneration, and there is widespread involvement of the frontal, temporal parietal, insula, and septal cortices. Moderate densities of NFTs are found in olfactory bulbs, hypothalamus, thalamus, mammillary bodies, substantia nigra, and both dorsal and median raphe nuclei.

Stage IV: In Stage IV CTE, there are dense NFTs in widespread regions of the brain, with prominent neuronal loss and gliosis of the neocortex and increasing p-tau in astrocytes. There is prominent loss of CA1 neurons throughout the hippocampus and subiculum, cerebral cortices and increasing myelinated fiber and axonal loss in the white matter. Severe p-tau pathology is found in the cerebral cortex, diencephalon, basal ganglia, and brainstem, white matter tracts and spinal cord. The primary visual cortex is spared.

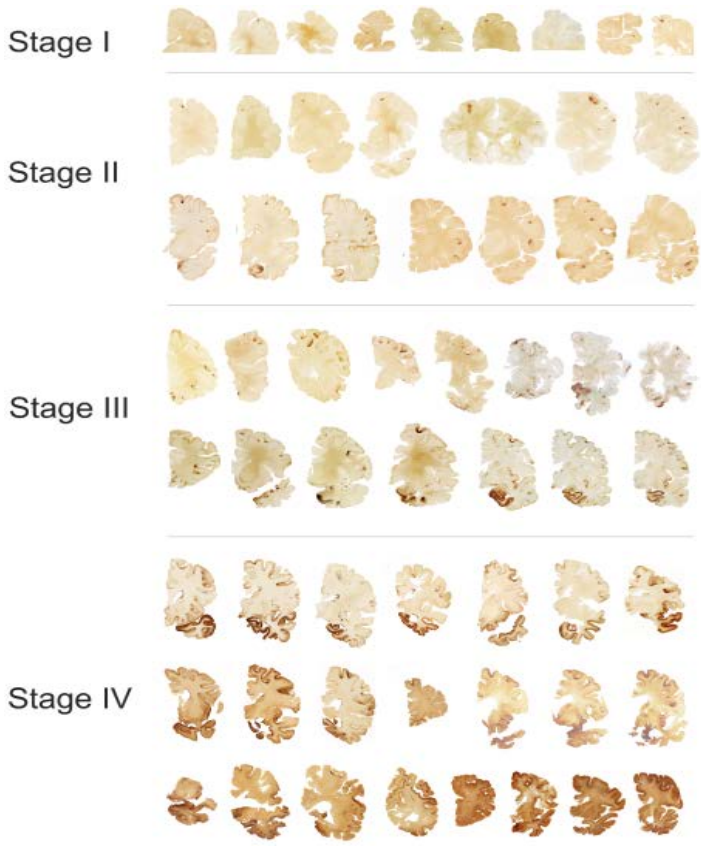

Figure 1.3 Histological Staging of CTE

Marked atrophy and concomitant tau deposition are noticeable with disease progression. In Stage I initial tau deposition is evident in sulcal depths within the frontal and temporal cortices. By Stage III and IV tau deposition is widespread. Figure reproduced with permissions (McKee et al., 2015).

Progression from multifocal in stage II to widespread disease in stage III suggests an exponential increase in tau deposition, which may result from a prion-like mechanism of self-propagating protein templating and other modes of interneuronal transmission (Morales et al., 2009, McKee et al., 2014). Clinical studies suggest that this stage of the disease correlates with the onset of intrusive neuropsychiatric symptoms such as depression and suicidality. Advancement to stage IV is clinically characterized by overt dementia. Here extensive underlying TDP-43 immunoreactive intraneuronal and glial inclusions are observed in the cortex, white matter, brainstem, diencephalon, and basal ganglia (McKee et al., 2013). Inevitably, the extent of tau and TDP-43 deposition, neuronal loss, and cerebral deterioration increases with lifespan, contributing to the unremitting progression of clinical symptoms (McKee et al., 2014).

1.5 General Purpose and Design of Thesis

Neuroimaging-based studies have acknowledged that both functional and structural damage persists for much longer than concussive symptoms are reported, and suggest that the return to neural homeostasis takes in excess of one month. However, neuropathological evaluations reveal that concussion-induced axonal damage may be evident for years after injury (Johnson et al., 2013a).

In this thesis, I discuss the underlying changes within the microstructural environment that occur with even mild concussion, and how damage is compounded with repetitive injury. I include the evolution of CTE to provide context for my subsequent study. In Chapter 2, I describe the use of DTI to evaluate microstructural changes that occur in white matter fibre tracts of concussed athletes. To offer greater understanding of how the organization of neural networks may change as a result of a single concussion, I utilize Complex Network Analysis to compare healthy adolescent individuals to their concussed counterparts. In Chapters 3 and 4, I address potential mechanisms that contribute to impaired neuronal function. I conducted PET with a newly developed radioligand, ^{11}C-PBB3, which specifically binds to hyperphosphorylated tau. The inherent properties of intraneuronal NFTs likely contribute to impaired axonal transport and may perpetuate or exacerbate dysfunction.

My investigations specifically evaluate baseline levels of abnormally phosphorylated tau in healthy controls, and provide preliminary results after testing the tracer in patients with a suspected and known tauopathy. This establishes the groundwork for subsequent comparison to neurodegenerative populations including patients with sports-induced CTE and varying forms of atypical Parkinsonism. The ultimate intent is to pursue tau-based imaging in a population of professional athletes to evaluate tau deposition from an early age. Longitudinal studies will be required to monitor changes in deposition as a function of time and exposure to injury, and determine whether this tracer may serve as a viable biomarker for neurodegenerative disease.

Chapter 2: Complex Network Analysis in Sports-Related Concussion

2.1 Introduction to Diffusion Tensor Imaging

Diffusion tensor imaging (DTI) is a non-invasive magnetic resonance imaging (MRI) technique that utilizes the diffusion properties of water molecules to reveal microscopic tissue architecture in-vivo (Le Bihan et al., 1986). The standard MR pulse sequence is supplemented with diffusion encoding gradients. Diffusion patterns reflect the interactions of water molecules within the surrounding milieu and may distinguish healthy and pathological states (Besga et al., 2012, Adamson et al., 2013), particularly of the white matter (WM). Collectively the tensor model identifies the structural orientation of fibres and measures both the rate (mean diffusivity, MD) and directionality of diffusion. The preferential direction of diffusion is expressed as a value of fractional anisotropy (FA), which averages both the axial (longitudinal) and radial (transverse) diffusivity measurements (Basser et al., 1994). DTI has emerged as a prominent imaging modality in the study of neurodegenerative conditions and brain injury (Greicius and Kimmel, 2012, Meijer et al., 2013, Abhinav et al., 2014, Acosta-Cabronero and Nestor, 2014, Keightley et al., 2014), for which the basic concepts and underlying principles of DTI have been comprehensively described, refined, and reviewed in the literature (Basser and Pierpaoli, 1996, Irimia et al., 2012, Fox et al., 2013, Hulkower et al., 2013, Shin et al., 2014, Khanna et al., 2015). A summary of the DTI acquisition process is described below.

The DTI process first requires a reference scan (B0 image) in which no diffusion weighting is applied. Next, the diffusion weighting of images is varied both in magnitude and orientation gradients indicated by a b-value. The particular combination of diffusion encoding gradients is provided in the b-matrix. Standard b-values are 1000 s/mm^2 for adults, 700 - 800 s/mm^2 for children and adolescents, and 600 s/mm^2 for infants (Hüppi and Dubois, 2006, Brown et al., 2014) diffusion produces darker pixels as the signal attenuates. Application of a diffusion weighted signal reveals that water molecules preferentially diffuse in parallel with the dominant orientation of WM fibers; this results in anisotropic diffusion (FA ≥0.8). The less organized microstructure of the gray matter and cerebral spinal fluid preferentially allow isotropic diffusion (FA close to 0); that which is independent of the direction of the applied gradient. The diffusion

weighted images (DWIs) are then compared to the reference scan. Tensor calculation relies on a minimum of six directions or gradients and allows a colour-coded representation of anterior vs. posterior, left vs. right, and superior vs. inferior orientations to be established as green, red, and blue, respectively. The tensor is arranged as a symmetric 3 x 3 matrix and may be split into diffusion directions defined as eigenvectors (*e*1, *e*2, *e*3*)* along the x, y, and z planes. Eigenvalues (λ1, λ 2, λ3) represent the magnitude of diffusion and are used to establish which eigenvector aligns with each of the aforementioned planes; larger eigenvalues indicate the primary direction of diffusion along a fibre. The resulting ellipsoid-shaped tensors may be mathematically combined in a process known as tractography (Gerig et al., 2004). Tractography discerns the complexity of WM networks, allowing for both qualitative and quantitative evaluation of the composite fibre tracts on a voxel-by-voxel basis.

2.2 Diffusion Tensor Imaging Applications in Sports-Related Concussion

Since the early 2000s the number of concussion-based research studies has increased dramatically, with emphasis on varsity and professional athlete populations in high contact sports. Current estimates suggest $1/10^{th}$ of published mTBI studies incorporate neuroimaging (Eierud et al., 2014). However, from a clinical perspective neuroimaging is impractical in the routine diagnosis of concussion. Conventional modalities such as anatomical MRI and CT scans, which are more frequently used in emergency departments to rule out more severe trauma, are insensitive to the subtle pathology and structural changes of mTBI. In recent years, DTI-based studies of concussive and subconcussive impact have provided a means to visualize the diffuse nature of what had previously been described as an invisible injury by capturing persistent microstructural alterations (Virji-Babul et al., 2013). Considerable efforts have been made to evaluate post-traumatic WM integrity, as abnormalities are purported to reflect damage to axon bundles and microtubule structures imposed by the violent shearing or stretching forces associated with such abrupt deceleration and impact on the skull (Buki and Povlishock, 2006, Blennow et al., 2012, McKee et al., 2014, Shin et al., 2014, Chong and Schwedt, 2015, Stemper et al., 2015). Previous studies suggest that the diffusion properties are altered following concussion; yet controversy remains over the directionality, anatomical localization, and timing of such changes.

First, published post-concussive changes in FA values have been inconsistent, with studies showing increases, decreases, or no detectable change at all (Henry et al., 2011, Lange et al., 2012, Alhilali et al., 2014, Lange et al., 2015). Explanations for these discrepancies suggest diffuse structural damage may impair the function of ion channels, leading to perturbances in ionic gradients. These fluctuations alter intra- and extracellular water content and thereby the acquired diffusion properties (Ito et al., 1996, Mayer et al., 2010). Additionally, constituents of the inflammatory cascade and processes such as cytotoxic edema may restrict overall diffusion or result in preferential directionality of the movement of water molecules during imaging (Cubon et al., 2011, Len and Neary, 2011, Ling et al., 2012). Collectively, these influences have sparked debate and challenged the correlations between neuropsychological evaluations and anisotropic values (Lange et al., 2012, Veeramuthu et al., 2015). While decreased FA values tend to follow more severe trauma (Ljungqvist et al., 2011), mounting evidence strongly supports an increase in FA values in the acute phase of mTBI (Wilde et al., 2008, Henry et al., 2011). A recent study found that adolescent athletes had a significant increase in whole brain FA values and a decrease in MD values up to two months post-concussion when compared to their non-concussed counterparts, and that these changes correlated with clinical measures on the Sports Concussion Assessment Tool version 2 (Virji-Babul et al., 2013).

Next, published findings of regional WM changes are highly heterogeneous. A recent meta-analysis examined the literature for anatomical consistency in concussion-induced lesions (Eierud et al., 2014). The authors reported a characteristic anterior-posterior gradient in which anterior WM tracts were more susceptible to traumatic insult. Additionally, the frontal association areas and dense crossing fibres of the commissural pathways including the anterior corona radiata and genu of the corpus callosum have shown high vulnerability to microstructural change post-concussion (Cubon et al., 2011, Virji-Babul et al., 2013). These findings substantiate that anterior microstructural injury may contribute to cognitive and executive function deficits frequently encountered in mTBI (McCrea et al., 2003), as these WM tracts are critical in higher cognitive functions such as sustained attention, working memory, and organizational skills.

Lastly, the timing of post-injury imaging and evaluations are known to influence the direction of change in diffusion properties. As previously discussed, studies have shown both increases and decreases in FA values in the acute phase of recovery; however, a shift toward decreased diffusion properties in chronic recovery has emerged (Ljungqvist et al., 2011, Murugavel et al., 2014). Differences in the time-course of imaging in concussion studies hinder comparisons in the literature. Current protocols have focused on recovery in the first three-month window with a distinct lack of long term follow up (Gardner et al., 2012). Longitudinal studies are needed to better understand the time-course of recovery, and associated structural and functional changes. Here we investigate structural changes in the sub-acute phase of recovery (up to two months post-injury) in adolescent athletes.

2.2.1 Distinction between Adolescent and Adult Concussion

Age has been identified as an important influential factor in the concussion literature. Younger populations experience increased risk for more severe injury, delayed recovery processes (McCrory et al., 2013), and worse overall outcomes (Giza et al., 2005, Anderson et al., 2009). Pediatric concussions warrant specific concern as the developing brain appears increasingly susceptible to the effects of mTBI. This is likely due to differences in structural features such as a lesser degree of myelination and brain-to-water volume ratios (Shrey et al., 2011). Children and adolescents also tend to show increases in inflammatory responses and lesser BBB integrity in response to trauma than adults (Falcone et al., 2015). Additionally, adolescents are particularly vulnerable in the instances of hypoxic and ischemic events or traumatic axonal injury due to ongoing brain development (Adelson and Kochanek, 1998, Kochanek, 2006). Damage in the frontal and temporal lobes is correlated with executive dysfunction, behavioural disturbance, and deficits in learning and working memory that may be more pronounced at a younger age (Di Stefano et al., 2000). Next, the majority of adults report their concussion symptoms resolve within 7 - 10 days, yet recovery times in children and adolescents are notably longer (McCrory and Davis, 2005, Purcell et al., 2015). Young age has been suggested to extend recovery times to average between two to four weeks; however, in a study of children as young as six-years-old, 14% reported concussive symptoms enduring beyond three months post-injury (Barlow et al., 2010). Given the prevalence of pediatric concussion, this number is not insignificant. Lastly,

following a concussion there is a distinct window of vulnerability in which children and adolescents are at greater risk for a second injury than adults. An early return to sport or other activity greatly increases the likelihood and severity of injury, as a second impact compounds the damage and significantly delays recovery (Bazarian et al., 2014).

2.2.2 Post-Concussive Functional Connectivity and Insight into Structural Connectivity

Despite unchanged gross anatomy following concussion, such injury is known to disrupt both functional and structural connectivity in the brain (Xiong et al., 1997, Langlois et al., 2006, Johnson et al., 2012). Blood oxygenation level dependent imaging is a functional MRI (fMRI) sequence that detects changes in neural blood flow and identifies areas of activity. fMRI provides two distinct avenues for investigation of concussion by capturing brain activity while engaged in task-based or resting-state paradigms. Task-based studies involve either passive or active engagement in a cognitive or physical task while in the scanner. Conversely, in resting-state fMRI there is no explicit task. These protocols have reliably detected changes in functional connectivity between healthy and concussed individuals, identified post-concussion functional irregularities in various brain regions, helped elucidate the time course of recovery, and identified regions of activity that may be further evaluated as structural correlates of post-concussive dysregulation (Abbas et al., 2015, Astafiev et al., 2015, Borich et al., 2015, Mayer et al., 2015). The contributions of each fMRI modality to the concussion literature, and influence on this study are described below.

Mounting evidence in adults suggests functional alterations may be detected for months after symptomatic relief (Shumskaya et al., 2012, Dettwiler et al., 2014). Interhemispheric connectivity in the dorsolateral prefrontal cortex (DLPFC), hippocampus, and primary visual cortex have been reduced in concussed adults who were asymptomatic at the time of imaging (Cao and Slobounov, 2010). Reduced functional connectivity has similarly been found in parietal and posterior cingulate cortices (PCC), and correlations identified between resting state measures and decreased neurocognitive performance (Johnson et al., 2012, Tang et al., 2012). A recent rs-fMRI pilot study in nine concussed collegiate football players reported functional connectivity within the Default Mode Network (DMN) was significantly reduced in the acute recovery phase

(Days 1 to 7) compared to control athletes, with partial recovery over the first month (Zhu et al., 2015). These functional changes were evident despite clinical improvement; however, the authors did not identify any structural changes in the DMN. Additionally, fMRI investigations of individuals who suffer persistent TBI symptoms have detected changes in localization and levels of activity in the brain despite scoring within normal limits on neurocognitive evaluations (Chen et al., 2008; Gosselin et al., 2011; Lovell et al., 2007).

A comprehensive review of the literature has incited our exploratory efforts to evaluate subnetworks for persistent structural change based on regions commonly identified as showing alterations in functional connectivity following a concussion. As discussed, functional studies using both resting state and task-based MRI have shown particular alterations in executive function, attention, and Default Mode Networks. A previous DTI study by Virji-Babul et al. (2013) suggests that subtle, diffuse structural changes are evident up to two months post-injury in concussed adolescent athletes between the ages of 14 - 17 years old. We sought to evaluate the corresponding structural components of each of the aforementioned functional networks in adolescent athletes in the sub-acute phases of recovery following a concussion. We propose a new methodology for understanding the changes in diffusion-based measures by evaluating topological network properties using a mathematical model of Complex Network Analysis. The findings of our subnetwork analysis may serve as a means to detect areas of prolonged structural change that underlie protracted symptoms.

2.3 Graph Theory Modeling of Structural Change

2.3.1 Introduction to Graph Theory and Complex Network Analysis

Graph Theoretical Analysis has been used to model relationships and interactions amongst a plethora of complex systems. While the original algorithms have been adapted for use in vast physical and social networks for the purposes of city-wide transportation planning (Quintero et al., 2013) or analytics of emerging trends on the World Wide Web (Otte and Rousseau, 2002), recent efforts to understand biologically relevant interactions have been fruitful (Ma'ayan, 2011). The complexity of neural networks may be distilled into structural pathways based on WM tracts. The efficiency with which the brain relays information, both within and between various

regions, is contingent upon the organization and integrity of these WM connections (Filley, 2005, Schmahmann et al., 2008). Complex Network Analysis (CNA), a derivative of Graph Theory, is a set of mathematical tools that has recently been used to quantify topologies and describe neural networks with respect to their organizational arrangements (Bullmore and Sporns, 2009, Brown et al., 2014, De Vico Fallani et al., 2014, Papo et al., 2014). CNA evaluates associations between entities in terms of symmetry or asymmetry, and structural integration and segregation (Bullmore and Sporns, 2009). By characterizing general and localized patterns of anatomical circuitry in both mTBI subjects and controls, the composite CNA measures provide a means to assess and track potential structural changes following traumatic insult.

In healthy individuals, brain connectivity structure has been described as analogous to a "small-world" network (Sporns and Honey, 2006, Rubinov and Sporns, 2010) and more recently, as a small-world network with hierarchical modularity (Kaiser and Hilgetag, 2010, Hilgetag and Goulas, 2015). The WM facilitates the flow of information within and between various brain regions, thereby offering local specialization and global integration in unison. However, studies of various neurodegenerative conditions have demonstrated focal atrophy yields widespread consequences for WM brain networks at both the local and global levels (Acosta-Cabronero et al., 2010, Zhang et al., 2013, Caso et al., 2015). Network measures are helpful in identifying changes pertaining to the clustering of activity, and density and length of connections; which likely reflect overall neural plasticity (Castellanos et al., 2011). However, more research is needed to elucidate whether injury-induced reorganizational responses are part of a dynamic compensatory process, or in fact contribute to the degenerative dysfunction by increasing energetic demands in certain regions as the efficiency and organization of the existing structures falter (Irimia et al., 2012).

Current efforts to identify subtle network changes often rely on regional atlases that parcellate the brain into anatomical regions in each hemisphere (McKenna et al., 2015). In terms of WM brain networks, each region represents a 'node', while the pathways between regions delineate 'edges'. This network represents the microstructural integrity between regions. CNA measures analyze the efficiency and organizational structure of this network to reveal topological

properties at both the whole brain (global) and subnetworks (local) levels. These measures can include quantities of degree and density; clustering, core, and community structures; path lengths; centrality; and motifs (Bullmore and Sporns, 2009).

The application of Graph Theory to measures of structural connectivity is a new avenue in DTI, and mTBI studies are in their infancy. A shift towards hemispheric asymmetries and suboptimal module organization and efficiency were reported in studies of concussed military personnel (Han et al., 2014, Yeh et al., 2014); however, currently there is no comparable study in younger individuals. In order to evaluate post-concussive structural brain connectivity, anatomical WM tracts between regions of previously described vulnerability to mTBI should be evaluated. Here we described the applications of CNA to subnetworks of structures associated with cognitive deficits and resting state changes in concussed adolescent athletes.

2.3.2 Global and Local Metrics

Complex Network Analysis offers an extensive list of measures, many of which have been adapted for use in brain-based investigations. Scripts for the CNA metrics relevant to structural connectivity networks, and yielding neurobiologically meaningful output, were extracted from the Brain Connectivity Toolbox (Rubinov and Sporns, 2010). A comprehensive overview of network metrics is provided in Appendix A, while descriptions of common network terminology and the primary global and local metrics included in our analysis are provided below.

Common Network Descriptors

- **Robustness:** describes network fragmentation following the loss of critical nodes or edges. This represents a phase transition from a more highly ordered structure to a disordered one in which components of a network become smaller, disconnected clusters. Robust networks will continue to function despite damage.

- **Modules:** modules are subnetworks in which the composite nodes are more strongly linked to each other than to nodes outside of the network. Modules represent regions of specialized function and are highly relevant to neural networks.

- **Small World Topology:** a network structure in which most nodes are not neighbours, but any given node may be reached following a small number of connections. This is true of the anatomical connections comprising neural circuitry. Small-worldness facilitates both global integration and local segregation; a key to lean wiring within complex systems, especially the brain (Watts and Strogatz, 1998).

Network Measures

- **Clustering Coefficient:** is a measure of segregated network structure. It identifies the extent to which nodes of interest tend to cluster together in a given network, and may be global or locally derived with values ranging between 0 and 1 (see Figure 2.1). Calculations identify the fraction of triangle motifs around a node (i.e. triplets where three vertices are fully connected by intervening edges). In the application to subnetworks, clustering coefficients measure 'local connectivity', where higher values are associated with network resilience to damage (i.e. robustness).

- **Transitivity:** evaluates the likelihood that, for a given node with connections to two different nodes, there will also be a connection between the two outlying nodes thus creating an enclosed triangle. Transitivity relies on the formation of subgraphs of three nodes called triplets. This measure is related to clustering coefficient, with values between 0 and 1. Higher values indicate greater likelihood that a node will form a triplet.

- **Characteristic Path Length:** paths are series of edges that connect nodes, but never visit any given node more than once. Characteristic Path Length is calculated as the average shortest path length between every pair of nodes in a network. Short path lengths are indicative of global and local integration. See Figure 2.1.

- **Efficiency:** describes how information flows within a network. This measure is inversely proportional to the characteristic path length of the same network. It may be computed as *global efficiency* for the whole brain, or *local efficiency* for a subnetwork or region of interest.

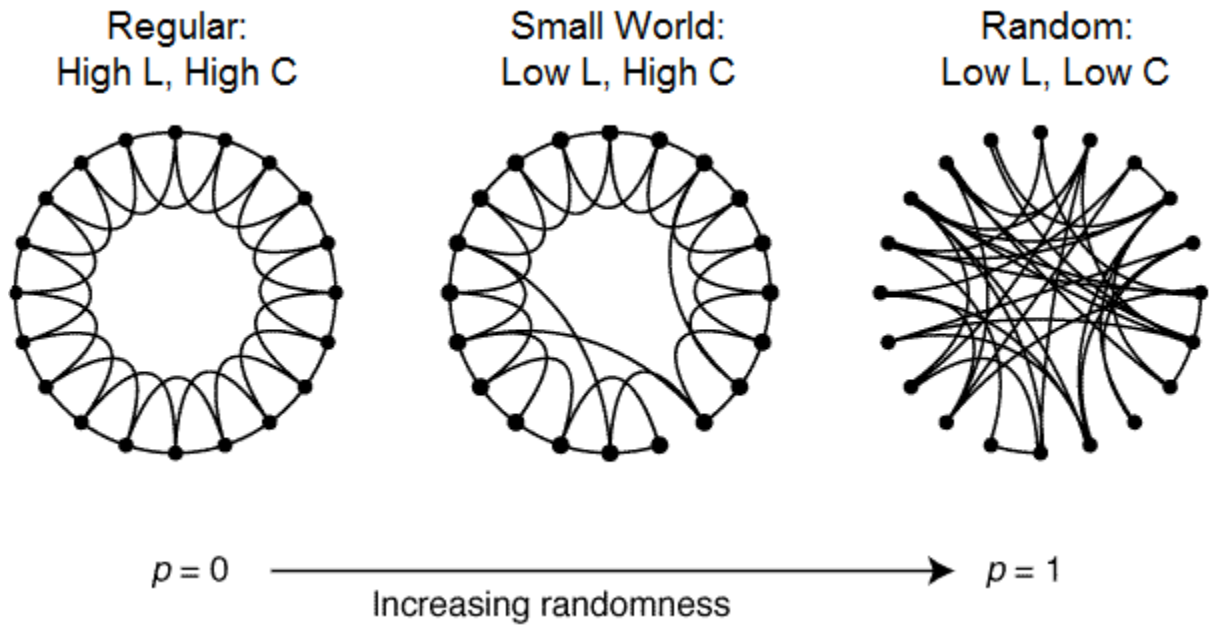

Figure 2.1 Connectome Properties of Neural Networks
Here both local segregation and global integration of small-world networks are facilitated by shorter path lengths (Low L) than regular networks, and higher clustering coefficients (High C) than random networks. Figure reproduced and revised with permissions (Watts and Strogatz, 1998). L = path length, C = clustering coefficient.

2.4 Statement of Purpose

This investigation sought to evaluate the microstructural changes in WM tracts in the sub-acute phase of recovery from a single sports-related concussion in adolescent athletes using DTI. The application of Complex Network Analysis to the study of subnetworks of interest enables the characterization and quantification of structural changes.

2.4.1 Hypothesis

We hypothesize that concussed individuals will show distinct microstructural changes in WM integrity when compared to controls. Specifically, network properties will reflect decreases in global integration and increases in local connectivity in each of the four subnetworks (attention, executive function, DMN, and frontal association areas) in concussed individuals. Based on our previous functional connectivity work, we predict the greatest changes in connectivity profiles will occur in the DMN.

2.5 Methodology

2.5.1 Participants

Twelve adolescent athletes who suffered a recent (within two months) sports-related concussion were recruited from local baseball, ice hockey, and rugby teams in the Greater Vancouver Area. At the time of imaging, all concussed athletes remained symptomatic. An additional ten healthy, physically active age-matched adolescents with no previous history of concussion or head injury were enrolled as controls. Participants were excluded if they had a pre-existing neurological or psychiatric condition. Parents signed an informed consent, and player assent was obtained prior to participation. This study was approved by the Clinical Research Ethics Board at the University of British Columbia.

2.5.2 Magnetic Resonance Imaging Protocol

Whole-brain, high-angular resolution diffusion MR scans were performed on a 3.0 Tesla Philips Achieva whole-body MRI scanner (Philips Healthcare, Andover, MD) at the University of British Columbia Magnetic Resonance Imaging Research Centre. Scans used an eight-channel sensitivity encoding head coil. Participants first underwent a high resolution anatomical scan (repetition time (TR) = 12.4 ms, echo time (TE) = 5.4 ms, flip angle = 8°, field of view (FOV) = 256 mm, 170 slices, 1 mm thickness). Next, two diffusion-weighted scans were performed with a single-shot echo planar imaging sequence (TR = 7465, TE = 75 ms, FOV = 212 x 212 mm, 60 slices, voxel dimension = 2.2 mm^3, scan time = 7 minutes). Diffusion weighting was performed across 60 different non-collinear orientations (b = 700 s/mm^2), with an acquisition of 10

minimally weighted diffusion images (b = 0). The total scanning time for each participant averaged 45 minutes.

2.5.3 Image Pre-Processing

Pre-processing and analysis of diffusion imaging data was conducted using ExploreDTI software version 4.8.4 (Leemans A., 2009) run through Matlab (version 2013b). First, the acquired DICOM files were converted to Neuroimaging Informatics Technology Initiative (NIfTI) format and structurally concatenated into a 4D file. To ensure images were imported correctly, a visual inspection was conducted in which raw images were sequentially run through a viewing window enabling the three orthogonal planes to be examined simultaneously. This allowed for the identification of missing slices, motion artifacts, and image distortions. Images were corrected for eddy-current induced geometric distortions and subject motion using affine registration to the corresponding b0 image (Leemans et al., 2009). A visual examination of the resulting tensor orientations was also conducted. Additional Quality Control measures included individual review of the average residuals per DWI after fitting tensors via the "assess data quality summary' feature in Explore DTI and inspection of outlier profiles. The anterior and posterior corpus callosum were inspected to ensure the corresponding gradient tables were appropriately aligned (i.e. left-to-right crossing fibres appeared red). High anisotropy around the perimeter would indicate misregistration. All files were batch processed to ensure consistent analytic parameters. Lastly, summary measures from quantitative parametric maps (FA, MD, and the number of tracts passing through each region) were extracted for the whole brain and specific regions of interest.

2.5.4 Fibre Tractography

Each participant's DTI was first registered in Standard Space then whole brain tractography was conducted using a deterministic streamline approach as previously described in Leeman et al. (2009). The fractional anisotropy threshold for initiating fibre tracking was set at 0.2 with a tract turning angle threshold of 30 degrees. Tractography delineates the 3D trajectories of white matter fibre tracts, both within and between different brain regions. Next, the Automatic Anatomical Labeling (AAL) Atlas was applied through ExploreDTI. This template delineates 45

different brain regions in each hemisphere (Tzourio-Mazoyer, 2002; Leemans, 2015). Here we focus on evaluating the structural integrity between brain regions directly connected by a fibre bundle. By examining fibre tracts between each pair of atlas regions, 90 x 90 Connectivity Matrices (CM) were generated for each subject. In particular, CMs were constructed which measured mean FA, mean MD, and the number of tracts for bundles between each region pair.

2.5.5 Connectivity Matrices

In the CM, each brain region is representative of one node in the subsequent network analysis (total 90 nodes/participant). Graph Theory metrics were applied to the CM output and thus the structural features of neural networks. Here we applied CNA to characterize network features by the following measures: clustering coefficient, transitivity, global and local efficiency, characteristic path length, density, modularity, mean authority/hub value and assortativity. Network measures were selected from the Brain Connectivity Toolbox and extracted using a custom Matlab script written by Colin J. Brown at Simon Fraser University. Our aim was to understand the way in which nodes were structurally embedded in their local or global networks, and identify whether CNA would be sensitive to characterizing the microstructural changes in regions of vulnerability. An illustration of the pre-processing and imaging pipeline is provided in Figure 2.2.

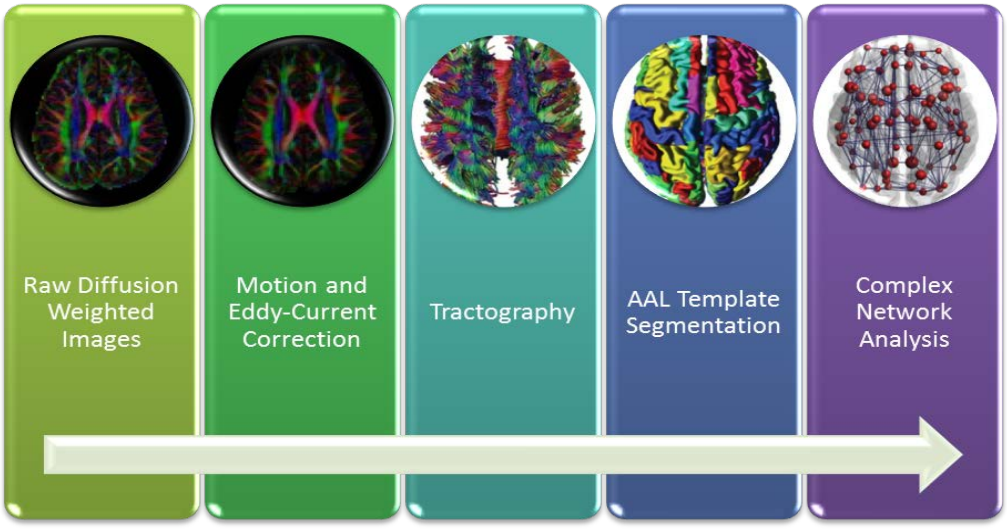

Figure 2.2 ExploreDTI Pre-Processing Pipeline

2.5.6 Subnetwork Analysis

To evaluate both global and local metrics, a whole brain network and four subnetworks (attention, executive function, DMN, and frontal association areas) of interest were established. Subnetworks were extracted individually following AAL template parcellation. Networks were selected a priori based on regions that had previously shown to be vulnerable to injury and areas responsible for cognitive functions commonly known to be impacted by concussions. Published data by Virji-Babul et al. (2013) show functional changes between control and concussed patients in the DMN, anterior commissural pathways, and the genu of the corpus callosum. We sought to evaluate the WM integrity in these same regions by constructing subnetworks of nodes representing the corresponding region in the AAL template (see Appendix B for a summary of each network based on the AAL template). The composite regions are listed below, and both left and right hemispheres were included for each subnetwork:

1. **Attention Networks:** inferior frontal gyrus (opercular, triangular, and orbital parts), anterior cingulate and paracingulate gyri, and the angular gyrus.

2. **Executive Function Network:** superior frontal gyrus (dorsolateral and medial parts).

3. **Default Mode Network:** superior frontal gyrus (medial and medial orbital parts), posterior cingulate gyrus, superior parietal gyrus, angular gyrus, precuneus, and middle temporal gyrus.

4. **Frontal Association Area Network:** superior frontal gyrus (dorsolateral, orbital, medial, and medial orbital parts), middle frontal gyrus (including the orbital part), inferior frontal gyrus (opercular, triangular, and orbital parts).

2.5.7 Statistics

The microstructural integrity of WM tracts was quantified using mean FA and MD values, and the number of tracts at both the global and local network levels. Group averages were obtained for each measure and differences between concussed and control groups examined using an

independent samples t-test (two-tailed significance uncorrected $p < 0.05$). To correct for multiple comparisons, a more conservative threshold ($p < 0.01$) was included. Due to the differing number of nodes, comparisons between different subnetworks could not be made and only group differences within subnetworks evaluated.

2.6 Results

2.6.1 Demographics

A total of twelve concussed athletes completed imaging (mean age 15.5 ± 1.2 years) within two months of their injury (mean days since concussion 35.7 ± 15.0 days). Ten controls completed imaging (mean age 15.7 ± 0.94 years). One control subject was excluded due to excessive head motion. Subject demographics are described in Table 2.1. All participants were right handed.

Table 2.1 Demographics for Adolescent Athletes

Participant ID	Gender	Age	Concussions	Days Post- Concussion
Control Participants				
HC003	M	15		
HC004	M	17		
HC008	M	14		
HC009	F	16		
HC010	M	16		
HC107	M	15		
HC109	M	16		
HC110	M	15		
HC113	M	16	*	
HC406	M	17		
Concussed Participants				
PC001	M	14	1	18
PC002	M	15	3	30
PC004	M	16	2	31
PC007	M	14	4	56
PC011	M	14	1	30
PC108	M	15	1	30
PC316	F	17	3	17
PC411	M	16	3	29
PC501	F	17	3	50
PC610	M	16	1	52
PC614	M	17	2	24
PC617	M	15	2	61

M = Male, F = Female, * = removed from analysis due to excessive head motion

2.6.2 Whole Brain Diffusivity Metrics

The average whole brain values for FA and MD for each group are described by Virji-Babul et al. (2013). Diffusivity metrics were assessed using an independent-samples t-test (two-tailed significance, $p < 0.05$). The concussed participants show significantly increased FA ($p = 0.01$) and decreased MD ($p = 0.04$) compared to controls (Figure 2.3). FA values are indicative of preferential flow of water molecules along fibre tracks, while MD represents the overall amount of diffusion taking place.

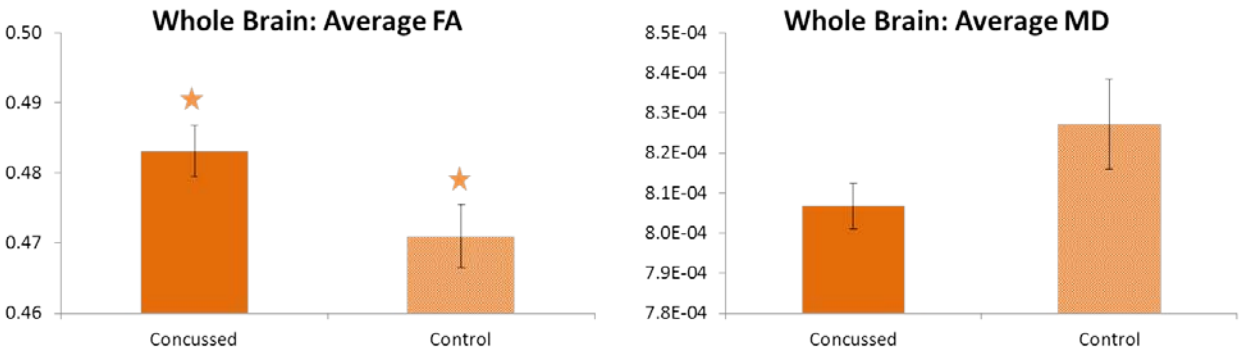

Figure 2.3 Whole Brain Diffusivity Metrics

Concussed participants show persistent increases in FA and decreases in MD metrics up to two months post-injury. Error bars represent the standard error of the mean (SEM). Stars denote significance at $p < 0.01$.

2.6.3 Complex Network Analysis

We subsequently extracted FA, MD, and the number of tracts from our four subnetworks of interest from the ExploreDTI output. We then applied Complex Network Analysis through our customized script from the Brain Connectivity Toolbox in Matlab to whole brain and local regions. Results showing network composition across each diffusivity metric are provided in the following sections.

2.6.3.1 Fractional Anisotropy

No significant differences were found for network measures in the whole brain, attention, executive function, or frontal association subnetworks. However, network organization in the DMN shows distinct alterations following concussion. Using a more conservative threshold, a significant increase in transitivity ($p = 0.009$), and significant decrease in the characteristic path length ($p = 0.006$) were detected. Here a trend towards increases in clustering coefficient ($p = 0.045$), and local efficiency ($p = 0.038$) were shown in the concussed adolescents. These metrics are indicative of increases in local segregation (Figure 2.4).

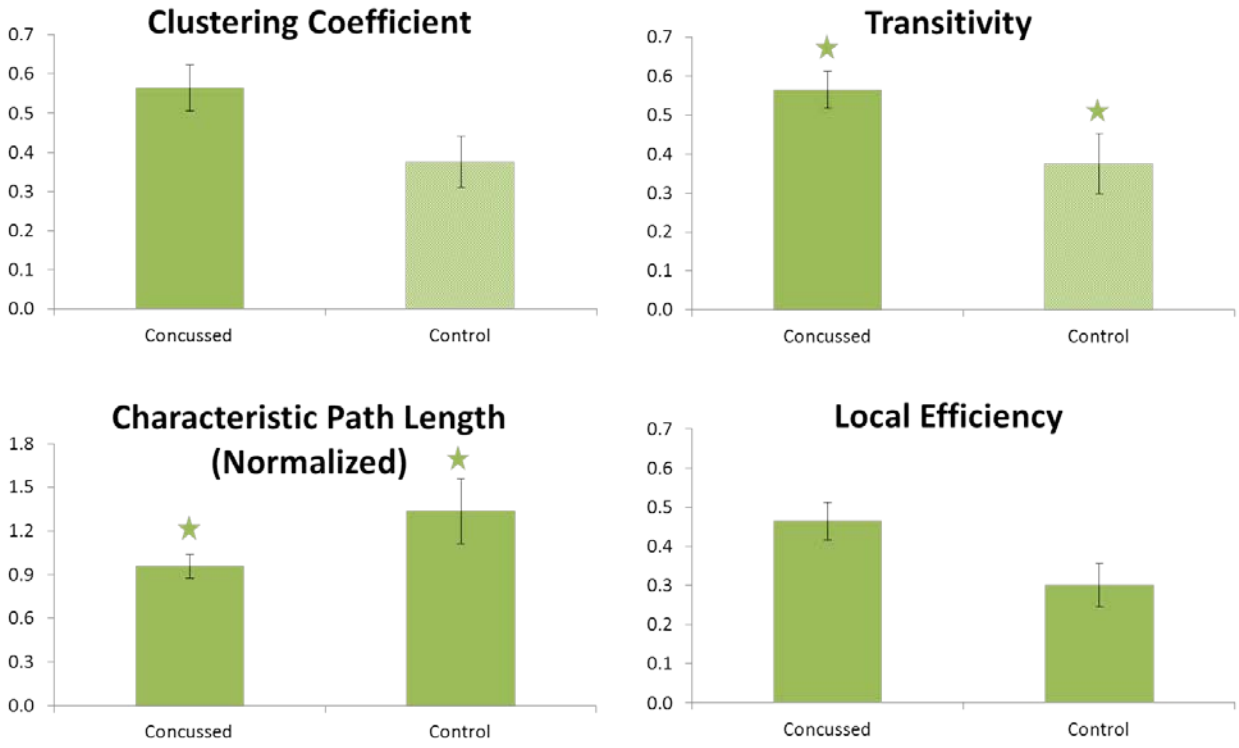

Figure 2.4 Changes in Structural Connectivity within the DMN using FA Values

Group averages reveal increases in metrics pertaining to local community structure and reflect changes in structural connectivity within the DMN of concussed individuals. Error bars represent SEM. Stars denote significance at $p < 0.01$.

2.6.3.2 Mean Diffusivity

There were no significant differences in network properties of the whole brain, executive function, attention or frontal association subnetworks using our conservative threshold ($p < 0.01$) to assess MD values. However, when using a more liberal threshold ($p < 0.05$) the structural properties of the attention subnetwork showed a weak trend towards increased local efficiency ($p = 0.06$), while the executive function network showed a significant decreased path length ($p = 0.03$) for concussed athletes. The greatest structural changes were evident in the DMN and parallel the FA findings. Here a significant increase in transitivity ($p = 0.016$) and decrease in characteristic path length ($p = 0.006$) are evident in athletes post-concussion. Lastly, a liberal trend towards increased local efficiency ($p = 0.06$) and increased clustering coefficient ($p = 0.07$) in the DMN of concussed players was also noted (see Figure 2.5).

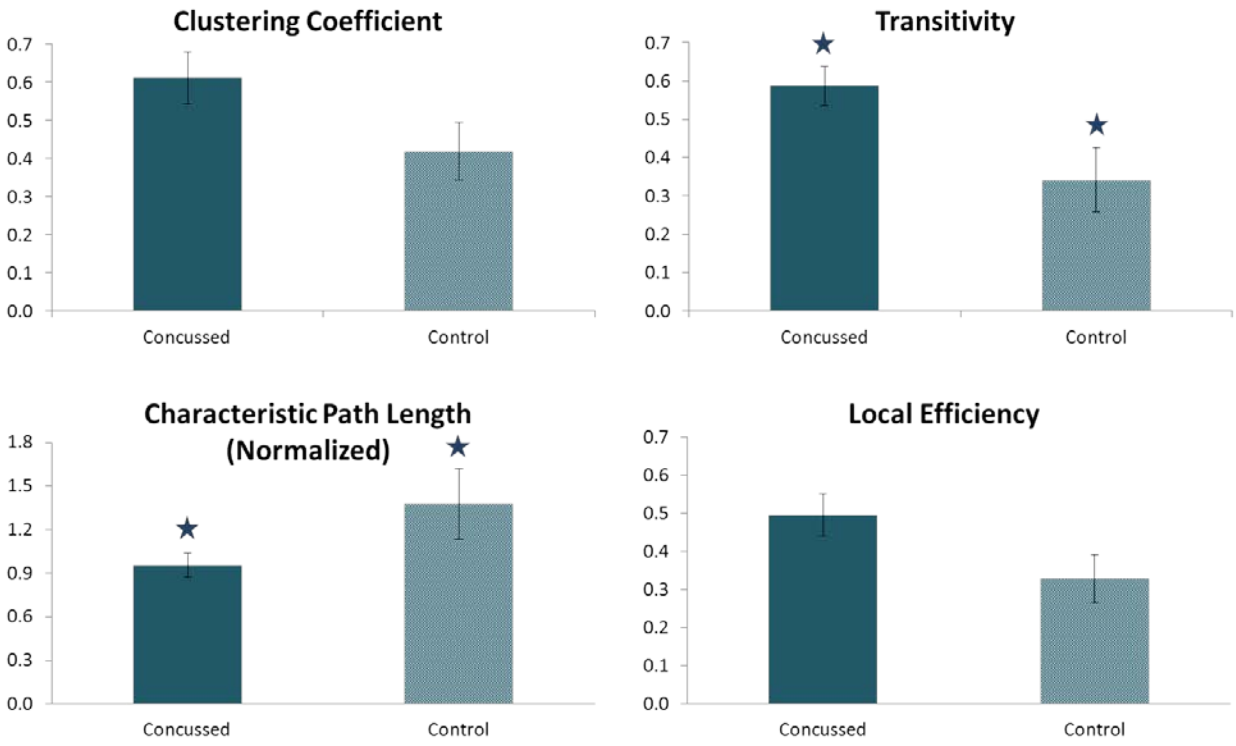

Figure 2.5 Changes in Structural Connectivity within the DMN using MD Values

Connectivity Analysis using MD metrics show a similar pattern of structural change as detected by FA values. Error bars represent SEM. Stars denote significance at $p < 0.01$.

2.6.3.3 Number of Tracts

No significant differences in graph theory measures were found for the whole brain, attention, and frontal association subnetworks. Characteristic path lengths were significantly shorter in the concussed group ($p = 0.007$) in the executive function network, but no other measures reached significance. The greatest structural differences between groups were evident in the DMN. Here concussed athletes showed shorter characteristic path lengths ($p = 0.006$), with trends towards decreased global efficiency ($p = 0.031$), and decreased density ($p = 0.024$) when compared to controls. A liberal trend in mean authority was also evident showing an increase in the concussed athletes ($p = 0.059$). These measures show trends toward decreased global integration, and are summarized in Figure 2.6.

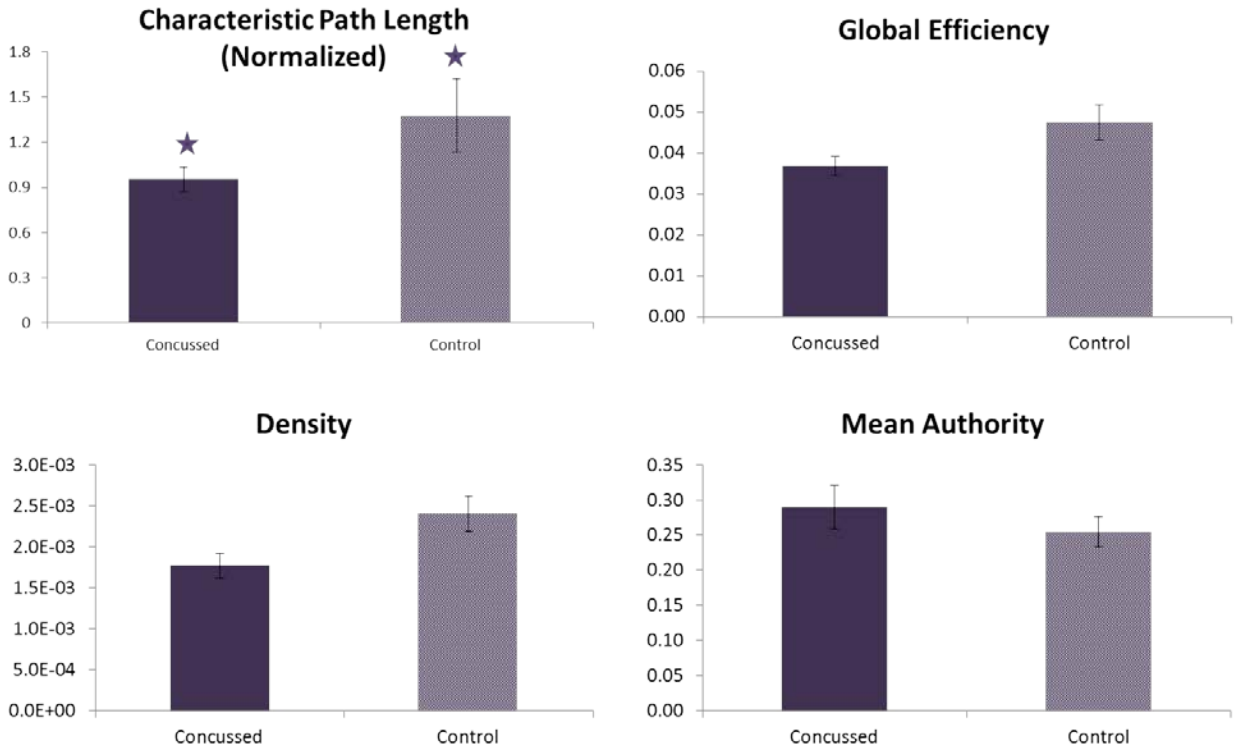

Figure 2.6 Changes in Structural Connectivity within the DMN using the Number of Tracts

Connectivity profiles within the DMN show trends towards decreased global integration across composite nodes. Error bars represent SEM. Stars denote significance at $p < 0.01$.

2.7 Discussion

Whole brain diffusivity metrics reflect WM integrity. As previously discussed, acute changes in diffusivity have been inconsistent in the literature showing both increases and decreases post-mTBI (Henry et al., 2011, Lange et al., 2012, Alhilali et al., 2014, Lange et al., 2015). It has been argued that compromised WM integrity results in decreased FA values and likely shows a corresponding increase in MD. This is common in moderate to severe TBI, whereby decreased FA values are thought to result from pathological disruption to the cytoskeletal organization, axotomy, Wallerian degeneration (axonal degradation and progressive demyelination), as well as neuronal loss (Cubon et al., 2011, Len and Neary, 2011, Ling et al., 2012). Neuronal loss may contribute to decreased FA by facilitating a comparative increase in the interstitial space between cells. Additionally, cytotoxic edema may occur in the acute phase of recovery in moderate to severe TBI. Here decreased FA may result from altered membrane integrity which increases intracellular fluid retention and consequently promotes cellular swelling. However, studies specific to mTBI tend to show the opposite response in diffusivity metrics. A report in young athletes (mean age 22.0 years, SD = 1.7 years) has shown increased FA in both the acute and chronic phases of recovery (6 months) from mTBI (Henry et al., 2011). Our results support this emerging trend toward a global increase in directionality accompanied by a decrease in overall diffusivity in the sub-acute and chronic stages of recovery from mTBI (Ljungqvist et al., 2011, Murugavel et al., 2014). Increased FA values in concussed athletes may reflect an inflammatory response that restricts diffusion or subtle vasogenic (extracellular) edema. Here an increase in extracellular pressure may temporary deform or constrict axonal processes, leading to an increase in the directional follow of water molecules during imaging. Elevated FA values in the chronic phases of recovery may suggest that neuroinflammation persists long after the initial injury. Additionally, regional increases in post-concussive FA values have been reported in the corticospinal tract and corpus callosum (Henry et al., 2011); further suggesting that a compressed intracellular space promotes directionality. Overall, our results support the notion that damage to axonal networks is detectable up to two months after concussive injury; however, the severity of injury and important of time-course cannot be underestimated as FA values are expected to normalize over the course of recovery. The nature of the underlying pathology warrants a more comprehensive evaluation.

To further investigate underlying anatomical changes in subnetworks of regions commonly affected by concussive and subconcussive forces, we applied principles of Graph Theory to our diffusivity metrics. To our knowledge, this was the first study to apply Complex Network Analysis to structurally derived subnetworks of interest in adolescent mTBI. Connectivity analysis using FA revealed significant structural alterations in the DMN of concussed athletes. Here an increase in clustering coefficient, transitivity, and local efficiency was accompanied by a decrease in the characteristic path length of fibre tracts. These results suggest that persistent axonal damage along certain fibre tracts in regions of the DMN may subsequently promote branching and development of new, shorter connections in certain neighbourhoods. New pathways in concentrated areas would explain a decrease in path length with a corresponding increase in local information flow (efficiency), clustering, and ultimately the likelihood of triangular motifs (transitivity). The CNA of MD values mirror that of the aforementioned FA findings. The decrease in overall mean diffusivity may similarly reflect a weakening of WM integrity and structural connections between certain modules, and a concurrent increased reliance on new or undamaged fibre bundles. Together these structural changes in the DMN suggest greater local segregation. However, we are currently limited in our ability to determine whether these changes occur across the entire DMN or only in specific regions.

Next, we applied CNA to the overall number of fibre tracts connecting various regions of interest. This approach revealed that concussed athletes show significantly shorter characteristic path lengths and decreased global efficiency across the DMN. Erosion of a highly organized neural network leads to decreased integration and a simultaneous increase in the likelihood of random connections. We suspect that damage to longer projections, as a result of diffuse axonal injury within the DMN, promotes growth of shorter connections between adjacent regions, increasing the local efficiency but decreasing the overall ease with which information is transferred across the entirety of the network. These results complement the connectivity profiles of our aforementioned diffusivity metrics, and support the notion that longer fibre tracts are most susceptible to injury (Buckner RL, 2008). Similar decreases in global efficiency and weaker

overall integration have been reported in patients with moderate to severe TBI (Caeyenberghs et al., 2012, Caeyenberghs et al., 2014). It remains unclear if such a response reflects a dynamic compensatory mechanism in which rewiring and reorganization of new connections serve to counteract functional deficits.

Characteristic small world networks exhibit dense connectivity within, and few long range projections between, hubs (Watts and Strogatz, 1998). Mounting evidence suggests TBI shifts structural organization away from this highly efficient information processing architecture (Pandit et al., 2013, Sharp et al., 2014). First, fragmented patterns of reduced structural connectivity in the frontal, parieto-premotor, and temporal cortices (fundamental to the DMN) have been reported in adults and children with brain injury (Caeyenberghs et al., 2012). Second, previous Graph Theory Analyses of healthy and pathological brain states have revealed a high concentration of hubs within the DMN and attention networks (Guye et al., 2010). Selective damage has been described in DMN hubs, particularly in the PCC, following moderate to severe TBI (Pandit et al., 2013). These injuries resulted in the reorganization of the spatial distribution of hubs and were accompanied by an increased reliance on certain hubs within the DMN (Pandit et al., 2013, Stam, 2014). This situation increases the risk of 'hub failure'; a collapse within a region of the network that deflates its' ability to efficiently and reliably transfer information. Our results suggest redistribution and reorganization of DMN hubs occurs even in mild TBI. This proposition is further supported by our trend in the increased importance of certain nodes (mean authority) with an overall decreased density evident in the concussed athletes. These results are of particular interest as the DMN requires 60 - 80% of the brain's basal metabolism to maintain resting state function (Raichle and Mintun, 2006, Guye et al., 2010). An increase in localized activity within DMN hubs is inextricably linked to an increase in regional energy demands; which is of paradoxical importance given the network is active predominantly while the brain is 'at rest'(Raichle et al., 2001). This is supported by research employing ^{18}F-Fluorodeoxyglucose PET to evaluate post-injury changes in metabolic activity within the DMN (Kato et al., 2007, Garcia-Panach et al., 2011). These studies further substantiate that dynamic irregularities in patterns of activity correlate with changes in performance on tasks of executive function and attention. Additional exploration is warranted as alterations in regional activity in the resting

state due to underlying structural change may create a period of vulnerability; detract from recovery, repair, or processes such as memory consolidation; and contribute to the post-injury cognitive symptom profile.

Currently, there is emerging evidence that structural disconnection within the DMN may lead to abnormalities in cognitive control and attention deficits (Bonnelle et al., 2011). A correlation between the extent of damage to cingulum bundle fibres, a tract that connects the PCC and ventromedial PFC, and decreased attention span has been shown both at structural and functional levels (Greicius et al., 2009, Bonnelle et al., 2011). This adds to evidence of structural alterations in the DMN manifesting with functional, and in turn, cognitive consequences. Additionally, effective modulation of DMN activity is influenced by the structural integrity of reciprocal network connections with the saliency network (Bonnelle et al., 2012). The extent of WM damage in the saliency network tracts joining the right anterior insula to the dorsal ACC and pre-supplementary motor areas has been shown to predict DMN dysfunction. Ineffective regulation has resulted in cognitive deficits. Collectively, disruption to the WM projection fibres likely explains how seemingly minor ultrastructural damage may have widespread consequence.

While the DMN has been a focus of many structural and functional studies, disruptions outside the DMN may similarly underlie common mTBI symptoms such as distractibility, impaired short term and working memory, and contribute to cognitive fatigue and headache (Kinnunen et al., 2011, Fagerholm et al., 2015). Damage to hubs that join spatially or functionally different networks is clinically significant as it may be the origin of disrupted higher level cognitive functioning that relies on the integration of information. Thus, it is plausible that diffuse axonal injury is the primary mechanism underlying TBI-induced cognitive impairments, driving large-scale network disconnection. An understanding of how information is processed and integrated within hubs between structurally and functionally connected networks, such as those between the DMN and its counterpart the saliency network, will be fundamental to advance our clinical approaches to concussion management strategies and treatment (Sharp et al., 2014).

Exposing the relationship between structure and function is the focus of many multimodal MR sequence studies. Regions strongly connected by WM tracts are more likely to bear similar functional properties. This is certainly true of the DMN, as regions with synchronous baseline activity that correspond to the DMN feature both direct and indirect anatomical connections (Greicius et al., 2003, Greicius et al., 2009). Surprisingly, no significant structural changes were detected in the executive function or attention-based networks in our study. This may be a result of the limited number of nodes included in the analysis or the parcellation mask (AAL template) which may over or underrepresent the regions corresponding to these networks based on the selection of composite nodes. Our future analysis will include a node-by-node evaluation and additional scrutiny by hemisphere which may be more sensitive to the subtle structural changes we believe underlie alterations in functional connectivity and electrical output, as informed by our previous work. Based on the aforementioned principles we have made three predictions: First, we hypothesize that the increase in clustering coefficient in certain DMN neighbourhoods aligns with findings from our functional connectivity study in the same patients in which probabilistic independent component analysis (ICA) of rs-fMRI data showed increased functional connectivity in the PCC (Borich et al., 2015). Borich et al. also report reduced connectivity in the parietal regions and the medial prefrontal areas, which we suspect will correspond to a decrease in clustering coefficient in these regions that would have been overshadowed in our current analysis. Second, we suspect underlying changes are in fact present in the executive function and attention networks based on our previous rs-fMRI data in these same participants. We have previously shown increased functional connectivity in both the executive function (right frontal pole) and ventral attention (left frontal operculum) networks (Borich et al., 2015). Third, we believe independent evaluation of nodes in these regions is likely to reveal structural anomalies in the white matter in adolescents recovering from concussion. We have applied Graph Theory principles to resting state activity in an electroencephalography (EEG) study of adolescents with concussion (Virji-Babul et al., 2014). Here each electrode served as a node. Increased local metrics related to the number of shortest paths between two nodes (betweenness) and the number of connections to a given node (degree) were reported in regions of the DLPFC and right inferior frontal regions.

In conclusion, our findings suggest that CNA is useful in detecting altered topology and neural reorganization following concussion. Here CNA measures showed that disruptions to the structural underpinnings of the DMN of concussed adolescent athletes were easily distinguished from that of normal controls up to two months after the initial injury. These results add to the growing body of knowledge surrounding connectivity profiles and the structural reorganization that takes place following concussive and sub-concussive injury. These changes in structural connectivity may be the foundation of functional disturbances, though the structure-function link between the two is still being elucidated.

2.7.1 Limitations

The application of Graph Theory and CNA to the study of adolescent concussion is subject to inherent limitations in methodology and study population. First, the current script analyzes the nodes of the each subnetwork as one structural identity, and may dilute regional changes that may be occurring in different directions. This is particularly relevant in the DMN given the integration across several distinct brain areas, and our previous findings of regional changes in functional connectivity in opposing directions. This was our first investigation using CNA in DTI and will inform future investigations to identify the direction of change occurring within each composite node. Next, the application of the AAL template to appreciate anatomical connectivity is a widely accepted methodology; however, other parcellation tools and templates are available. Slight differences in thresholding exist between various programs, and may result in the connectivity profiles that vary in both the number and degree of composite nodes, thus influencing network measures. The utility of various parcellation platforms and overall patterns of structural change following TBI will continue to be an area of active research. Additionally, while DTI has advanced our understanding WM integrity, the diffusivity metrics may be influenced by factors such as the extent of myelination, axonal packing density, and neuronal cytoarchitecture (Alexander et al., 2007). Further study is needed to understand the contributions of each factor in influencing the FA and MD output. Lastly, CNA relies heavily on multiple comparisons. To correct for this, we used a more conservative approach ($p < 0.01$); however, we additionally acknowledged findings under a more liberal statistics thresholds common across other connectivity studies. Future endeavours may look for additional statistical approaches to

evaluate structurally significant alterations in WM integrity and connectivity.

Second, despite the limited small sample size, the study of adolescents' reveals that even at a young age athletes may have sustained numerous concussions. The influences of the type of sport that resulted in concussive injury, fluctuations between the time of injury and imaging, and varying number of concussions between participants cannot be overlooked. The representative sports played and number of injuries seen in our study are common across many larger scale studies of sports-related concussion. A recent study of adolescent hockey players found the likelihood of having sustained a previous concussion increased as a function of age (Smith-Forrester, 2015). Here 22% of participants between the ages of 13 - 14 years old reported a history of concussion; this dramatically increased to 42% of participants between the ages 15 - 17 years old. Within these populations, over 10% of athletes had sustained more than one previous concussion. Additionally, there is a discrepancy between behavioural recoveries and resolution of underlying pathophysiological processes which makes it difficult to know whether those who had previously suffered a head injury had fully recovered. Given that concussion is a dynamic injury, having only collected data across a single time point further limits our interpretation. There is no baseline data for each participant, thus we are unable to tell the extent of structural damage and/or recovery. This gives merit to future longitudinal studies that rigorously track adolescent athletes from acute injury (between 24 – 72 hours) through chronic phases of recovery (1, 3, 6, and 12 months post-injury), and that monitor the influences of repetitive concussion and subsequent developmental responses. Lastly, our control group was matched for age, handedness, and athletic ability (team mates of concussed individuals); however, there is no means to account for the influence of injury type (concussion versus non-head injury). Future studies may look at including an additional study group to account for the psychosomatic influence of injury on overall network structure.

2.7.2 Application of Complex Network Analysis to the Study of CTE

CNA may serve as a useful tool in identifying early changes in the structural (re-)organization of WM tracts. CNA enhances our understanding of the dynamic response to injury, beyond what has been previously described by FA and MD metrics. In particular, CNA characterizes the

microstructural correlates of how information is processed within a damaged or recovering system. Changes in characteristic path lengths, and identifying core hubs and 'community structures' provides information on network efficiency and resilience to damage. Head injury provokes a shift away from the optimal neural network architecture; lean wiring that facilitates both local specialization and global integration of information. Correlating CNA metrics with functional connectivity and behavioural outcomes may provide a critical link between structure and function that underlies clinical presentation.

We provide evidence of structural changes in neural networks, specifically the DMN, that persist for up to two months and likely longer, following a single concussive injury. In light of this we suggest the applications of CNA may yield great benefit in characterizing structural changes following repetitive head injury; and in turn advance our understanding of the causal mechanisms linking frequent trauma to conditions such as CTE.

First, we suggest that adolescent athletes at the beginning of their sporting careers serve as valuable study subjects. The opportunity to perform longitudinal studies that track individuals through their first concussion and recovery, as well as after repeated injury will further our understanding of the extent and time course of injury-induced structural changes, offer opportunities to correlate structural changes with behavioural and cognitive recovery, and clarify the roles of age-related plasticity on recovery. Training often begins from a very young age, and while it is known that repetitive injury in early life serves as a risk factor for CTE, the independent contributions of a frequency and severity have yet to be determined. Additionally, training and competition expose players to hundreds and even thousands of subconcussive and concussive injuries (Beckwith et al., 2007, Greenwald et al., 2008) over the course of their careers. CNA may help quantify the cumulative damage, and characterize patterns of change in structural networks prior to the onset of clinical symptoms.

Second, considerable efforts have been made to evaluate post-traumatic WM integrity, as abnormalities are purported to reflect damage to axon bundles and microtubule structures (Buki and Povlishock, 2006, Blennow et al., 2012, McKee et al., 2014, Shin et al., 2014, Chong and

Schwedt, 2015, Stemper et al., 2015). Tau protein serves to stabilize microtubules; however, injury-induced disruption to cytoskeletal structure, such as becoming uncoupled from tubulin, may trigger protein dysfunction, abnormal phosphorylation, and misfolding. Interestingly, hyperphosphorylation of tau provokes prion-like self-assembly. Converging evidence from the study of other tauopathies (frontotemporal lobe dementia and AD) suggest that tau propagation occurs along anatomical connections such as WM fibre tracts. We believe that intraneuronal tau in the form of PHFs and NFTs would disrupt diffusivity metrics, producing noticeable alterations in FA and MD values. We suspect that the applications of CNA to CTE would easily distinguish connectivity profiles between healthy individuals and affected subjects. Knowing that tau deposition is first noted in frontal and temporal cortices of patients, with late stages of disease showing widespread intraneuronal deposition, white-matter imaging may serve a prominent role in tracking pathological progression (Ahmed et al., 2014, Boluda et al., 2015). Future longitudinal studies will be necessary to look at whether changes in network properties may be predictive of, or associated with, future regions of tau accumulation.

Lastly, DTI is more cost-effective and accessible means of detecting pathological CTE processes than PET-based tau-imaging. CNA offers an unparalleled framework to amalgamate anatomical and functional connectivity-based MRI data, providing a more comprehensive clinical picture. Collectively, early detection and monitoring of structural changes may help identify individuals that are pre-disposed, or at an increased risk of subsequent (earlier onset) neurodegenerative diseases and may one day serve as a diagnostic aid (Guye et al., 2010).

Chapter 3: Tau Imaging with ^{11}C-PBB3 in Healthy Controls

3.1 Introduction to Positron Emission Tomography

Positron Emission Tomography (PET) permits high resolution functional imaging of biological processes at tissue and cellular levels by utilizing a scanner capable of detecting traces of radiation (Phelps et al., 1975). Since the technology was first established in the 1950s the long-standing applications of PET to the study of brain function in health and disease have improved diagnostics and broadened our understanding of both disease mechanisms and progression (Ravina et al., 2005, Nandhagopal et al., 2008, Mitsis et al., 2014, Stoessl, 2014, Blennow et al., 2015). While the process has been refined and the resolution improved over generations, a summary of current details surrounding the radiotracer production and delivery, the scanner, and image reconstruction, especially those most pertinent to PET at UBC, are described below.

Tracer: PET imaging requires an exogenous tracer; a radioisotope linked to a biologically relevant carrier molecule that will bind to a target of interest. For our purposes, the tracer will bind to hyperphosphorylated tau protein. Commonly utilized positron-emitting isotopes include ^{11}C ($t_{1/2}$= 20.3 minutes) and ^{18}F ($t_{1/2}$ = 109.7 minutes). The production of these unstable isotopes relies on a cyclotron for particle acceleration. Due to the short half-lives of the aforementioned particles the imaging centre must be in close proximity to a cyclotron; as is the case between the Nuclear Medicine Department at the UBC Hospital and TRIUMF. Here an underground delivery system facilitates transportation between the two locations in under two minutes. Upon delivery, the tracer is injected through an intravenous bolus and circulates in the bloodstream. The level of radioactivity in brain tissue is monitored as the isotope decays throughout the scan.

Scanner: The crux of PET resides in coincidence detection. As the radiolabeled isotope decays a β+ particle (a positron) is ejected, and upon losing its kinetic energy interacts with an electron. This results in the complete annihilation of both particles and produces two gamma rays (photons). Linear Conservation of Momentum implies that the emitted photons will each have an energy level of 511keV and travel in equal but opposite directions. When gamma photons from

β+ nuclear decay processes occur within the scanner's field of view, the coincident arrival of two photons separated by nearly 180° is recorded and stored by the scanner.

A PET scanner superficially resembles a CT scanner in that a patient is supine on a gurney and positioned in the gantry by an imaging technician. Behind the plastic exterior, imaging is enabled when the patient's head is placed inside the cylindrical configuration of numerous detector rings comprised of eight flat panels, each housing 117 block detectors (936 detectors total). The detector block is made of LSO/LYSO crystals which act as a scintillator (de Jong et al., 2007). Scintillators convert the energy of the emitted photons into visible light. Additionally, each block of crystals is coupled to photomultiplier tubes that detect the intensity of light and in turn calculate the location in which the photon entered the detector. A temporal window of 10 – 15 nanoseconds is used to establish the arrival of photon pairs; events registered outside this window are ignored. By following the line between the two activated detectors (the line of response, LOR), the origin of the emission may be determined. The configuration of detector rings enables detailed 3D mapping of these decay events; however, the increased sensitivity to detect events across different detector rings results in some degradation of resolution. Data acquired throughout the scan are exported to external hard drives and subsequently used to reconstruct the images for analysis.

Image Reconstruction: The information collected by the ring receivers (the coordinates of the two detectors indicating the LOR for each event) is assembled into a sinogram; a two-dimensional histogram of the LOR coordinates in a particular plane. The overall number of sinograms depends on the acquisition mode of the scanner (2D or 3D); however, the resulting sinograms are trimmed into matrices of 128 angular x 96 radial elements. 2D acquisition results in decreased sensitivity as only LORs from nearby rings are considered while oblique LORs are rejected. 3D acquisition takes into account all events but significantly increases reconstruction times. A further distinction in image reconstruction depends on whether scans were conducted as static or dynamic. Static scans synthesize all sinograms into a single frame that runs the full duration of data acquisition. Alternatively, dynamic scanning uses multiple frames of varying lengths to allow for the analysis of tracer kinetics. For our phenyl/pyridinylbutadienyl-

benzothiazole/benzothiazolium compound (^{11}C-PBB3) PET scans, dynamic imaging with 17 frames was used. Lastly, irrespective of acquisition mode, co-registration of PET data with anatomical (T1) MRI improves spatial accuracy for interpretation. Once reconstructed by computer analysis, images show the tissues in which the tracer has become concentrated using a colour-coded 'heat map' on a voxel-by-voxel basis.

3.2 Applications of PET Imaging to Neurotrauma

The application and utility of PET imaging to brain injury relies heavily on tracer selection. In the past, PET studies have looked at changes in cerebral blood flow and glucose metabolism in TBI using ^{15}O-H_2O and ^{18}F-Fluorodeoxyglucose (^{18}F-FDG), respectively, whereas more recent efforts have concentrated on tracers targeting specific proteins of interest such as Aβ and tau. The contributions of each to the study of neurotrauma are discussed below.

Initial ^{18}F-FDG PET studies of TBI date back to the late 1980s (Humayun et al., 1989). While investigations of glucose uptake and metabolism have varied in their post-injury time-course and discussions over global versus local changes have waged on, the trend toward decreased tracer uptake (hypometabolism) in populations of athletes and war veterans with repetitive concussive and subconcussive injury compared to healthy controls is evident (Peskind et al., 2011, Nariai et al., 2013). Interestingly, an ^{18}F-FDG study of 105 patients evaluating neurotrauma-induced changes in metabolism suggested the vermis/cerebellum ratio may be a predictor of future recovery (Lupi et al., 2014). The authors reported hypermetabolism of the vermis (ratio >1) correlated with scores on the Disability Rating Scale and inverse associations were noted with initial Glasgow Outcome Scores and Levels of Cognitive Function over the first year of recovery. While the heterogeneity of TBI populations complicate cross-study comparisons, a distinct pattern of hypometabolism in the frontal regions, PCC, and cerebellum was reported in study of 19 boxers suspected of CTE (Provenzano et al., 2010). The diagnostic utility of ^{18}F-FDG PET in TBI remains controversial; however, it has proven a valuable tool for detecting pathological processes that may contribute to the overall clinical picture (Byrnes et al., 2013).

Further advances in neuroimaging targeting the pathophysiological mechanisms of head injury are helping to define the relationship between trauma and neurodegeneration (Sundman et al., 2014). The development of tracers for amyloid imaging has contributed to our understanding of the long term sequelae. A study employing both ^{18}F-FDG and Pittsburg Compound B (PiB) PET looked at the influence of prior head injury on amyloid deposition in cognitively normal participants and those with a history of Mild Cognitive Impairment (MCI) (Mielke et al., 2014). PiB revealed that a history of TBI was associated with an 18% higher deposition of amyloid in individual's with MCI. Interestingly, no associations between prior head injury and ^{18}F-FDG were reported in either the normal or MCI group. While increases in post-traumatic PiB uptake have been replicated, a definitive link to subsequent decline in cognitive or motor function has not been clearly established (Hong et al., 2014, Malkki, 2014). To date, no neuroimaging studies have used PiB to investigate CTE.

Most recently tau imaging has become a focal point in the study of head injury and CTE. As a new field of exploration, case studies using various tau-specific ligands have been published though further validation by the scientific community is needed. For example, a study of five retired NFL players using ^{18}F-FDDNP revealed increased tracer accumulation in subcortical regions and the amygdala compared to controls (Small et al., 2013). Similarly, a case study of a retired athlete with suspected CTE employed ^{18}F-Florbetapir (for amyloid imaging) and a novel tau tracer, ^{18}F-T807. ^{18}F-Florbetapir imaging was negative, thereby excluding a diagnosis of AD, while ^{18}F-T807 tracer concentrated in striatal and nigral regions, consistent with the presentation of an underlying tauopathy (Mitsis et al., 2014). While these studies are hindered by small sample sizes, a distinct lack of longitudinal follow-up, and no autopsy to provide a definitive CTE diagnosis, they suggest that tau imaging may be useful in improving in vivo diagnostic capacities and serve as objective biomarkers for treatment efficacy and/or monitoring of the associated progressive neuropathology (Sundman et al., 2014). Undoubtedly, addressing these shortcomings will be areas of active and future study. A summary of the recently developed tau tracers is provided in the next section.

3.3 Review of Tau Tracers

The recent interest in tau imaging has resulted in numerous ligands with varying degrees of utility. In creating a new tau ligand, scientists seek an agent with high binding selectivity and specificity for the intended target, desirable pharmacokinetic properties such as rapid uptake (permeability to the BBB) and clearance, high specific activity, and minimal radiolabeled metabolites which complicate the interpretation of reconstructed images. A comprehensive review article summarizes additional barriers unique to tau tracer production including the necessity to bind the six isoforms irrespective of post-translational modifications, the need to cross the extra membrane to label intraneuronal deposits, and properties that enable detection of tau aggregates in white matter (Shah and Catafau, 2014).

To date, the greatest shortcoming is concurrent binding of Aβ; however, current efforts are committed to improving the specificity for aberrant tau protein. In light of these challenges, rapid progress in tracer development may be attributed to advances in tangential technologies that facilitate large-scale screening of molecular precursors as well as iterative learning for refinement of structural modifications. The application of liquid chromatography coupled to mass spectrometry to aid radiotracer identification and performance enhancement is one such instance (Barth and Need, 2014).

^{18}F-FDDNP was the first tracer described to knowingly bind tau. This tracer predominates in the Alzheimer's-related literature as it binds to the secondary structures (β-pleated sheets) strongly associated with amyloid deposition (Shoghi-Jadid et al., 2002, Shin et al., 2011, Small et al., 2012); however, it's utility in binding tau aggregates in non-AD tauopathies such as Progressive Supranuclear Palsy (PSP) has been demonstrated (Kepe et al., 2013). A recent study of 14 National Football League (NFL) players with a suspected CTE diagnosis revealed ^{18}F-FDDNP uptake in brainstem white matter and subcortical regions in a pattern consistent with models of repetitive concussion (Barrio et al., 2015). This likely reflects the compounded and cumulative damage to white matter tracts. Though minimal, the non-specific binding of concurrent α-synuclein and Aβ must be acknowledged (Collins-Praino et al., 2014). The study of CTE would benefit from a more selective tracer.

A series of arylquinoline tracers have been introduced beginning with ^{18}F-6-(2-fluoroethoxy)-2-(4-aminophenyl)-quinolone (^{18}F-THK5223) (Fodero-Tavoletti et al., 2011, Villemagne et al., 2014), and following compound optimization, it's higher affinity derivatives ^{18}F-THK5105 and ^{18}F-THK5117 (Harada et al., 2013, Okamura et al., 2013, Okamura et al., 2014). When tested in non-AD tauopathies ^{18}F-THK5223 failed to label tau aggregates and lesions (Fodero-Tavoletti et al., 2014), thereby eliminating it's utility in the study of CTE and questioning that of it's successors.

Another series of tracers called ^{18}F-T807 and ^{18}F-T808 have entered clinical trials, demonstrating 27 times greater affinity for p-tau than amyloid plaques and low retention in white matter (Chien et al., 2013, Mitsis et al., 2014), though studies have not yet been published in non-AD populations.

To date, only one ^{11}C-tracer has entered clinical trials (Maruyama et al., 2013, Wood, 2013); while several others such as ^{11}C-N-methyl lansoprazole are in the pre-clinical trials pipeline (Shao et al., 2012, Tago et al., 2014). Pre-clinical trials with ^{11}C-PBB3 show promise in binding p-tau in non-AD tauopathies such as corticobasal degeneration (CBD), suggesting the ability to detect various protein isoforms. It remains to be seen which of the aforementioned tracers will predominate in the tau literature. A summary of the tracer properties, as well as the most prominent advantages and limitations of the contending tau ligands, are provided in Table 3.1.

Table 3.1 Summary of Newly Developed Tau Radioligands

Tracer	Properties	Advantages	Limitations
^{18}F-FDDNP Small et al. (2012) Kepe et al. (2013)	• 320 MBq (8.4 mCi) • 120 min scan	• **First ^{18}F-labeled tracer aimed at tau imaging** • Well characterized in AD, MCI and now mTBI • FDDNP-PET binding differentiates diagnostic groups better than metabolism on FDG-PET or volume on MRI • High midbrain and subthalamic binding was distinctive for PSP patients compared to PD and controls	• Concurrent binding to Aβ and α-synuclein
^{18}F-T807 Chien et al. (2013) Mitsis et al. (2014)	• 370 MBq (10 mCi) • 100 min scan • K_d = 14.6	• **25x more selective for tau than Aβ** • Favourable kinetics in brain uptake, clearance from WM • Low non-specific binding in WM and cortical gray matter in controls • MCI and AD patients show retention consistent with Braak staging • Case Report: nigral and striatal retention in retired NFL player revealed subcortical tauopathy: identified as a novel form of CTE	• Limited data on suitability in non-AD tauopathies • May bind non-tau TDP-43 and C9orf72 expansions
^{18}F-T808 Chien et al. (2013) Mitsis et al. (2014)	• 370MBq (10 mCi) • 100 min scan • K_d = 22	• **27x more selective for tau than Aβ** • Faster kinetics and washout than T807, rapid distribution suggests possible imaging as early as 30 min after injection • Good signal-to-noise ratio, rapid clearance from cerebellum, minimal non-specific binding • Binding correlated with dementia severity and distribution follows Braak staging • Immunostaining (with AT 100 Ab) of post-mortem AD sections show the frontal, temporal and parietal lobes and the hippocampus agreed with the regions lit up by the PET ligand	• Intense bone uptake in the skull due to defluorination • High binding in the striatum, a region without tau deposits in AD
^{18}F-THK523 Villemagne et al. (2014) Fodero-Tavoletti et al. (2014)	• 1st gen. arylquinoline • 200 MBq (5.4 mCi) • 90 min scan • K_{d1}= 2.0, K_{d2}= 50.7	• **15x more selective for tau than Aβ** • Half-life = 110 min, does not require onsite cyclotron, offering wider distribution (true of all ^{18}F-labeled tracers) • Radioactivity peaked 3 - 6 min post-injection with rapid clearance • Selectively binds to PHF tau in AD, patients retained 40% more THK523 than semantic dementia and controls • Retention follows Braak staging and hippocampal retention correlates with cognitive parameters	• High non-specific retention in WM may obscure cortical uptake and precludes simple visual inspection of images • Failure to label tau lesions in non-AD tauopathies or to α-synuclein in PD brains

Tracer	Properties	Advantages	Limitations
^{18}F-THK5105 Okamura et al. (2014)	• 2nd gen. arylquinoline • Enantiomer of THK5107 • K_{d1}=1.45, K_{d2}=7.40	• **25x more selective for tau than Aβ** in vitro (high affinity and selectivity for recombinant tau) • Tracer binds to corticobasal lesions • Significantly higher retention in the parietal, posterior cingulate, frontal and mesial temporal cortices of AD • Retention correlated with cognitive parameters	• Insensitive to Pick bodies and the tangles in PSP
^{18}F-THK5117 Okamura et al. (2014) Harada et al. (2014)	• 2nd gen. arylquinoline • Enantiomer of THK5015 • K_d= 10.5	• **Faster kinetics and higher signal-to-background ratio than ^{18}F-THK5105** • Labels certain forms of tau in non-AD tauopathies (sections including 3 and 4 repeat tau lesions) • In CBD sections, THK5117 intensely labeled argyrophilic threads and coiled bodies containing 4 repeat tau • Retention follows Braak staging and hippocampal retention correlates with cognitive parameters	• Insensitive to Pick bodies and tau tangles in PSP • Failed to label inclusion bodies in FTLD, senile plaques, Lewy bodies, and TDP-43 deposits.
^{11}C-PBB3 Maruyama et al. (2013) Wood (2013)	• Benzothiazole derivative • 370 MBq (10 mCi) • 70 min scan • K_{d1}= 2.5 • K_{d2}= 100	• **40-50x more selective for tau than Aβ** • Retention correlates with clinical symptoms • Rapidly uptake, unbound tracer promptly washed out • Label tau-containing lesions in non-AD tauopathies, suggests ability to recognize multiple isoforms • Limited WM background signal and minimal Aβ detection compared to ^{11}C-PiB • Retention follows Braak staging and hippocampal retention correlates with cognitive parameters	• Photo-isomerization caused by ultraviolet light (10 - 380nm) • 11C half-life is 20 min, requiring on site cyclotron • Tracer metabolite crosses BBB and may also bind tau
Tau Tracers in Pre-Clinical Trials			
^{11}C-N-Methyl Lansoprazole Shao et al. (2012)	• ^{11}C-labeled version of lansoprazole	• Exceptionally high affinity for tau in rodent and primate microPET • Autoradiography conducted in post-mortem PSP tissue	• No human data have been published yet
^{11}C-THK-951 Tago et al. (2014)	• Hydroxylated 2-arylquinoline derivative	• High binding affinity for tau pathology (NFTs) in an AD brain section and K18Δ280K fibrils (K_i = 20.7 nM) • Excellent kinetics in normal mouse brain	• No human data have been published yet

3.4 Selection of ^{11}C-PBB3

Following comprehensive evaluation of the utility of recently described tau ligands we have pursued imaging with the novel ^{11}C-PBB3 for its selectivity, preferable dosimetry, and capacity to perform multi-tracer studies (Hashimoto et al., 2014). First, the ^{11}C-PBB3 tracer exhibits low non-specific binding to white matter whilst selectively binding abnormally phosphorylated tau independent of Aβ deposition. ^{11}C-PBB3 demonstrates a 40 - 50 times greater selectivity for tau than Aβ, and importantly binds to areas of pathology in non-AD related tauopathies including PSP and CBD. Next, ^{11}C-PBB3 has been synthesized with high radiochemical purity and specific activity, and sufficient brain uptake has been demonstrated (approximately 2% of the injected dose at 1 minute). Most notably, in vivo characteristics allow for a reference tissue input function thereby avoiding the cumbersome requirement for an arterial line and metabolite determination.

Furthermore, the compound has undergone rigorous pre-clinical evaluation and it's safety demonstrated in human subjects by the research team at the National Institute for Radiological Science (NIRS) in Chiba, Japan (Maruyama et al., 2013). At the time of publication, no known side effects for ^{11}C-PBB3 exposure have been documented. In following the Canadian Nuclear Safety Commission guidelines for research involving radiation exposure, the recommended maximum exposure limit for participants is 50 millisieverts (mSv) per year or 100 mSv over five years. The PPRC adheres to more conservative guidelines in which critical organ (gonads, blood forming organs, and lens of the eye) limits of 30 mSv per study are imposed. All tracer doses were well within these guidelines and a breakdown of the relevant organ doses based on a maximum 20 mCi injection are provided in Table 3.2.

Table 3.2 Maximum ^{11}C-PBB3 Radiation Exposure Doses by Organ for 20 mCi Injection

Organ	Dose (mSv)
Kidney	15.02
Ovary	1.6
Testes	0.74
Red Marrow	2.7
Lungs	25.1*
*Indicates the critical organ for this tracer (Maruyama et al., 2013, Hashimoto et al., 2014).	

Lastly, the PPRC is among the first research groups worldwide with access to this tracer. The accessibility of TRIUMF and an on-site cyclotron ensures that the PPRC is well poised to capitalize on the ^{11}C-isotopes capacity for multi-tracer studies as a result of the short half-life ($t_{1/2}$ = 20 minutes). Collectively, these characteristics suggest ^{11}C-PBB3 has the most favourable characteristics of currently available tau tracers and is thus desirable for pursuing tau-based imaging in head injury, CTE, and other related tauopathies. Our early access to this tracer is instrumental in performing these studies.

3.5 Statement of Purpose

The overarching purpose of this study was to assess the potential utility of a new radioligand, ^{11}C-PBB3, as an in vivo marker of abnormally phosphorylated tau deposition. The significance of this tracer is multifactorial as it holds promise both in the study of trauma-induced degeneration and disease progression, and also advances the PPRC's objectives to better understand the potential basis for cognitive impairment prevalent in atypical Parkinsonism (PSP, MSA, and CBD). We investigated the presence and extent of tau deposition across a range of healthy, elderly individuals to test tracer validity. Establishing baseline values in healthy aging provides the foundation for future studies to assess the interplay between tau deposition, neuroinflammation, and dopamine denervation. This work is widely applicable to the study of many neurodegenerative tauopathies.

3.5.1 Hypothesis

We hypothesize that in healthy, elderly individuals there will be no substantial deposition of abnormally phosphorylated tau, and thus minimal to no uptake and retention of the ^{11}C-PBB3 tracer in brain tissue.

3.6 Methodology

3.6.1 Study Design

The UBC Clinical Research Ethics Board approved the investigation and issued the Certificate of Approval under the "Tau Imaging with PBB3 in Healthy Controls" (H14-02375) protocol. Participants were invited to complete one ^{11}C-PBB3 PET scan and one anatomical MRI. All

participants completed examinations of mood (BECK Depression Inventory, BDI), cognitive function (Montreal Cognitive Assessment, MoCA), and motor function (the Movement Disorder Society-Sponsored Revision of the Unified Parkinson's Disease Rating Scale, MDS-UPDRS III), on their first study visit. Subjects whose scores were indicative of active depression or mild cognitive impairment were excluded from the study.

3.6.2 Study Subjects

Healthy control subjects (males between the ages of 19 – 85 years old, and females between ages 30 – 85 years old) were recruited through advertisements in the Metro News in Vancouver, BC. Additional recruitment strategies included approaching healthy spouses of patients attending the Movement Disorders Clinic at the PPRC and healthy individuals who had previously taken part in PET-based imaging studies with the research group. Informed consent was obtained for each participant prior to all study procedures and re-obtained before the PET scan. Subjects were excluded if they met any of the following criteria:

1. Outside the desired age bracket;
2. Have a personal history or presence of a neurological or psychiatric condition;
3. Have a family history (first degree blood relative) with a movement disorder or dementia;
4. Have a history of head injury, including a concussion with or without loss of consciousness, or stroke;
5. Have a history of major episodes of drug or alcohol abuse;
6. Female participants that may be pregnant or breastfeeding;
7. Have a body mass index greater than 35;
8. Have a history of radiation therapy treatment;
9. Have recurring metastasis;
10. Meet exclusion criteria for MRI Scanning:
    a. Subjects who have been/are metal workers or machinists;
    b. Subjects who have had an injury where a piece of metal lodged in their eye;
    c. Subjects who have pierced body parts (other than earrings) or recent tattoos;
    d. Subjects who have had an injection into any joint in the previous 4 weeks.

Additionally, there could be no instance of any of the following present in the subject's body:

1. Cardiac pacemakers, wires, or defibrillator;
2. Artificial heart valve;
3. Brain aneurysm clip;
4. Electrical stimulator for nerves or bones;
5. Deep brain stimulator;
6. Implanted drug infusion pump;
7. Coil, catheter, or filter in any blood vessel;
8. Orthopedic hardware (artificial joint, plate, screws);
9. Harrington rod for scoliosis;
10. Other metallic prosthesis;
11. Shrapnel, bullets, or other metal fragments;
12. Dentures, braces, or retainer.

The MR technician reviewed each patient’s record prior to scanning, and surgical reports were acquired as necessary.

3.6.3 PET Image Acquisition

PET tracer production, image acquisition procedure, and analytic techniques were established by our collaborators at the NIRS in Chiba, Japan (Maruyama et al., 2013), and modified by the chemists and technicians at TRIUMF in Vancouver, BC. PET imaging was conducted in the Nuclear Medicine Department at the UBC Hospital on the Siemens High Resolution Research Tomograph (HRRT). The HRRT captures 207 planes with a plane thickness of 1.21875 mm. Data were acquired over 17 frames obtained over 70 minutes. Scan lengths (in seconds) for the 17 frames were: 20, 20, 20, 40, 40, 40, 60, 180, 180, 360, 360, 360, 360, 360, 600, 600, and 600. In preparation for scanning, participants were positioned using external lasers such that the inferior orbital-external metal line was parallel to the scanner gantry, following a well-established protocol. A thermoplastic mask was molded to each individual and attached to the headrest of the scanner to reduce head movement. A motion detector was also positioned on a thin cap to monitor and later correct for changes in the position of the subject's head during the

scan. Prior to tracer injection, a 6 - 10 minute transmission scan was performed for attenuation correction using ^{137}Cs rods. Following the pre-scan, the ^{11}C-PBB3 tracer was administered through intravenous bolus and the emission data collection process initiated. Approximately 740 MBq (20 mCi) of tracer with a maximum effective dose of 5.4 mSv was administered per scan. Due to the photosensitivity of the tracer, each scan was performed under low lighting conditions with special amber syringes and tubing for transport and injection.

3.6.4 PET Image Analysis

^{11}C-PBB3 data were analyzed using standardized uptake value ratios (SUVRs) with the cerebellum as the reference region (Maruyama et al., 2013). As this is a novel tracer, more sophisticated analysis will be adopted as the research supporting these methodologies becomes available.

For image reconstruction, the participant's MRI files were first converted to Neuroimaging Informatics Technology Initiative (NIfTI). The patient's T1 image was resized to the PET scan pixel sizes (1.21875 for x, y, and z) in MedX to improve co-registration to PET. Frame-to-frame realigned HRRT PET images were converted to NIfTI, and a mean image created from the dynamic images across the 70 minutes (frames 0 – 17). The MRI was reoriented along the Anterior Commissure to Posterior Commissure line, and subsequently co-registered to the PET images. The T1 MRI image was then segmented to calculate the inverse transform from MNI space back to the patient's own MRI space. The inverse transform was applied to the atlas based regions of interest (ROIs), using the normalize function in SPM. PET images were smoothed by 3 mm to reduce noise. Next, a mean image was created from the last 40 minutes of dynamic PET imaging and the average value of the last half hour of tracer uptake in the cerebellum extracted independently. Every pixel of the image was divided by the cerebellar average to establish a SUVR image. The average of each ROI region was calculated against the SUVR image using the MarsBar tool in SPM, and subsequently written to a text file. These are the final SUVR values used for each patient.

3.6.5 Clinical Measures of Motor and Non-Motor Function

To ensure a subject met all designated inclusion criteria, and as the current protocol is intended for a future comparison to individuals with atypical Parkinsonism, standard evaluations of mood (BDI), cognition (MoCA), and motor function (MDS-UPDRS III) were performed. Examples of each clinical measure of motor and non-motor function are provided in Appendices C - E.

3.6.6 MR Imaging

Participants completed a 7 minute 59 second anatomical T1-weighted MR scans, and a 6 minute 34 second resting state functional MRI (rs-fMRI) scan at the UBC MRI Research Centre. All scans were performed on a Philips Achieva 3.0 Tesla scanner. An MR technician reviewed the MRI Screening Form with each participant prior to participation. T1 images were necessary for PET re-alignment, whereas rs-fMRI data are not included in this thesis but may be used in future analysis by the research team at the PPRC.

3.7 Results

3.7.1 Subject Demographics and Clinical Assessments

A total of eight participants between the ages of 45 to 76 years old (five females, three males) completed tau imaging. At the time of manuscript preparation, seven had completed the associated MRI scans; however, one was incomplete due to the participant's feeling of anxiety in the scanner. Demographics and individual scores for the clinical assessments of mood, cognition, and motor function are provided in Table 3.3. Depression scores were low (4.3 ± 5.1), with the exception of one individual who scored in the mild range (14). All participants scored within the normal range (26 or greater) on cognitive testing (average = 27.9 ± 1.0). While all but one participant had non-zero MDS-UPDRS III motor scores (average 4.8 ± 3.6), this is within acceptable limits and expected with normal aging. Additionally, one participant reported mild arthritis that increased motor scores.

Table 3.3 Demographics and Clinical Assessments for Healthy Controls

PET Scan Number	Age at PET	Gender	Clinical Assessments						
			BDI	MoCA	MDS - UPDRS III				
					Total	Right	Left	Common	H&Y
H1042	45	M	0	29	10	4	3	3	0
H1035	55	M	14	26	3	2	1	0	0
H1034	59	F	4	28	5	2	3	0	0
H1069	66	F	9	27	7	2	3	2	0
H1038	67	F	6	28	2	0	2	0	0
H1040	68	F	0	29	0	0	0	0	0
H1074	72	M	0	28	2	2	0	0	0
H1036	76	F	1	28	9	2	5	2	0

F = Female; M = Male; BDI = Beck Inventory Depression; MoCA = Montreal Cognitive Assessment; H&Y = Hoehn & Yahr Rating Scale; MDS - UPDRS III = Movement Disorder Society - Unified Parkinson's Disease Rating Scale

3.7.2 ^{11}C-PBB3 Image Analysis in Healthy Controls

All participants that received the radiotracer completed the 70 minute PET scan and no adverse events were reported. The mean injected dose of radioactivity was 510.3 MBq (13.8 mCi) ± 68.4 MBq (1.8 mCi). The ^{11}C-PBB3 images from a representative healthy control (H1040) are presented in Figure 3.1 as SUVRs that have been averaged over the last 40 minutes of the scan. Here axial slices 64 - 159 (of 207) are presented. The sum of nine images corresponding to the basal ganglia have been collapsed into three slices and are provided in Figure 3.2. Images pertaining to the cerebellum and placement of the reference ROI are presented in Chapter 4 with the clinical cases. There is no tracer uptake in the basal ganglia or cerebellum of our controls. Increased signal in the aforementioned scans seems to align with venous sinuses rather than brain tissue. To facilitate anatomical interpretation, an MR overlay is also provided across the three orthogonal planes in Figure 3.3. Visual inspection of the coronal image suggests that the tracer is predominately in the venous sinuses, with little to no deposition in brain tissue. This is further supported by the coronal and sagittal views, in which tracer uptake appears concentrated in the cavernous sinus, bilaterally. Lastly, minimal tracer activity in the superior sagittal sinus appears both dorsally and posteriorly. Uptake in the torcula (confluence of the sinuses) is evident in the sagittal section.

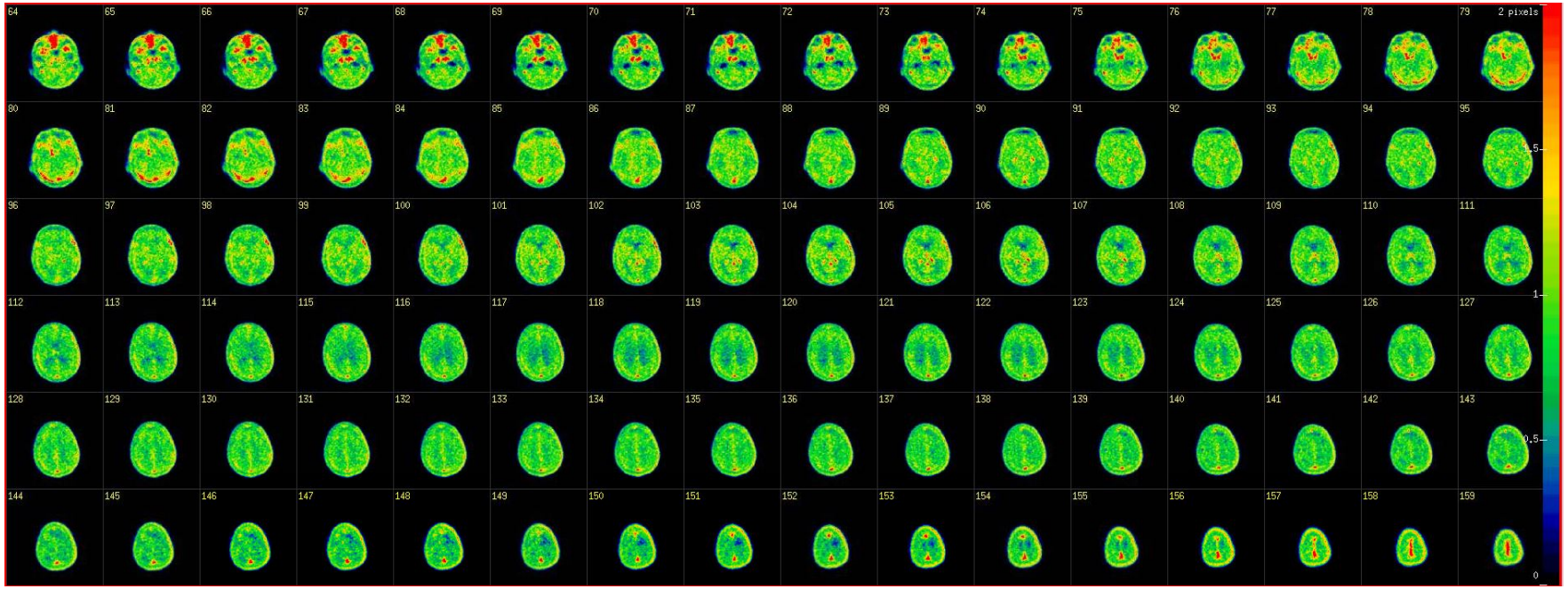

Figure 3.1 ^{11}C-PBB3 Scan in a Healthy Control

^{11}C-PBB3 images from a representative healthy control (H1040) are depicted for slices 64-159 (of 207). Images represent the SUVRs and were averaged over the last 40 minutes of the scan. Regions that show uptake similar to that in the cerebellar reference region appear green, with an SUVR near 1. Cooler colours indicate minimal or absent tracer accumulation, whereas warmer colours reflect increased radioactivity. Hot colours in the image sequences 64 - 77 likely pertain to the circulation through ethmoid and maxillary sinuses, and are not reflective of tau deposition in brain tissue.

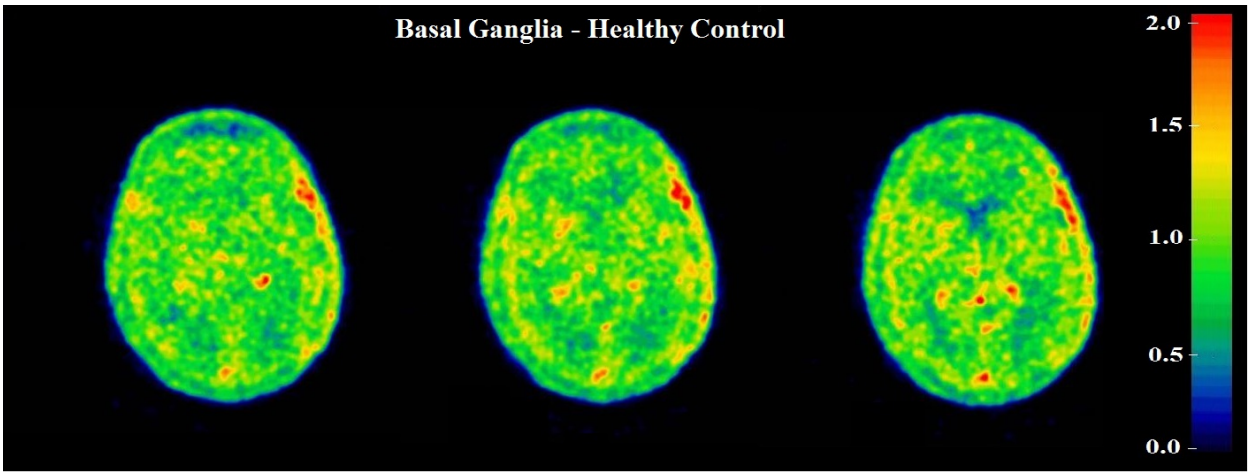

Figure 3.2 Enlargement of Axial Slices Corresponding to the Basal Ganglia

Representative ^{11}C-PBB3 scans in the basal ganglia of a healthy control show limited tracer retention in brain tissue. The sum of nine images corresponding to the basal ganglia have been collapsed into three axial slices. The warmer colours clustered in the middle of each image and the signal around the perimeter of the brain suggest the tracer remains in the vasculature.

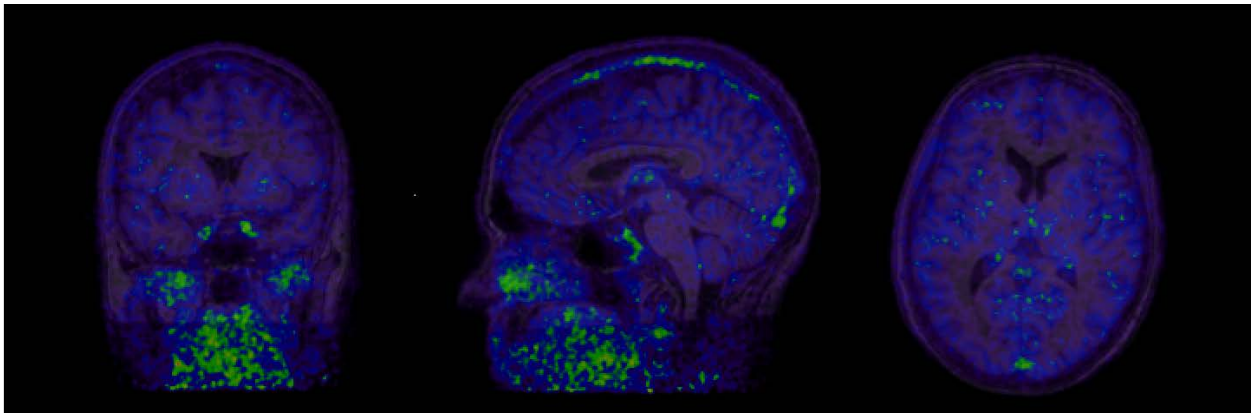

Figure 3.3 ^{11}C-PBB3 Scan in a Healthy Control with MR Overlay

Visual interpretation across representative coronal (left), sagittal (middle), and axial (right) perspectives is enhanced with the MR overlay. Images reflect the mean tracer uptake averaged over the last 40 minutes of the scan. The coronal image confirms the tracer is predominately in the venous sinuses, with little to no deposition in brain tissue. The coronal and sagittal views show uptake in the cavernous sinus, bilaterally. Additional activity in the superior sagittal sinus both dorsally and posteriorly, and in the torcula (confluence of the sinuses), is evident in the sagittal section.

Time Activity Curves (TACs) for the dynamic images (from 0 to 70 minutes) were generated for each participant who successfully completed both PET and MRI (n = 6). TACs were generated for a total of 21 ROIs including the reference region (cerebellum). Group averages for each region are displayed by left (Figure 3.4) and right (Figure 3.5) hemisphere. Rapid and complete tracer distribution is evident throughout the brain, with peak activity occurring between two to three minutes post-injection. Participants showed similar clearance rates across all ROIs. Here peak activity ranges between 5,000 – 6,200 Bq/ml, with retained activity leveling off at approximately 2,500 Bq/ml after 30 minutes. Similar patterns of activity are seen in both left and right hemispheres. TAC kinetics were corrected to account for differences in the injected dose of tracer and individual body weight.

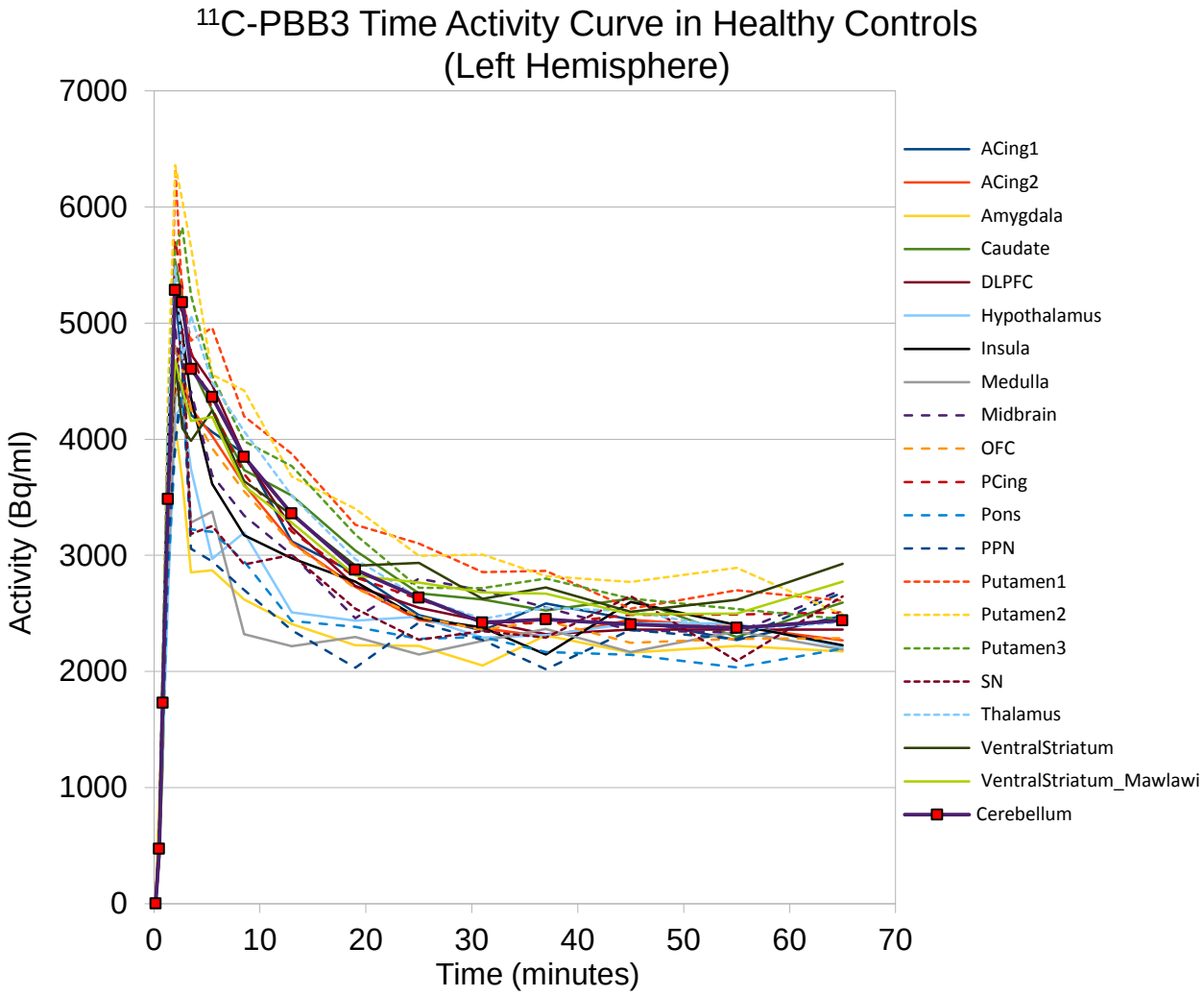

Figure 3.4 Time Activity Curves for ^{11}C-PBB3 Across Left Regions of Interest

TACs were generated for 21 ROIs and averaged across all participants who had completed ^{11}C-PBB3 PET and a corresponding anatomical MRI (n = 6). Radioactivity levels peak within minutes of injection and are followed by a steady decay for approximately 30 minutes. Retained activity levels of between 2,000 – 3,000 Bq/ml are evident for the remainder of the scan. Plotted values were corrected for injected dose and weight. Red squares denote the TAC for the reference region (cerebellum).

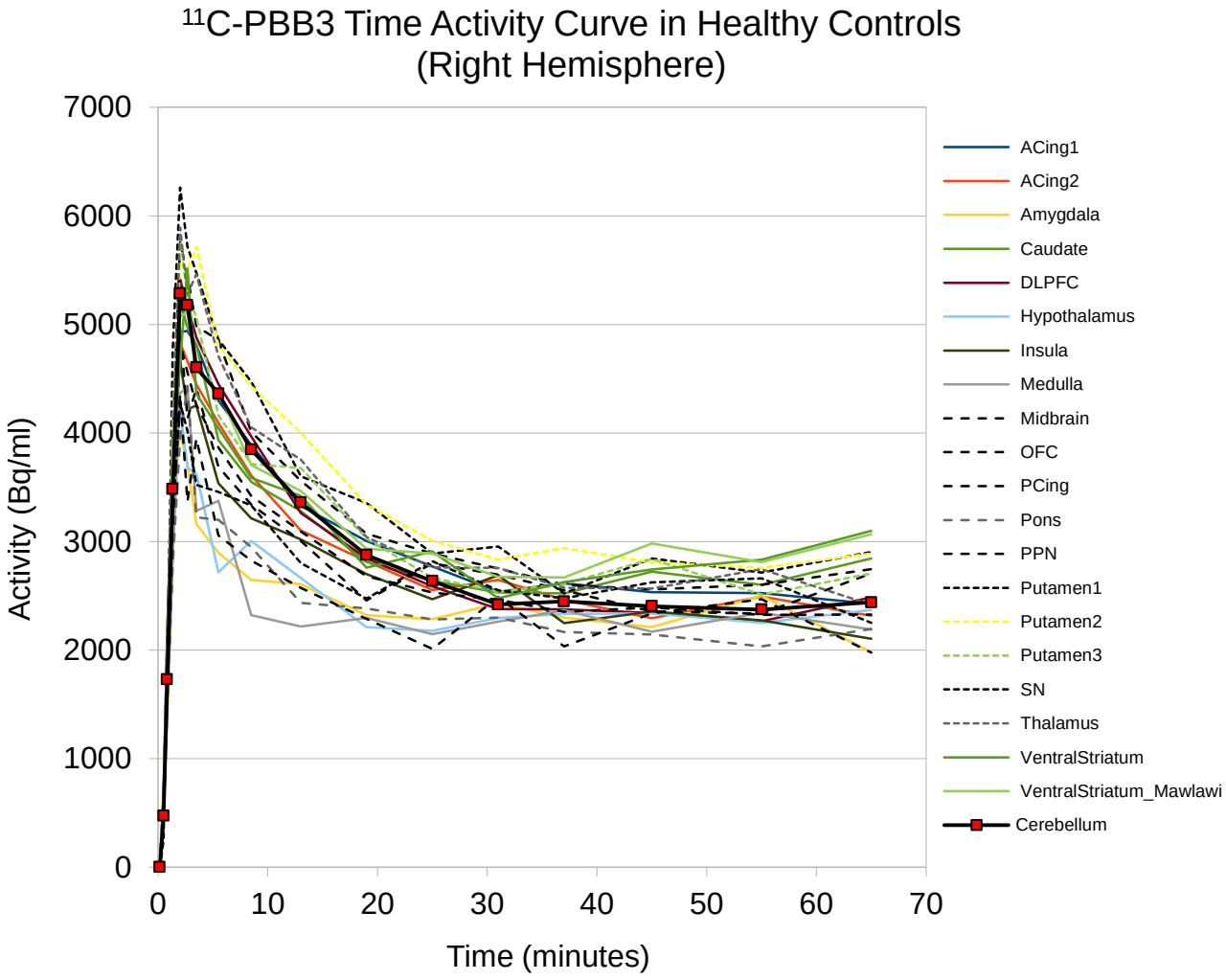

Figure 3.5 Time Activity Curves for ^{11}C-PBB3 Across Right Regions of Interest

TACs were generated for 21 ROIs and averaged across all participants who had completed ^{11}C-PBB3 PET and a corresponding anatomical MRI (n = 6). Radioactivity levels peak within minutes of injection and are followed by a steady decay for approximately 30 minutes. Retained activity levels of between 2,000 – 3,000 Bq/ml are evident for the remainder of the scan. Plotted values were corrected for injected dose and weight. Red squares denote the TAC for the reference region (cerebellum).

Lastly, as ^{11}C-PBB3 is a distributed tracer, Standard Uptake Values (SUVs) for each ROI were generated. Ratios were established by dividing each pixel in a given region by the mean of the cerebellum for the last 40 minutes. The ratio of the SUV for each ROI compared to the cerebellum approaches 1:1 for all regions. On average, the lowest ratios were reported in the pons (0.83) and the right pedunculopontine nucleus (0.87), with the highest ratios in the right ventral striatum (1.18) and putamen (1.14). A summary of the SUVRs is depicted in Figure 3.6.

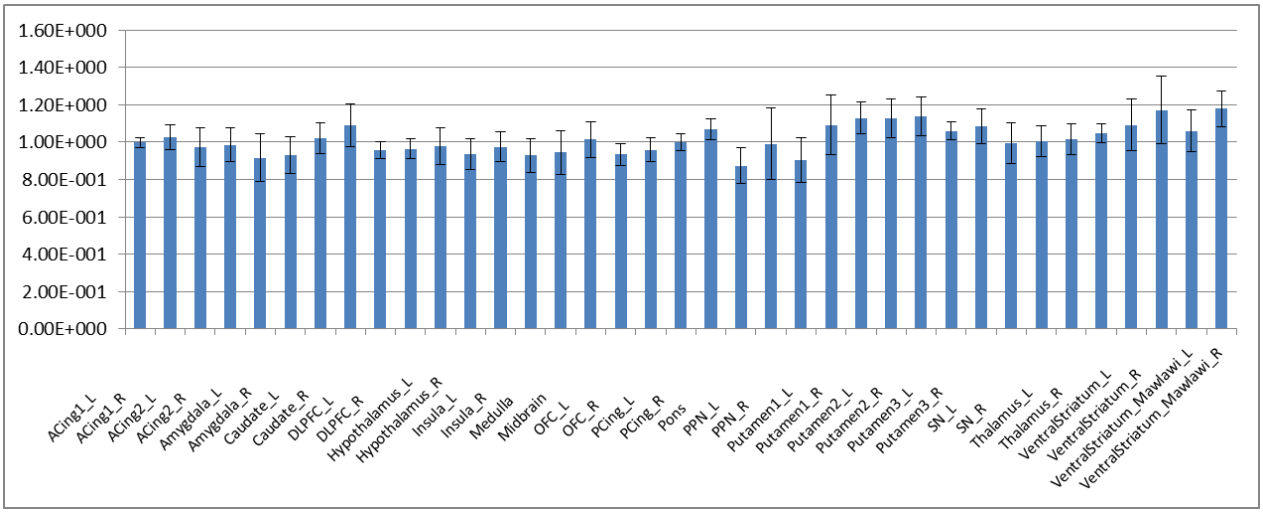

Figure 3.6 Standard Uptake Value Ratios Across Regions of Interest

SUVs for each ROI were averaged across participants (n = 6). The tracer uptake in each region was divided by the uptake in the reference region (cerebellum) over the same time frame to generate the SUVR. Here all regions show uptake and clearance at similar rates as the cerebellum, thus ratios are close to one. Error bars represent SEM.

3.8 Discussion

This was the first study using ^{11}C-PBB3 at the PPRC. We successfully completed tau imaging in eight participants. Demographics and clinical assessments reflect anticipated variability within the healthy, elderly population. Depression scores were low (4.3 ± 5.1), with the exception of one individual who scored in the mild range (14). This was attributed to recent and unforeseen circumstances; however, this individual did not report having a previous history of depression. Additionally, the tracer kinetics in the eldest participant (F, 76 years old) show much higher uptake and retained activity in the cerebellum compared to all other subjects. Anecdotally, the participant reported having taken a Cafergot tablet in the morning (at least 5 hours prior to the scan) to prevent the onset of a vascular headache. Cafergot is a combination of caffeine and ergotamine, both of which are vasoconstrictors. Therapeutic benefit may additionally result from circulating metabolites; the half-life for the parent drug is approximately 2.7 hours while the half-life of the metabolites is significantly longer, in excess of 21 hours (Diener et al., 2002). The influence of such compounds may have constricted vasculature within the brain thus slowing both uptake and clearance of the tracer, resulting in elevated values; however, this would presumably occur to a similar extent throughout the entire brain and thus maintain a ratio of close to 1 when comparing the SUVs for ROIs to the cerebellum. This was not the case as all other ROI values for this participant fell within the normal and expected ranges. Lastly, visual inspection of this participant's images show increased signal in the areas corresponding to the venous sinuses. This raises the question of whether the tracer might persist in the vasculature and thereby introduce artificially elevated values in adjacent brain tissue, especially in the cerebellum. This finding was not replicated in our other participants. Collectively, our results fit in the context of the emerging literature and replicate the findings of the developers of the ^{11}C-PBB3 tracer in Chiba, Japan (Maruyama et al., 2013).

The ^{11}C-PBB3 images in Figures 3.1 - 3.2 represent SUVRs averaged over the last 40 minutes of the each scan. This is a common practice to assess areas of tracer retention. Our current interpretations remain limited; however, kinetic analyses of TACs show rapid uptake and widespread distribution. Peak radioactivity levels were achieved between two to three minutes post-injection. Our results show limited to no retention of the ^{11}C-PBB3 tracer, suggesting that there is no substantial deposition of abnormally phosphorylated tau protein in physically and

cognitively healthy, elderly individuals. This is similarly supported by the average ratios of each SUV to the cerebellar reference region, which approaches 1:1 for all assessed ROIs. This suggests clearance from each region is comparable to that of the reference region, and that no significant regional tracer accumulation is evident. These results appear to support our hypothesis; however, testing the tracer in a known tauopathy would serve as a methodological control to assess whether the tracer is capable of detecting and binding various tau isoforms. Preliminary results to help address this question are presented in Chapter 4.

In conclusion, this study has successfully added ^{11}C-PBB3 into the PPRC's neuroimaging repertoire. The visual interpretations of ^{11}C-PBB3 images and ROI-analysis of both TACs and SUVRs suggest that no significant tau deposition was evident in our healthy, aging population. The compilation of this data will serve as our baseline metrics, and subsequent investigations will build on this newly established framework. Specifically, future research will look to incorporate tau imaging into longitudinal multi-tracer studies across numerous neurodegenerative disease profiles.

3.8.1 Limitations

The study is not without inherent limitations pertaining to tracer production and recruitment. First, following an extensive period in research and development, logistical challenges were introduced with the photosensitivity of the tracer. Amber tubing and syringes were used to minimize light exposure during injection in the PET Suite, and participants were scanned under low light conditions. However, despite these methodological considerations the tracer may still experience more rapid decay. Further challenges were introduced as tracer production and delivery were consistently lower than anticipated throughout the study. Our average injected dose was 510 MBq rather than our intended 740 MBq. The impact of such a reduced dose may be elucidated with further study and learned experience with the tracer. Lastly, the varying specific activity of the tracer across participants introduces additional confounds. Here injection with a lower specific activity could ultimately decrease the radioactive retention and therefore signal as a greater percentage of hyperphosphorylated tau binds to 'cold' unlabeled tracer. To account for this, the production of larger volumes and higher specific activities may warrant further discussion.

Second, the sample population was recruited through advertisements in a local newspaper and follow-up with previous participants in PET-based studies. While screening procedures ensure participant's mood, cognitive, and motor functions do no introduce unwarranted variability, the use of radiation inevitably deters a significant number of eligible participants. This is a frequent challenge in PET-based studies, and one that is not easily overcome. Finally, our comprehensive screening practices specifically filter out participants with predispositions to increased tau levels, such as a family history of Alzheimer's disease or participants who have experienced a previous concussion or head injury. Despite our efforts, emerging evidence strongly suggests that subconcussive injury may also increase neuronal dysfunction and contribute to tau misfolding and deposition (Gavett et al., 2011, Baugh et al., 2012). Controlling for these incidences is more difficult as many individuals may overlook this type of injury, or be unable to recall the frequency and severity. This is common among individuals with a history of amateur or competitive sport.

3.8.2 Applications of Tau Imaging to the Study of CTE

Establishing the current baseline tracer kinetics and retention patterns (or lack thereof) is an essential step in investigating subsequent tauopathies. Here we propose three areas of future interest that capitalize on tau imaging to advance our understanding of CTE.

First, ^{11}C-PBB3 likely offers great benefit to translational research in the study of CTE. Bench-based investigations of the underlying and instigative pathophysiological processes may employ ^{11}C-PBB3 as a non-invasive means of tracking tau deposition. In turn, this has potential clinical applications as earlier, definitive diagnosis in vivo may facilitate increased educational awareness for both the patient and their families. This may enable earlier interventions and/or coping strategies to help mitigate risk for negative psychological symptoms such as depression, aggression, and suicidal tendencies. However, widespread application of this is unlikely due to the limited access and high cost of tau imaging.

Next, given the emerging evidence on the role of inflammation in obstructing recovery and perpetuating cytotoxic environments (Fitch and Silver, 2008), multi-tracer studies with ^{11}C-PBB3 and ^{11}C-PBR28, a tracer that is known to bind to peripheral benzodiazepine receptors on activated microglia (Fujita et al., 2008), would be advantageous in understanding the confluence of inflammation and tau deposition. Furthermore, CTE is often described as having an insidious onset and ambiguous presentation. Concurrent investigations of neuroinflammation and dopamine denervation are necessary to understand the initial mechanisms and potential biomarkers the relationship between trauma and the onset of potential sequelae.

Lastly, longitudinal tracking with the tracer will need to evaluate the contributions of frequency and severity of trauma on tau deposition. This will broaden our understanding of how injury serves as a risk factor of earlier onset and increased likelihood of disease. As described in Chapter 1, the stereotypical pattern of tau deposition begins in the cerebral cortices, in close proximity to cerebral vasculature in the sulcal folds (Courville, 1962, Morales et al., 2009, McKee et al., 2014). Early detection of tau in these areas offers further opportunity to monitor cognitive decline as a function of progressive tau deposition, and, in the future, a way to monitor treatment efficacy. While currently there is no therapy to slow, stop, and/or reverse tau deposition, efforts are underway in each of these domains (Jin et al., 2014, Lei et al., 2015).

Chapter 4: Preliminary Investigation with ^{11}C-PBB3 in Clinical Tauopathies

4.1 Introduction to Progressive Supranuclear Palsy

Progressive Supranuclear Palsy (PSP) is a tauopathy that was first described by two Canadian neurologists and a neuropathologist in 1964; and at the time, recognized as Steele-Richardson-Olszewski Syndrome (Steele et al., 1964). The condition is generally of unknown etiology, affecting 1.4 - 4.0 per100, 000 individuals with an average age of onset in the mid-sixties (Nath et al., 2001). However, the true prevalence is likely masked by misdiagnosis. PSP mimics a Parkinsonian presentation but is characterized by the insidious onset of postural instability, deficits in eye movements, and impaired cognitive function. The cardinal manifestations include severe disruptions of balance or gait ataxia resulting in recurrent backwards falls, bradykinesia, and supranuclear vertical gaze palsy; though dizziness, depression, apathy, fatigue, axial rigidity, and neck dystonia are also prominent. Although the initial presentation may appear similar to Parkinson's disease, distinguishing features include a more rapid progression and poor response to Levodopa treatment (Mitra et al., 2003). Survival averages seven years from diagnosis, with later stages of disease showing impaired autonomic processes such as breathing and swallowing, dysarthria, bradyphrenia, and frequently, retrocollis posturing (Higginson et al., 2012). Currently, no laboratory or neuroimaging tests provide a definitive diagnosis thus decisions are exclusively clinically derived, highlighting the need for early detection. Treatment options for symptom alleviation may include use of dopamine agonists or tricyclic antidepressants, Botulinum toxin injections, eye drops for dry eyes or prisms for vision correction, and at end stages, use of a feeding tube (Long et al., 2015, Stamelou and Bhatia, 2015). These may temporarily improve quality of life; however, there is currently no cure or means to slow or stop the course of disease.

Abnormal tau protein is implicated in the pathogenesis. The underlying pathology indicates that PSP is characterized by significant and progressive deposition of NFTs and gliosis (Williams et al., 2007). Tau deposition appears to be primarily 4-repeat tau filaments, though further investigation of the representatives isoforms is warranted (Yokoyama et al., 2015). These entanglements generally occur in the absence of senile plaque formation. Interestingly, tau

oligomers, not NFTs, are purported to be the most detrimental; seeding and facilitating pathological tau transmission (Gerson et al., 2014). This finding is generalizable amongst neurodegenerative tauopathies, inclusive of PSP and CTE. Histological preparations indicate gliosis and marked deposition of hyperphosphorylated tau in both primary motor regions and subcortical nuclei (Yokoyama et al., 2015). Pathophysiologically, this enigmatic disease presents with atrophy throughout the brainstem (medulla, pons, and midbrain), basal ganglia (substantia nigra, globus pallidus, and subthalamic nucleus), and cerebellum (Yagishita and Oda, 1996). Later stages of the disease present with a distinguishing pattern of atrophy in the midbrain, revealing a 'hummingbird' sign on MR imaging (Shukla et al., 2009). Concurrent enlargement of the third ventricle and wasting of the superior cerebellar peduncles are also noted.

4.2 Statement of Purpose

In this preliminary report, we sought to further validate our ^{11}C-PBB3 tracer by scanning two patients with probable and known tauopathies. These scans serve the critical purpose of evaluating whether the tracer will detect and specifically bind to abnormally phosphorylated tau, and to what extent. Identification of selective tau markers may aid in early identification of individuals who are at increased risk or predisposition to tau-related disease such as CTE, and may eventually assist with prognosis and distinguishing disease trajectory.

4.3 Hypothesis

We hypothesize that patients with suspected and known tauopathies will differ in the degree and distribution of abnormal tau deposition both from each other, and from the healthy, elderly population. Specifically, we expect patterns of activity to reflect known pathophysiology such that tracer binding occurs in the cerebral cortex, basal ganglia (putamen), brainstem (midbrain), and cerebellum. We expect more significant and widespread tracer binding in the advanced stages of PSP than in our probable PSP-P participant.

4.4 Methodology

The UBC Clinical Research Ethics Board approved this investigation and issued the Certificate of Approval under the "Tau and Neuroinflammation Imaging in Parkinson's Disease and Related Disorders" protocol (certificate number: H14-03268). Eligible participants (males and females

over the age of 19 years old) were recruited from the Movement Disorders Clinic at the PPRC. Neurologists pre-screened patients who were diagnosed with atypical Parkinsonism. All participants had a MoCA of greater than 18. The methodology for this study mirrors that described in Chapter 3 for the study of tau imaging in the healthy, elderly controls. Next, a summary of each participant's clinical presentation is provided.

4.4.1 Case 1: Progressive Supranuclear Palsy - Parkinsonism

A 72-year-old woman's queries into neurological dysfunction began seven years ago, whereby initial presentation included uncoordinated movement followed by difficulties in writing, and later ambulating which led to recurrent falls. A diagnosis of probable Progressive Supranuclear Palsy - Parkinsonism (PSP-P) was made within the last six months following a poor response to Levodopa and increasing oculomotor deficits. She has mild, symmetric bradykinesia and progressive deficits in gait initiation and freezing (right > left), and significant postural instability now requiring the aid of a walker. Additional clinical features include hoarse voice, slight hypomimia, and mild hypophonia. There are no symptoms of tremor, rapid eye movement sleep behaviour disorder, sleep apnea, orthostatic hypotension, or bowel complaints; though slight loss of bladder control was noted.

The patient's daily medication regimens include eight tablets of Sinemet IR 100/25 mg, anti-depressants (Paroxetine, 20 mg), iron supplements (Ferrous gluconate, 300 mg), and vitamins (B12, 1000 μg; D, 1000 units). She reports improved mood with Paroxetine but no appreciable benefit from Sinemet.

Clinical examinations of blood pressure, cognition and mood are normal. No perseveration is detected in the Luria sequence, palmomental signs are present, and the applause sign is positive. Cranial nerve examination revealed significant olfactory and oculomotor deficits. Square wave jerks are present in the primary position with impairments in vertical saccades (decreased amplitude and velocity) in the upward direction. Horizontal saccades are equally slow. Visual fields and pupillary light responses are normal. Mild, symmetric rigidity is noted in the neck and extremities.

4.4.2 Case 2: Moderate to Severe Progressive Supranuclear Palsy

A 68-year-old wheelchair bound woman presents with moderate to severe PSP of five years duration. Her history is notable for increased frequency of backward falls, significant bradykinesia, and no tremor. She has significant postural instability and is unable to transition from her wheelchair unassisted. Additional presentation includes profound dysarthria associated with palilalia, severe hypophonia, and mild hypomimia. Fine motor movements of the upper limbs are moderately impaired. She reports significant lower back pain, worse on the left side with no radiation to lower extremities. There are minimal cognitive issues, and no problems with mood, anxiety, or hallucinations. While quantity of sleep is decreased, she retains a regular pattern with no symptoms of rapid eye movement sleep behaviour disorder. Urinary urgency and incontinence are present, as is minimal dysphagia.

Her daily medication regimen includes Sinemet IR 100/25 bid, an anti-depressant (Mirtazapine, 15 mg qhs), Co-enzyme Q10 (100 mg) and the non-steroidal anti-inflammatory, Naproxen. Treatment for co-morbid hypothyroidism (L-thyroxine, 50 mcg) and elevated cholesterol (atorvastatin, 10 mg qhs) are noted.

Clinical examination reveals slightly elevated blood pressure upon standing and elevated pulse (91 beats per minute). Cranial nerves and extraocular eye movements are normal. There is mild restriction of upward gaze, broken pursuit, and slow, hypometric saccades with delayed initiation. Optokinetic nystagmus is present but impaired vertically. Mild to moderate symmetric rigidity is noted in the neck and extremities.

4.5 Results

4.5.1 Subject Demographics and Clinical Assessments

In this preliminary report two female participants, ages 68 and 72 years old, completed tau imaging and the associated MRI scans. Participants did not stop their medications prior to scanning and no side effects or complications were reported throughout the study. Demographics and individual scores for the clinical assessments of mood, cognition, and motor function are provided in Table 4.1.

In the PSP-P case, mood (BDI = 10) and cognition (MoCA = 28/30) were normal. In the severe PSP case, mood was normal (BDI = 8) and only minimal cognitive decline was noted, scoring 24/28 on a modified MoCA. Here the two-points for language repetition were excluded. There were, however, no deficits in word finding or comprehension. Two points were lost for visuospatial testing and two points for delayed recall. There were marked differences in the mobility between cases as noted by the total motor scores on the MDS – UPDRS III (PSP-P = 38 versus severe = 73). As the woman with severe PSP was wheelchair bound, we were unable to assess the freezing of gait and accordingly no score was reported for this section.

Table 4.1 Demographics and Clinical Assessments for PSP Cases

Clinical Diagnosis	Age at PET	Gender	Clinical Assessments						
			BDI	MoCA	MDS - UPDRS III				
					Total	Right	Left	Common	H&Y
PSP-P	72	F	10	28/30	38	9	10	15	4
Severe PSP	68	F	8	24/28*	73	21	20	27†	5

F = Female; M = Male; BDI = Beck Inventory Depression; MoCA = Montreal Cognitive Assessment; H&Y = Hoehn & Yahr Rating Scale; MDS - UPDRS III = Movement Disorder Society - Unified Parkinson's Disease Rating Scale
* MoCA scaled to 28, language repetition not included
† No score for freezing of gait reported

4.5.2 ^{11}C-PBB3 Image Analysis in PSP

Participants underwent a 70 minute ^{11}C-PBB3 scan with injected doses of 550.3 MBq (PSP-P) and 557.5 MBq (severe PSP). ^{11}C-PBB3 PET images are presented as SUVRs using the individual's own cerebellum as their reference region. The signal was averaged across the last 40 minutes of the each scan. Visual assessments of realigned images show selective regional ^{11}C-PBB3 retention in the basal ganglia and thalamus, suggesting the tracer was effective in detecting tau deposition in an expected distribution in both PSP-P (Figure 4.1) and severe PSP cases (Figure 4.2). Images were produced using the same SUVR scale to facilitate comparison within and between healthy controls and the tauopathies.

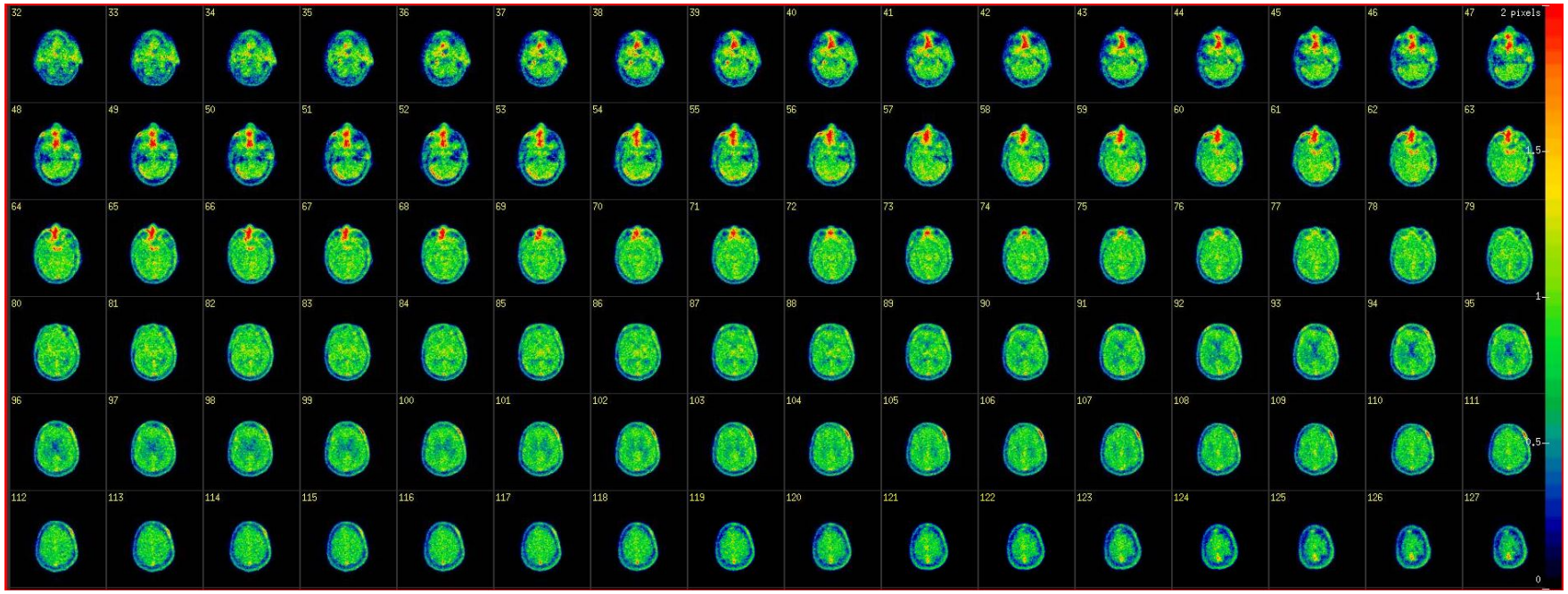

Figure 4.1 ^{11}C-PBB3 Scan in Probable Progressive Supranuclear Palsy – Parkinsonism

Slices 32 - 127 (of 207) are presented for the PSP-P case. Images reflect the SUVRs and were averaged over the last 40 minutes of the scan. Areas that appear green show similar uptake to the cerebellar reference region. Cool colours indicate minimal or absent tracer accumulation, whereas warmer colours reflect increased radioactivity and would suggest deposits of abnormally phosphorylated tau. Here tau deposition is noted in the regions corresponding to the basal ganglia (slices 83 - 88), and the transverse sinus (slices 48 - 55). Warmer colours in the anterior part of slices 40 – 60 likely pertain to the circulation through ethmoid and maxillary sinuses, and are not reflective of tau deposition in brain tissue.

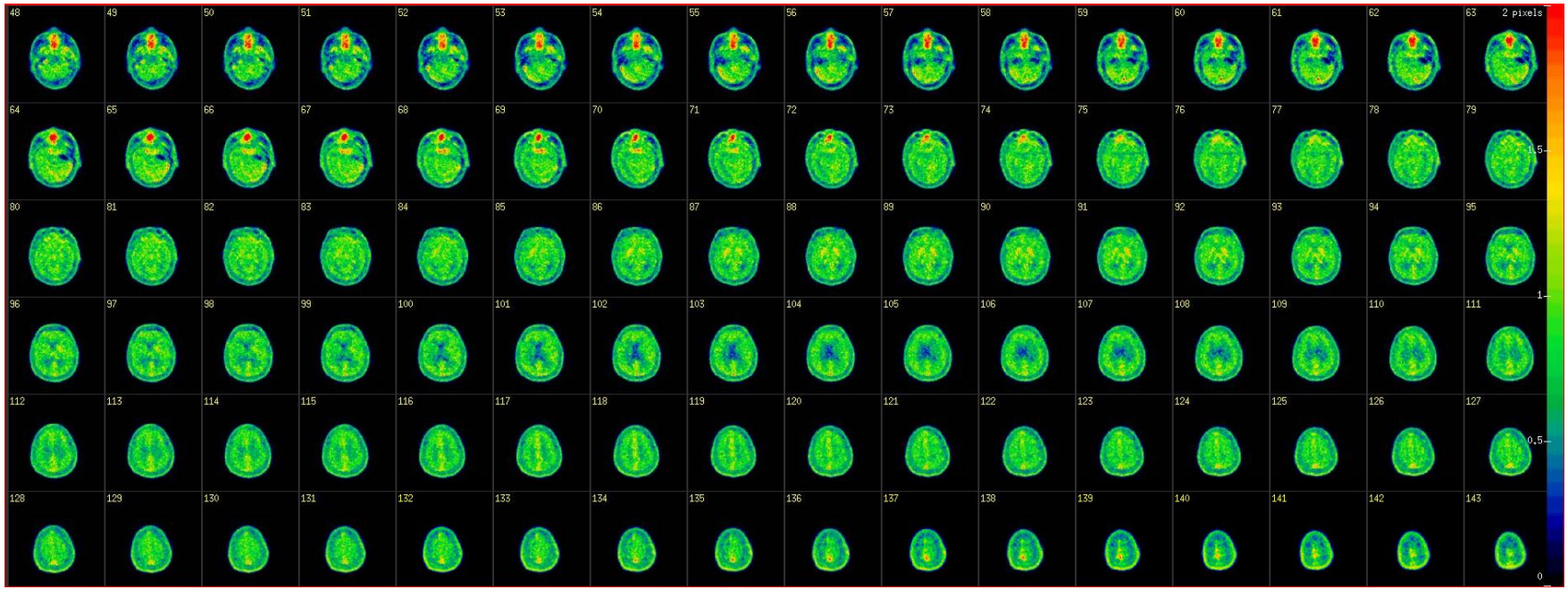

Figure 4.2 ^{11}C-PBB3 Scan in Severe Progressive Supranuclear Palsy

Slices 48 – 143 (of 207) are presented for the severe PSP-P case. Images reflect the SUVRs and were averaged over the last 40 minutes of the scan. Areas that appear green show similar uptake to the cerebellar reference region. Cool colours indicate minimal or absent tracer accumulation, whereas warmer colours reflect increased radioactivity and would suggest deposits of abnormally phosphorylated tau. Here tau deposition is noted in the regions corresponding to the basal ganglia and thalamus (slices 86 - 95), and the transverse sinuses (slices 53 - 63). Warmer colours in the anterior part of slices 48 - 63 likely pertain to the circulation through ethmoid and maxillary sinuses, and are not reflective of tau deposition in brain tissue.

Further investigation was completed by summing nine ^{11}C-PBB3 images in the regions corresponding to the basal ganglia and collapsing these across three axial slices for healthy and disease states (Figure 4.3). For comparison, images from an age and gender-matched healthy control (H1040, 68 year old female) were selected. Enhanced tracer uptake is suggestive of mild tau deposition in the basal ganglia of the PSP-P case. Greater retention patterns as indicated by an SUVR of greater than 1.5 are indicated in the basal ganglia and thalamus of the severe PSP case. In the healthy controls no retention in brain tissue is evident, but rather signal appears scattered in the venous system and near the perimeter of the brain suggesting continued circulation in the vasculature.

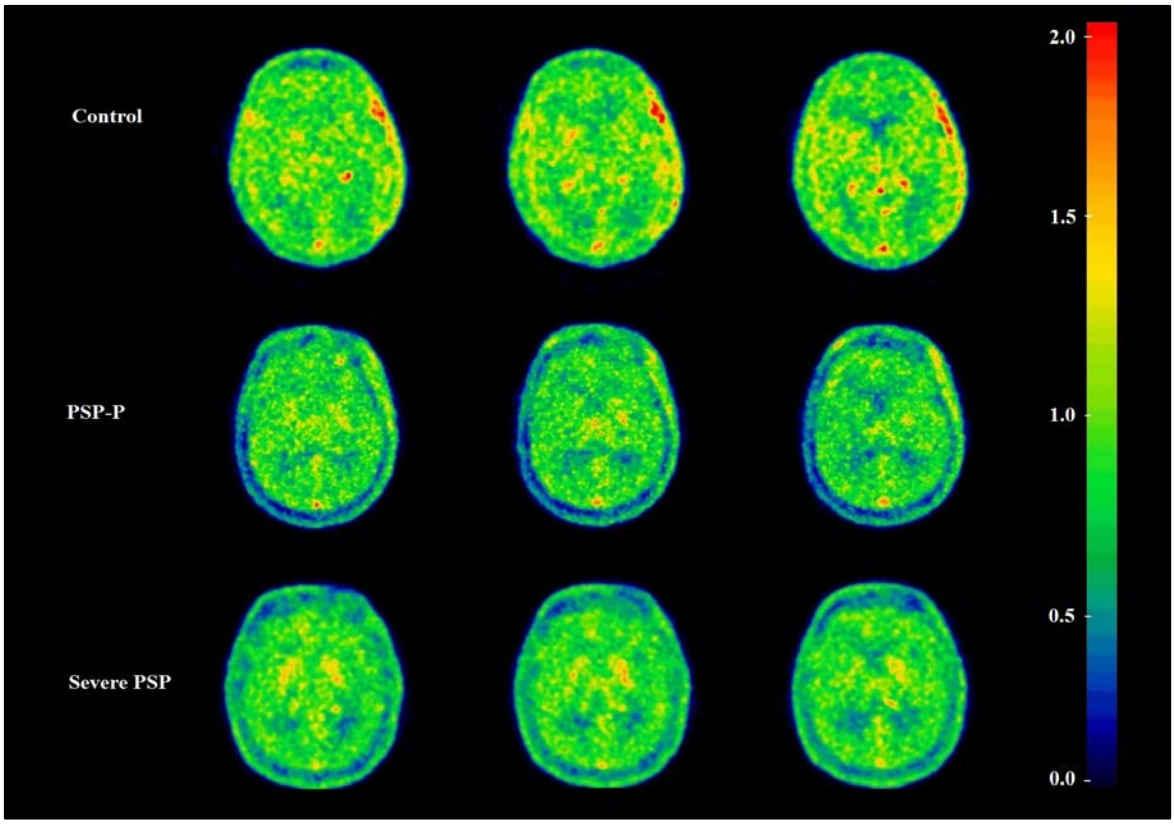

Figure 4.3 Comparison of ^{11}C-PBB3 Uptake in the Basal Ganglia by Tauopathy

A total of nine ^{11}C-PBB3 images corresponding to the basal ganglia were collapsed into three axial slices for each individual. Tracer uptake in the basal ganglia is suggested in the PSP-P case, whereas uptake in the basal ganglia and thalamus is seen in the severe PSP case.

To establish the placement of the cerebellar ROIs, a total of six images were summed and collapsed into a single axial slice for each individual (Figure 4.4). The anterior portion of each axial slice shows tracer uptake and is reflected by hot colours. This pattern of activity likely reflects uptake in the ethmoid and maxillary sinuses and is not reflective of tau deposition in brain tissue. Additionally, the control shows signal near the perimeter of the brain suggesting continued retention in the vasculature. Hot spots are evident in the right transverse sinus in the PSP-P case, and in the torcula of the severe PSP case.

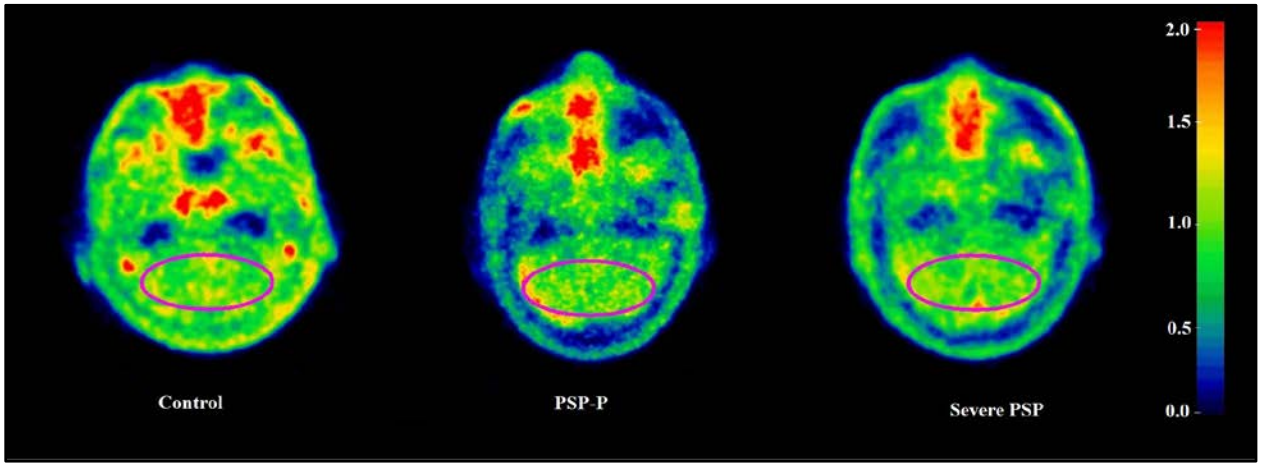

Figure 4.4 Comparison of ^{11}C-PBB3 Uptake and Cerebellar ROI Placement by Tauopathy

A total of six ^{11}C-PBB3 images in the region of the cerebellum were summed and collapsed into a single axial slice for each individual. Hot spots encroaching on the cerebellar ROIs likely reflect tracer uptake in the venous sinuses in both the PSP-P and severe PSP cases. In all scans, the hot colours in the anterior portion of each slice suggest tracer uptake in the sinuses and does not reflect tau deposition in brain tissue. Delineation of the cerebellar ROI is denoted by the magenta ellipse; the border is enhanced for visual purposes.

Orthogonal images help facilitate visual assessment. In Figure 4.5 the distinction between healthy and diseased states is evident. In comparing the coronal sections between individuals, uptake in the healthy control is concentrated in the cavernous sinuses bilaterally whereas diseased states show regionalized uptake in the basal ganglia and thalamus. Lastly, sagittal sections reveal the common uptake in the nasal sinuses. Healthy controls retained activity in the

vasculature, as indicated by the hot signal in the superior sagittal sinus, both dorsally, and posteriorly to the torcula (see Figure 3.3 for interpretation with MR overlay).

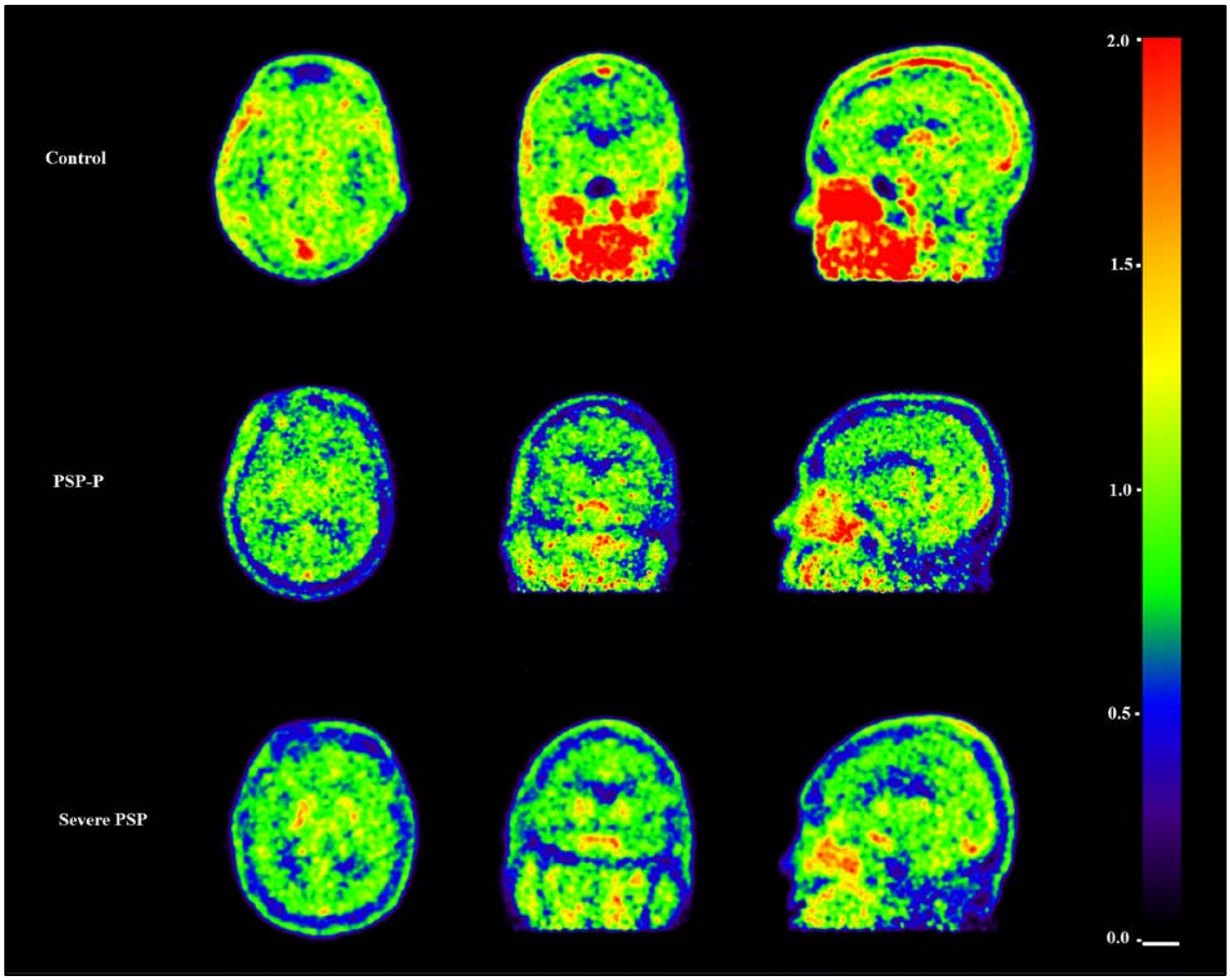

Figure 4.5 Comparison of ^{11}C-PBB3 Uptake in Orthogonal Views by Tauopathy

Orthogonal representations of ^{11}C-PBB3 images distinguish healthy and diseased states. Healthy controls retained activity in the vasculature, denoted in the sagittal view. Coronal sections show regional retention in the basal ganglia and thalamus in diseased states. Sagittal sections reveal the common uptake in the nasal sinuses.

Lastly, the TACs for the reference region (cerebellum) in diseased states show slightly enhanced tracer uptake and retention compared to controls (Figure 4.6); however, there is large variability within the control group. Peak activity is similarly achieved within 2 - 3 minutes of injection, and is followed by approximately 30 minutes of decay. The PSP-P case shows the greatest uptake achieving a maximum activity level of 8,000 Bq/ml and retained activity of approximately 3,800 Bq/ml throughout the latter half of the scan. However, some of this activity may reflect contamination from activity in the transverse sinus (see Figures 4.1 and 4.4). Comparative uptake values for the severe PSP case may change when overall brain atrophy is considered.

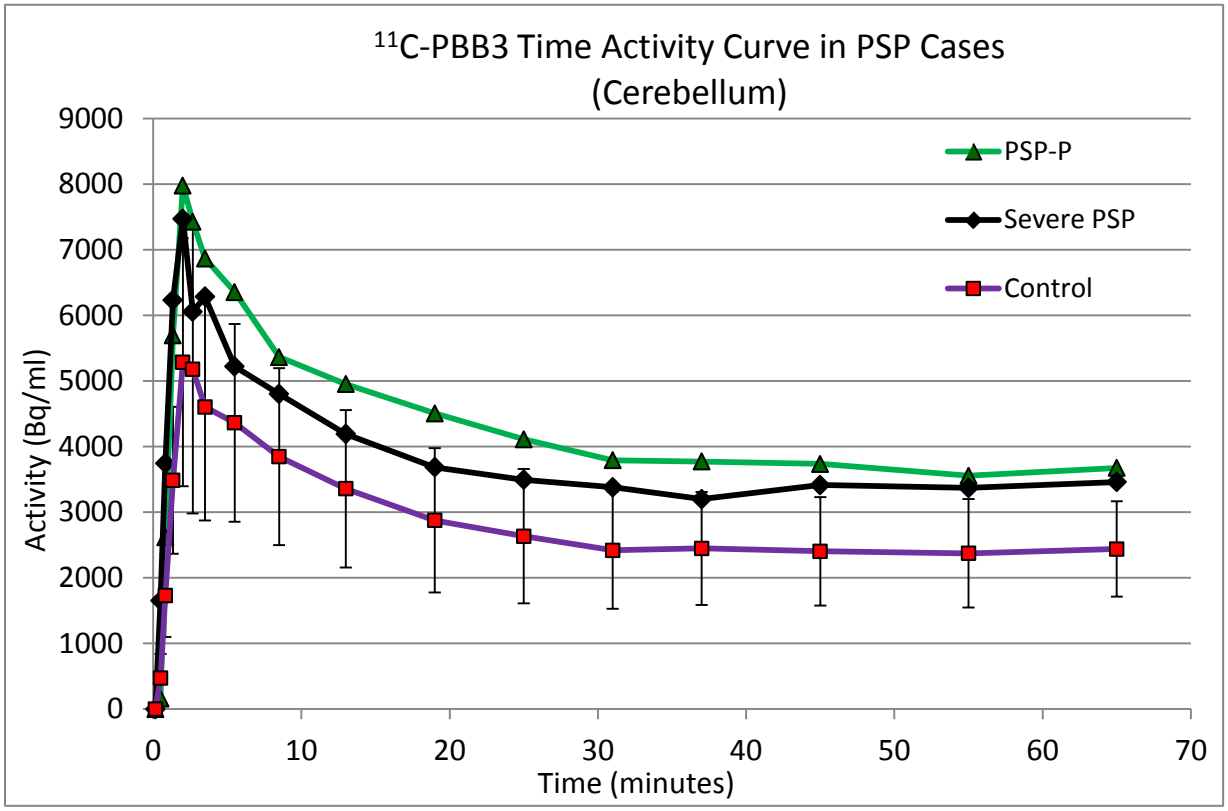

Figure 4.6 Cerebellar Time Activity Curve for ^{11}C-PBB3 in Healthy Controls and Tauopathies

Cerebellar TACs obtained for the PSP-P (n = 1) and severe PSP (n = 1) cases show both increased tracer uptake and retention throughout the scan when compared to the average uptake in the control group (n = 6). There is rapid uptake in each group, followed by a characteristic pattern of decay for 30 minutes. Error bars represent standard deviation.

4.6 Discussion

We are among the first groups to conduct tau imaging in PSP using the ^{11}C-PBB3 radioligand. In this preliminary report, we successfully scanned two elderly women, each with a clinically diagnosed tauopathy. Visual assessment of tracer binding distinguishes our healthy controls from our PSP-P and severe PSP cases. In both tauopathies, our images show an increase in signal retention throughout the basal ganglia and thalamus, patterns consistent with the known pathophysiology of tau deposition. Collectively, these findings support our hypothesis that the degree and distribution of abnormal tau would differ between our clinical and control cases.

Currently, our comparison between controls and our clinical tauopathies is limited to the cerebellar TAC. Although there was no obvious increase in cerebellar uptake in the PSP cases (other than that potentially arising from contamination from the transverse sinus) this is a potentially problematic area to use as a reference region, as the dentate nucleus may be affected in PSP. There is also moderate variability within our control population that warrants acknowledgement. We suggest the differences in uptake and retention may reflect the spectrum of aging, as there was more than 30 years difference between our youngest and oldest control participants. Further study is needed to draw conclusions on the comparative differences of tracer uptake between groups. Additional ROI analysis will be conducted across our 20 previously described ROIs (see Figure 3.4 and Figure 3.5). Comparison of regional TACs and SUVs may identify significant changes in structures that are not visible in the current gross images.
The cerebellum is often selected as a reference region in instances where it is known to remain unaffected in the condition of interest. Investigating tau deposition poses unique challenge here. While cognitively normal, healthy individuals show minimal uptake within the cerebellum, PSP and other tauopathies result in diffuse tau deposition as well as concomitant atrophy in the cerebellum with disease progression. This is significant for two reasons. First, increased tau deposition within the cerebellum would result in increased ^{11}C-PBB3 retention, and consequently a larger SUV. In this situation, an elevated cerebellar SUV may skew the overall interpretation of SUVRs for all remaining ROIs, producing artificially low ratios. Second, in the instance of marked brain atrophy, there is comparatively less brain volume available for tracer uptake. Here one would expect comparatively lower cerebellar SUVs, and in turn, elevated SUVRs across all

ROIs. The potential interaction between tau deposition and atrophy in the cerebellum complicates interpretations, and the possible direction of influence remains elusive. Further study may seek clarification in whether tau incites or accelerates localized atrophy, or vice versa, whereby atrophy promotes or accelerates abnormal tau deposition. A final caveat is that cerebellar ROIs may also be influenced by the specific placement methodology, either hand drawn or automated delineation. Previous studies have shown that the inclusion or exclusion of specific composite regions within the cerebellum such as deep cerebellar nuclei (dentate nucleus) are influential and must be carefully considered. Collectively, this suggests analysis of ^{11}C-PBB3 data should be interpreted with caution, and future analysis may look at alternative reference regions or ROI-based approaches.

In conclusion, our results fit with the emerging tau imaging literature. Similar findings have recently been presented in PSP cases using ^{18}F-AV1451, whereby voxel-wise contrasts and ROI analysis show increases in tau deposition in the subthalamic nucleus, dentate nucleus, pallidum, putamen, and frontal white matter (Ashall S., 2015). Other centres have also demonstrated the utility of ^{11}C-PBB3 in the study of other tauopathies including AD and CBD (Maruyama et al., 2013) . Our preliminary results suggest that ^{11}C-PBB3 appears superior to tau tracers such as ^{18}F-THK523, which identified PHFs in AD but failed to bind tau inclusion in PSP and other non-AD tauopathies (Fodero-Tavoletti et al., 2014).

4.6.1 Limitations

Our preliminary results are limited first and foremost by our small sample size (n = 2). More work is necessary to validate our findings and provide statistical significance; however, the differences in gross images provided here suggest that ^{11}C-PBB3 is a valuable tau imaging tool, with potentially widespread applications. The limitations previously discussed in Chapter 3 in regards to ^{11}C-PBB3 tracer production are also applicable here. A better understanding of tracer kinetics as well as the influences of the injected doses and specific activity, both in healthy and disease states, will requires further study. Lastly, the challenge of pursuing imaging in a rapidly progressive disease warrants acknowledgment. The physical manifestation of disease restricts eligibility and prevents many participants from completing PET scans. This may be due to cognitive decline (a minimum MoCA of 18 was required), or common symptoms of PSP such as

prominent neck dystonia and retrocollis posturing. The average disease duration is seven years from time of diagnosis, which further limits the ability to perform longitudinal imaging studies. Pronounced immobility and onset of autonomic symptoms and distress often prevent the study of more advanced stages of the disease.

4.6.2 Future Directions

Diseases characterized by the presence of pathologic tau, such as dementias, movement disorders, TBI, and CTE, could potentially benefit from tau PET imaging (Shah and Catafau, 2014). Future investigations at the PPRC will look to incorporate ^{11}C-PBB3 PET imaging into a number of current and upcoming studies across a spectrum of neurodegenerative conditions; one such study is described below.

Future studies will examine susceptibility to neurodegeneration following trauma. Previous efforts to study post-concussive tau deposition and neuroinflammation in professional athletes may be renewed following successful application of ^{11}C-PBB3 in our PSP cases. This investigation would compare middle aged athletes with a history of prior head trauma to PD patients with and without a prior history of head trauma. We hypothesize that athletes with early tau deposition and/or neuroinflammation following trauma will show imaging and clinical profiles suggestive of PD or other neurodegenerative conditions. Clinical and cognitive assessments would be complimented by PET measures of tau deposition, and cholinergic and dopaminergic dysfunction. This future study would also help establish whether correlations between in vivo imaging and cognitive status are present.

Chapter 5: Conclusions

5.1 Advancing the Study of CTE and Other Tauopathies

First, this thesis described the impact of a single sports-related concussion on the organizational structure of subnetworks previously identified as vulnerable to injury (Chapter 2). We applied the mathematical modeling construct of Complex Network Analysis to the study of adolescent athletes in the sub-acute phase of recovery. We selected brain regions associated with persistent deficits in attention, cognitive fatigue, distractibility, short term and working memory, and higher level executive functions. We demonstrated significant structural alterations in the Default Mode Network were evident up to two months post-injury in concussed athletes. This approach extends our knowledge of diffusivity metrics (FA and MD) to understand how information is processed in networks that are damaged or recovering. Previous studies have shown structural alterations in the DMN following more severe injury; however, we suggest even seemingly minor injuries can introduce persistent network damage. CNA offers the opportunity to combine powerful MR-based sequences (DTI and fMRI) of structure and function, providing a more comprehensive clinical picture. We propose broader applications of CNA may provide a more accessible option to study the effects of repetitive brain injury and characterization of in vivo structural dysfunction that may predispose individuals to CTE. The influence of intraneuronal tau deposits on DTI metrics, and consequently on CNA measures, offers an exciting new avenue of study.

Next, this thesis introduced a new tau-specific radioligand, ^{11}C-PBB3, to the Pacific Parkinson's Research Centre's investigative repertoire (Chapter 3). The focus of this investigation was establishing baseline scans for abnormally phosphorylated tau deposition in healthy aging. We successfully completed eight baseline scans and established that there was minimal to no retention of ^{11}C-PBB3 in our participants. While this suggests an absence of aberrant tau protein deposition, we sought preliminary results in which the tracer was employed in patients with clinically suspected and diagnosed tauopathies (Chapter 4). To determine whether ^{11}C-PBB3 would show a distinct pattern of activity and more significant uptake we conducted one scan in a suspected case of Progressive Supranuclear Palsy – Parkinsonism, and a second in a known severe case of PSP. ^{11}C-PBB3 data was analyzed using standardized uptake value ratios with the

cerebellum as the reference region (Maruyama et al., 2013). Visual interpretations of our results show tracer uptake and retention in the basal ganglia and thalamus, patterns consistent with known tau pathophysiology. As this is a newly developed tracer, more sophisticated methods of analysis will be employed as the research supporting these methods becomes available. Current interpretations remain limited, and further study in both PSP and other tauopathies is essential. We offer cautious optimism that ^{11}C-PBB3 may hold promise as a novel approach to study the progression of CTE, and in the future, a means to assess treatment efficacy.

In summary, this thesis builds a case for the utility of neuroimaging modalities as potential tracking progression in CTE. Here DTI-based approaches evaluated the structural integrity of neural networks which may be predictive of future dysfunction, whereas tau imaging serves as a concrete marker of current disease states. Longitudinal study with either modality would be beneficial, though the combination of both CNA and tau-imaging is likely most telling. Collectively, this work offers new directions to compare the effects of frequency and severity of head injury on long term sequelae. Knowing these studies will effectively take decades to complete, there is no time like the present to get started!

Bibliography

(ACRM) ACoRM (1993) Definition of mild traumatic brain injury. Journal of Head Trauma Rehabilitation 8:86-87.

Abbas K, Shenk TE, Poole VN, Robinson ME, Leverenz LJ, Nauman EA, Talavage TM (2015) Effects of repetitive sub-concussive brain injury on the functional connectivity of Default Mode Network in high school football athletes. Dev Neuropsychol 40:51-56.

Abhinav K, Yeh FC, Pathak S, Suski V, Lacomis D, Friedlander RM, Fernandez-Miranda JC (2014) Advanced diffusion MRI fiber tracking in neurosurgical and neurodegenerative disorders and neuroanatomical studies: A review. Biochim Biophys Acta 1842:2286-2297.

Acosta-Cabronero J, Nestor PJ (2014) Diffusion tensor imaging in Alzheimer's disease: insights into the limbic-diencephalic network and methodological considerations. Front Aging Neurosci 6:266.

Acosta-Cabronero J, Williams GB, Pengas G, Nestor PJ (2010) Absolute diffusivities define the landscape of white matter degeneration in Alzheimer's disease. Brain 133:529-539.

Adamson C, Yuan W, Babcock L, Leach JL, Seal ML, Holland SK, Wade SL (2013) Diffusion tensor imaging detects white matter abnormalities and associated cognitive deficits in chronic adolescent TBI. Brain Inj 27:454-463.

Adelson PD, Kochanek PM (1998) Head injury in children. J Child Neurol 13:2-15.

Ahmed Z, Cooper J, Murray TK, Garn K, McNaughton E, Clarke H, Parhizkar S, Ward MA, Cavallini A, Jackson S, Bose S, Clavaguera F, Tolnay M, Lavenir I, Goedert M, Hutton ML, O'Neill MJ (2014) A novel in vivo model of tau propagation with rapid and progressive neurofibrillary tangle pathology: the pattern of spread is determined by connectivity, not proximity. Acta Neuropathol 127:667-683.

Alexander AL, Lee JE, Lazar M, Field AS (2007) Diffusion tensor imaging of the brain. Neurotherapeutics 4:316-329.

Alhilali LM, Yaeger K, Collins M, Fakhran S (2014) Detection of central white matter injury underlying vestibulopathy after mild traumatic brain injury. Radiology 272:224-232.

Anderson V, Spencer-Smith M, Leventer R, Coleman L, Anderson P, Williams J, Greenham M, Jacobs R (2009) Childhood brain insult: can age at insult help us predict outcome? Brain 132:45-56.

Ashall S. JA, Siderowf A., Devous M., Roberson E., Russell D, Miller B., Johnson K., Jagust W., Boxer A., Rabinovici G. (2015) Tau Imaging in Progressive Supranuclear Palsy using 18F-AV1451. Poster Presentation, 19th International Congress of Parkison's Diease and Movement Disorders.

Astafiev SV, Shulman GL, Metcalf NV, Rengachary J, Mac Donald CL, Harrington DL, Maruta J, Shimony JS, Ghajar J, Diwakar M, Huang MX, Lee RR, Corbetta M (2015) Abnormal White Matter Blood-Oxygen-Level-Dependent Signals in Chronic Mild Traumatic Brain Injury. J Neurotrauma.

Barkhoudarian G, Hovda DA, Giza CC (2011) The molecular pathophysiology of concussive brain injury. Clin Sports Med 30:33-48, vii-iii.

Barlow KM, Crawford S, Stevenson A, Sandhu SS, Belanger F, Dewey D (2010) Epidemiology of postconcussion syndrome in pediatric mild traumatic brain injury. Pediatrics 126:e374-381.

Barrio JR, Small GW, Wong KP, Huang SC, Liu J, Merrill DA, Giza CC, Fitzsimmons RP, Omalu B, Bailes J, Kepe V (2015) In vivo characterization of chronic traumatic encephalopathy using [F-18]FDDNP PET brain imaging. Proc Natl Acad Sci U S A 112:E2039-2047.

Barth V, Need A (2014) Identifying novel radiotracers for PET imaging of the brain: application of LC-MS/MS to tracer identification. ACS Chem Neurosci 5:1148-1153.

Basser PJ, Mattiello J, LeBihan D (1994) MR diffusion tensor spectroscopy and imaging. Biophys J 66:259-267.

Basser PJ, Pierpaoli C (1996) Microstructural and physiological features of tissues elucidated by quantitative-diffusion-tensor MRI. J Magn Reson B 111:209-219.

Baugh CM, Stamm JM, Riley DO, Gavett BE, Shenton ME, Lin A, Nowinski CJ, Cantu RC, McKee AC, Stern RA (2012) Chronic traumatic encephalopathy: neurodegeneration following repetitive concussive and subconcussive brain trauma. Brain Imaging Behav 6:244-254.

Bazarian JJ, Zhu T, Zhong J, Janigro D, Rozen E, Roberts A, Javien H, Merchant-Borna K, Abar B, Blackman EG (2014) Persistent, long-term cerebral white matter changes after sports-related repetitive head impacts. Plos One 9:e94734.

Beckwith JG, Chu JJ, Greenwald RM (2007) Validation of a noninvasive system for measuring head acceleration for use during boxing competition. J Appl Biomech 23:238-244.

Bergsneider M, Hovda DA, Lee SM, Kelly DF, McArthur DL, Vespa PM, Lee JH, Huang SC, Martin NA, Phelps ME, Becker DP (2000) Dissociation of cerebral glucose metabolism and level of consciousness during the period of metabolic depression following human traumatic brain injury. J Neurotrauma 17:389-401.

Besga A, Termenon M, Grana M, Echeveste J, Perez JM, Gonzalez-Pinto A (2012) Discovering Alzheimer's disease and bipolar disorder white matter effects building computer aided diagnostic systems on brain diffusion tensor imaging features. Neurosci Lett 520:71-76.

Billingsley ML, Kincaid RL (1997) Regulated phosphorylation and dephosphorylation of tau protein: effects on microtubule interaction, intracellular trafficking and neurodegeneration. Biochem J 323 (Pt 3):577-591.

Blennow K, Hardy J, Zetterberg H (2012) The neuropathology and neurobiology of traumatic brain injury. Neuron 76:886-899.

Blennow K, Mattsson N, Scholl M, Hansson O, Zetterberg H (2015) Amyloid biomarkers in Alzheimer's disease. Trends Pharmacol Sci 36:297-309.

Blumbergs PC, Scott G, Manavis J, Wainwright H, Simpson DA, McLean AJ (1994) Staining of amyloid precursor protein to study axonal damage in mild head injury. Lancet 344:1055-1056.

Boluda S, Iba M, Zhang B, Raible KM, Lee VMY, Trojanowski JQ (2015) Differential induction and spread of tau pathology in young PS19 tau transgenic mice following intracerebral injections of pathological tau from Alzheimer’s disease or corticobasal degeneration brains. Acta Neuropathol 129:221-237.

Bonnelle V, Ham TE, Leech R, Kinnunen KM, Mehta MA, Greenwood RJ, Sharp DJ (2012) Salience network integrity predicts default mode network function after traumatic brain injury. Proc Natl Acad Sci U S A 109:4690-4695.

Bonnelle V, Leech R, Kinnunen KM, Ham TE, Beckmann CF, De Boissezon X, Greenwood RJ, Sharp DJ (2011) Default mode network connectivity predicts sustained attention deficits after traumatic brain injury. J Neurosci 31:13442-13451.

Borich M, Babul AN, Huang PH, Boyd L, Virji-Babul N (2015) Alterations in resting state brain networks in concussed adolescent athletes. J Neurotrauma.

Brorson JR, Manzolillo PA, Miller RJ (1994) Ca2+ entry via AMPA/KA receptors and excitotoxicity in cultured cerebellar Purkinje cells. J Neurosci 14:187-197.

Brown CJ, Miller SP, Booth BG, Andrews S, Chau V, Poskitt KJ, Hamarneh G (2014) Structural network analysis of brain development in young preterm neonates. Neuroimage 101:667-680.

Buckner RL A-HJ, Schacter DL (2008) The brain's default mode network: anatomy, function, and relevance to disease. Ann N Y Acad Sci 1124:1-38.

Buki A, Povlishock JT (2006) All roads lead to disconnection?--Traumatic axonal injury revisited. Acta Neurochir (Wien) 148:181-193; discussion 193-184.

Bullmore E, Sporns O (2009) Complex brain networks: graph theoretical analysis of structural and functional systems. Nat Rev Neurosci 10:186-198.

Byrnes KR, Wilson CM, Brabazon F, von Leden R, Jurgens JS, Oakes TR, Selwyn RG (2013) FDG-PET imaging in mild traumatic brain injury: a critical review. Front Neuroenergetics 5.

Caeyenberghs K, Leemans A, De Decker C, Heitger M, Drijkoningen D, Linden CV, Sunaert S, Swinnen SP (2012) Brain connectivity and postural control in young traumatic brain injury patients: A diffusion MRI based network analysis. Neuroimage Clin 1:106-115.

Caeyenberghs K, Leemans A, Leunissen I, Gooijers J, Michiels K, Sunaert S, Swinnen SP (2014) Altered structural networks and executive deficits in traumatic brain injury patients. Brain Struct Funct 219:193-209.

Cao C, Slobounov S (2010) Alteration of cortical functional connectivity as a result of traumatic brain injury revealed by graph theory, ICA, and sLORETA analyses of EEG signals. IEEE Trans Neural Syst Rehabil Eng 18:11-19.

Caso F, Agosta F, Mattavelli D, Migliaccio R, Canu E, Magnani G, Marcone A, Copetti M, Falautano M, Comi G, Falini A, Filippi M (2015) White Matter Degeneration in Atypical Alzheimer Disease. Radiology 142766.

Castellanos NP, Leyva I, Buldu JM, Bajo R, Paul N, Cuesta P, Ordonez VE, Pascua CL, Boccaletti S, Maestu F, del-Pozo F (2011) Principles of recovery from traumatic brain injury: reorganization of functional networks. Neuroimage 55:1189-1199.

Chien DT, Bahri S, Szardenings AK, Walsh JC, Mu F, Su MY, Shankle WR, Elizarov A, Kolb HC (2013) Early clinical PET imaging results with the novel PHF-tau radioligand [F-18]-T807. J Alzheimers Dis 34:457-468.

Chong CD, Schwedt TJ (2015) White matter damage and brain network alterations in concussed patients: a review of recent diffusion tensor imaging and resting-state functional connectivity data. Curr Pain Headache Rep 19:485.

Collins-Praino LE, Francis YI, Griffith EY, Wiegman AF, Urbach J, Lawton A, Honig LS, Cortes E, Vonsattel JP, Canoll PD, Goldman JE, Brickman AM (2014) Soluble amyloid beta levels are elevated in the white matter of Alzheimer's patients, independent of cortical plaque severity. Acta Neuropathol Commun 2:83.

Corsellis JA, Brierley JB (1959) Observations on the pathology of insidious dementia following head injury. J Ment Sci 105:714-720.

Corsellis JA, Bruton CJ, Freeman-Browne D (1973) The aftermath of boxing. Psychol Med 3:270-303.

Courville CB (1962) Punch drunk. Its pathogenesis and pathology on the basis of a verified case. Bull Los Angel Neuro Soc 27:160-168.

Creed JA, DiLeonardi AM, Fox DP, Tessler AR, Raghupathi R (2011) Concussive brain trauma in the mouse results in acute cognitive deficits and sustained impairment of axonal function. J Neurotrauma 28:547-563.

Cubon VA, Putukian M, Boyer C, Dettwiler A (2011) A diffusion tensor imaging study on the white matter skeleton in individuals with sports-related concussion. J Neurotrauma 28:189-201.

Daneshvar DH, Goldstein LE, Kiernan PT, Stein TD, McKee AC (2015) Post-traumatic neurodegeneration and chronic traumatic encephalopathy. Mol Cell Neurosci.

de Jong HW, van Velden FH, Kloet RW, Buijs FL, Boellaard R, Lammertsma AA (2007) Performance evaluation of the ECAT HRRT: an LSO-LYSO double layer high resolution, high sensitivity scanner. Phys Med Biol 52:1505-1526.

De Vico Fallani F, Richiardi J, Chavez M, Achard S (2014) Graph analysis of functional brain networks: practical issues in translational neuroscience. Philos Trans R Soc Lond B Biol Sci 369.

Dettwiler A, Murugavel M, Putukian M, Cubon V, Furtado J, Osherson D (2014) Persistent differences in patterns of brain activation after sports-related concussion: a longitudinal functional magnetic resonance imaging study. J Neurotrauma 31:180-188.

Di Stefano G, Bachevalier J, Levin HS, Song JX, Scheibel RS, Fletcher JM (2000) Volume of focal brain lesions and hippocampal formation in relation to memory function after closed head injury in children. J Neurol Neurosurg Psychiatry 69:210-216.

Diener HC, Jansen JP, Reches A, Pascual J, Pitei D, Steiner TJ (2002) Efficacy, tolerability and safety of oral eletriptan and ergotamine plus caffeine (Cafergot) in the acute treatment of migraine: a multicentre, randomised, double-blind, placebo-controlled comparison. Eur Neurol 47:99-107.

Eierud C, Craddock RC, Fletcher S, Aulakh M, King-Casas B, Kuehl D, LaConte SM (2014) Neuroimaging after mild traumatic brain injury: Review and meta-analysis. Neuroimage Clin 4:283-294.

Faden AI, Simon RP (1988) A potential role for excitotoxins in the pathophysiology of spinal cord injury. Ann Neurol 23:623-626.

Fagerholm ED, Hellyer PJ, Scott G, Leech R, Sharp DJ (2015) Disconnection of network hubs and cognitive impairment after traumatic brain injury. Brain 138:1696-1709.

Falcone T, Janigro D, Lovell R, Simon B, Brown CA, Herrera M, Myint AM, Anand A (2015) S100B blood levels and childhood trauma in adolescent inpatients. J Psychiatr Res 62:14-22.

Filley CM (2005) White matter and behavioral neurology. Ann N Y Acad Sci 1064:162-183.

Fitch MT, Silver J (2008) CNS injury, glial scars, and inflammation: Inhibitory extracellular matrices and regeneration failure. Exp Neurol 209:294-301.

Fodero-Tavoletti MT, Furumoto S, Taylor L, McLean CA, Mulligan RS, Birchall I, Harada R, Masters CL, Yanai K, Kudo Y, Rowe CC, Okamura N, Villemagne VL (2014) Assessing THK523 selectivity for tau deposits in Alzheimer's disease and non-Alzheimer's disease tauopathies. Alzheimers Res Ther 6:11.

Fodero-Tavoletti MT, Okamura N, Furumoto S, Mulligan RS, Connor AR, McLean CA, Cao D, Rigopoulos A, Cartwright GA, O'Keefe G, Gong S, Adlard PA, Barnham KJ, Rowe CC, Masters CL, Kudo Y, Cappai R, Yanai K, Villemagne VL (2011) 18F-THK523: a novel in vivo tau imaging ligand for Alzheimer's disease. Brain 134:1089-1100.

Fox WC, Park MS, Belverud S, Klugh A, Rivet D, Tomlin JM (2013) Contemporary imaging of mild TBI: the journey toward diffusion tensor imaging to assess neuronal damage. Neurol Res 35:223-232.

Fujita M, Imaizumi M, Zoghbi SS, Fujimura Y, Farris AG, Suhara T, Hong J, Pike VW, Innis RB (2008) Kinetic analysis in healthy humans of a novel positron emission tomography radioligand to image the peripheral benzodiazepine receptor, a potential biomarker for inflammation. Neuroimage 40:43-52.

Garcia-Panach J, Lull N, Lull JJ, Ferri J, Martinez C, Sopena P, Robles M, Chirivella J, Noe E (2011) A voxel-based analysis of FDG-PET in traumatic brain injury: regional metabolism and relationship between the thalamus and cortical areas. J Neurotrauma 28:1707-1717.

Gardner A, Kay-Lambkin F, Stanwell P, Donnelly J, Williams WH, Hiles A, Schofield P, Levi C, Jones DK (2012) A systematic review of diffusion tensor imaging findings in sports-related concussion. J Neurotrauma 29:2521-2538.

Gavett BE, Stern RA, McKee AC (2011) Chronic traumatic encephalopathy: a potential late effect of sport-related concussive and subconcussive head trauma. Clin Sports Med 30:179-188, xi.

Gerig G, Gouttard S, Corouge I (2004) Analysis of brain white matter via fiber tract modeling. Conf Proc IEEE Eng Med Biol Soc 6:4421-4424.

Gerson JE, Sengupta U, Lasagna-Reeves CA, Guerrero-Munoz MJ, Troncoso J, Kayed R (2014) Characterization of tau oligomeric seeds in progressive supranuclear palsy. Acta Neuropathol Commun 2:73.

Giza CC, Griesbach GS, Hovda DA (2005) Experience-dependent behavioral plasticity is disturbed following traumatic injury to the immature brain. Behav Brain Res 157:11-22.

Giza CC, Hovda DA (2001) The Neurometabolic Cascade of Concussion. J Athl Train 36:228-235.

Giza CC, Hovda DA (2014) The New Neurometabolic Cascade of Concussion. Neurosurgery 75:S24-S33.

Goldberg MP, Weiss JH, Pham PC, Choi DW (1987) N-methyl-D-aspartate receptors mediate hypoxic neuronal injury in cortical culture. J Pharmacol Exp Ther 243:784-791.

Greenwald RM, Gwin JT, Chu JJ, Crisco JJ (2008) Head impact severity measures for evaluating mild traumatic brain injury risk exposure. Neurosurgery 62:789-798; discussion 798.

Greicius MD, Kimmel DL (2012) Neuroimaging insights into network-based neurodegeneration. Curr Opin Neurol 25:727-734.

Greicius MD, Krasnow B, Reiss AL, Menon V (2003) Functional connectivity in the resting brain: a network analysis of the default mode hypothesis. Proc Natl Acad Sci U S A 100:253-258.

Greicius MD, Supekar K, Menon V, Dougherty RF (2009) Resting-state functional connectivity reflects structural connectivity in the default mode network. Cereb Cortex 19:72-78.

Guskiewicz KM, Marshall SW, Bailes J, McCrea M, Cantu RC, Randolph C, Jordan BD (2005) Association between recurrent concussion and late-life cognitive impairment in retired professional football players. Neurosurgery 57:719-726; discussion 719-726.

Guskiewicz KM, McCrea M, Marshall SW, Cantu RC, Randolph C, Barr W, Onate JA, Kelly JP (2003) Cumulative effects associated with recurrent concussion in collegiate football players: the NCAA Concussion Study. Jama 290:2549-2555.

Guye M, Bettus G, Bartolomei F, Cozzone PJ (2010) Graph theoretical analysis of structural and functional connectivity MRI in normal and pathological brain networks. MAGMA 23:409-421.

Hammoud DA, Wasserman BA (2002) Diffuse axonal injuries: pathophysiology and imaging. Neuroimaging Clin N Am 12:205-216.

Han K, Mac Donald CL, Johnson AM, Barnes Y, Wierzechowski L, Zonies D, Oh J, Flaherty S, Fang R, Raichle ME, Brody DL (2014) Disrupted modular organization of resting-state cortical functional connectivity in U.S. military personnel following concussive 'mild' blast-related traumatic brain injury. Neuroimage 84:76-96.

Harada R, Okamura N, Furumoto S, Tago T, Maruyama M, Higuchi M, Yoshikawa T, Arai H, Iwata R, Kudo Y, Yanai K (2013) Comparison of the binding characteristics of [18F]THK-523 and other amyloid imaging tracers to Alzheimer's disease pathology. Eur J Nucl Med Mol Imaging 40:125-132.

Hashimoto H, Kawamura K, Igarashi N, Takei M, Fujishiro T, Aihara Y, Shiomi S, Muto M, Ito T, Furutsuka K, Yamasaki T, Yui J, Xie L, Ono M, Hatori A, Nemoto K, Suhara T, Higuchi M, Zhang MR (2014) Radiosynthesis, Photoisomerization, Biodistribution, and

Metabolite Analysis of 11C-PBB3 as a Clinically Useful PET Probe for Imaging of Tau Pathology. J Nucl Med.

Hemphill MA, Dabiri BE, Gabriele S, Kerscher L, Franck C, Goss JA, Alford PW, Parker KK (2011) A possible role for integrin signaling in diffuse axonal injury. Plos One 6:e22899.

Henry LC, Tremblay J, Tremblay S, Lee A, Brun C, Lepore N, Theoret H, Ellemberg D, Lassonde M (2011) Acute and chronic changes in diffusivity measures after sports concussion. J Neurotrauma 28:2049-2059.

Higginson IJ, Gao W, Saleem TZ, Chaudhuri KR, Burman R, McCrone P, Leigh PN (2012) Symptoms and quality of life in late stage Parkinson syndromes: a longitudinal community study of predictive factors. Plos One 7:e46327.

Hilgetag CC, Goulas A (2015) Is the brain really a small-world network? Brain Struct Funct.

Hippocrates (460-370 BC).

Hong YT, Veenith T, Dewar D, Outtrim JG, Mani V, Williams C, Pimlott S, Hutchinson PJ, Tavares A, Canales R, Mathis CA, Klunk WE, Aigbirhio FI, Coles JP, Baron JC, Pickard JD, Fryer TD, Stewart W, Menon DK (2014) Amyloid imaging with carbon 11-labeled Pittsburgh compound B for traumatic brain injury. JAMA Neurol 71:23-31.

Hulkower MB, Poliak DB, Rosenbaum SB, Zimmerman ME, Lipton ML (2013) A decade of DTI in traumatic brain injury: 10 years and 100 articles later. AJNR Am J Neuroradiol 34:2064-2074.

Humayun MS, Presty SK, Lafrance ND, Holcomb HH, Loats H, Long DM, Wagner HN, Gordon B (1989) Local cerebral glucose abnormalities in mild closed head injured patients with cognitive impairments. Nucl Med Commun 10:335-344.

Hüppi PS, Dubois J (2006) Diffusion tensor imaging of brain development. Seminars in Fetal and Neonatal Medicine 11:489-497.

Irimia A, Wang B, Aylward SR, Prastawa MW, Pace DF, Gerig G, Hovda DA, Kikinis R, Vespa PM, Van Horn JD (2012) Neuroimaging of structural pathology and connectomics in traumatic brain injury: Toward personalized outcome prediction. Neuroimage Clin 1:1-17.

Ito J, Marmarou A, Barzo P, Fatouros P, Corwin F (1996) Characterization of edema by diffusion-weighted imaging in experimental traumatic brain injury. J Neurosurg 84:97-103.

Jin G, Wang LH, Ji XF, Chi TY, Qi Y, Jiao Q, Xu Q, Zhou XY, Zhang R, Zou LB (2014) Xanthoceraside rescues learning and memory deficits through attenuating beta-amyloid deposition and tau hyperphosphorylation in APP mice. Neurosci Lett 573:58-63.

Johnson B, Zhang K, Gay M, Horovitz S, Hallett M, Sebastianelli W, Slobounov S (2012) Alteration of brain default network in subacute phase of injury in concussed individuals: resting-state fMRI study. Neuroimage 59:511-518.

Johnson VE, Stewart JE, Begbie FD, Trojanowski JQ, Smith DH, Stewart W (2013a) Inflammation and white matter degeneration persist for years after a single traumatic brain injury. Brain 136:28-42.

Johnson VE, Stewart W, Smith DH (2013b) Axonal pathology in traumatic brain injury. Exp Neurol 246:35-43.

Kaiser M, Hilgetag CC (2010) Optimal hierarchical modular topologies for producing limited sustained activation of neural networks. Front Neuroinform 4:8.

Kato T, Nakayama N, Yasokawa Y, Okumura A, Shinoda J, Iwama T (2007) Statistical image analysis of cerebral glucose metabolism in patients with cognitive impairment following diffuse traumatic brain injury. J Neurotrauma 24:919-926.

Kawamata T, Katayama Y, Hovda DA, Yoshino A, Becker DP (1995) Lactate accumulation following concussive brain injury: the role of ionic fluxes induced by excitatory amino acids. Brain Res 674:196-204.

Keightley ML, Sinopoli KJ, Davis KD, Mikulis DJ, Wennberg R, Tartaglia MC, Chen JK, Tator CH (2014) Is there evidence for neurodegenerative change following traumatic brain injury in children and youth? A scoping review. Front Hum Neurosci 8:139.

Kepe V, Bordelon Y, Boxer A, Huang SC, Liu J, Thiede FC, Mazziotta JC, Mendez MF, Donoghue N, Small GW, Barrio JR (2013) PET Imaging of Neuropathology in Tauopathies: Progressive Supranuclear Palsy. J Alzheimers Dis 36:145-153.

Khanna N, Altmeyer W, Zhuo J, Steven A (2015) Functional Neuroimaging: Fundamental Principles and Clinical Applications. Neuroradiol J.

Khlistunova I, Biernat J, Wang Y, Pickhardt M, von Bergen M, Gazova Z, Mandelkow E, Mandelkow EM (2006) Inducible expression of Tau repeat domain in cell models of tauopathy: aggregation is toxic to cells but can be reversed by inhibitor drugs. The Journal of biological chemistry 281:1205-1214.

Kiernan PT, Montenigro PH, Solomon TM, McKee AC (2015) Chronic traumatic encephalopathy: a neurodegenerative consequence of repetitive traumatic brain injury. Semin Neurol 35:20-28.

Kinnunen KM, Greenwood R, Powell JH, Leech R, Hawkins PC, Bonnelle V, Patel MC, Counsell SJ, Sharp DJ (2011) White matter damage and cognitive impairment after traumatic brain injury. Brain 134:449-463.

Kochanek PM (2006) Pediatric traumatic brain injury: quo vadis? Dev Neurosci 28:244-255.

Lange RT, Iverson GL, Brubacher JR, Madler B, Heran MK (2012) Diffusion tensor imaging findings are not strongly associated with postconcussional disorder 2 months following mild traumatic brain injury. J Head Trauma Rehabil 27:188-198.

Lange RT, Panenka WJ, Shewchuk JR, Heran MK, Brubacher JR, Bioux S, Eckbo R, Shenton ME, Iverson GL (2015) Diffusion tensor imaging findings and postconcussion symptom reporting six weeks following mild traumatic brain injury. Arch Clin Neuropsychol 30:7-25.

Langlois JA, Rutland-Brown W, Wald MM (2006) The epidemiology and impact of traumatic brain injury: a brief overview. J Head Trauma Rehabil 21:375-378.

Le Bihan D, Breton E, Lallemand D, Grenier P, Cabanis E, Laval-Jeantet M (1986) MR imaging of intravoxel incoherent motions: application to diffusion and perfusion in neurologic disorders. Radiology 161:401-407.

Leemans A. JB, Sijbers J., Jones DK. (2009) ExploreDTI: a graphical toolbox for processing, analyzing, and visualizing diffusion MR data. 17th Annual Meeting of Intl Soc Mag Reson Med p. 3537.

Lei P, Ayton S, Appukuttan AT, Volitakis I, Adlard PA, Finkelstein DI, Bush AI (2015) Clioquinol rescues Parkinsonism and dementia phenotypes of the tau knockout mouse. Neurobiol Dis.

Len TK, Neary JP (2011) Cerebrovascular pathophysiology following mild traumatic brain injury. Clin Physiol Funct Imaging 31:85-93.

Liliang PC, Liang CL, Lu K, Wang KW, Weng HC, Hsieh CH, Tsai YD, Chen HJ (2010) Relationship between injury severity and serum tau protein levels in traumatic brain injured rats. Resuscitation 81:1205-1208.

Ling H, Hardy J, Zetterberg H (2015) Neurological consequences of traumatic brain injuries in sports. Mol Cell Neurosci.

Ling JM, Pena A, Yeo RA, Merideth FL, Klimaj S, Gasparovic C, Mayer AR (2012) Biomarkers of increased diffusion anisotropy in semi-acute mild traumatic brain injury: a longitudinal perspective. Brain 135:1281-1292.

Ljungqvist J, Nilsson D, Ljungberg M, Sorbo A, Esbjornsson E, Eriksson-Ritzen C, Skoglund T (2011) Longitudinal study of the diffusion tensor imaging properties of the corpus callosum in acute and chronic diffuse axonal injury. Brain Inj 25:370-378.

Long L, Cai XD, Wei XB, Liao JC, Xu YQ, Gao HM, Chen XH, Wang Q (2015) Progressive supranuclear palsy: what do we know about it? Curr Med Chem 22:1182-1193.

Lupi A, Bertagnoni G, Borghero A, Picelli A, Cuccurullo V, Zanco P (2014) 18FDG-PET/CT in traumatic brain injury patients: the relative hypermetabolism of vermis cerebelli as a medium and long term predictor of outcome. Curr Radiopharm 7:57-62.

Lynall RC, Laudner KG, Mihalik JP, Stanek JM (2013) Concussion-assessment and -management techniques used by athletic trainers. J Athl Train 48:844-850.

Ma'ayan A (2011) Introduction to Network Analysis in Systems Biology. Sci Signal 4:tr5.

Malkki H (2014) Traumatic brain injury: PET imaging detects amyloid deposits after TBI. Nat Rev Neurol 10:3.

Maroon JC, Winkelman R, Bost J, Amos A, Mathyssek C, Miele V (2015) Chronic Traumatic Encephalopathy in Contact Sports: A Systematic Review of All Reported Pathological Cases. Plos One 10.

Martland HS (1928) PUnch drunk. Journal of the American Medical Association 91:1103-1107.

Maruyama M, Shimada H, Suhara T, Shinotoh H, Ji B, Maeda J, Zhang MR, Trojanowski JQ, Lee VM, Ono M, Masamoto K, Takano H, Sahara N, Iwata N, Okamura N, Furumoto S, Kudo Y, Chang Q, Saido TC, Takashima A, Lewis J, Jang MK, Aoki I, Ito H, Higuchi M (2013) Imaging of tau pathology in a tauopathy mouse model and in Alzheimer patients compared to normal controls. Neuron 79:1094-1108.

Mayer AR, Bellgowan PS, Hanlon FM (2015) Functional magnetic resonance imaging of mild traumatic brain injury. Neurosci Biobehav Rev 49:8-18.

Mayer AR, Ling J, Mannell MV, Gasparovic C, Phillips JP, Doezema D, Reichard R, Yeo RA (2010) A prospective diffusion tensor imaging study in mild traumatic brain injury. Neurology 74:643-650.

McBride DL (2012) Concussion: the hidden injury. J Pediatr Nurs 27:763-764.

McCrea M, Guskiewicz K, Randolph C, Barr WB, Hammeke TA, Marshall SW, Kelly JP (2009) Effects of a symptom-free waiting period on clinical outcome and risk of reinjury after sport-related concussion. Neurosurgery 65:876-882; discussion 882-873.

McCrea M, Guskiewicz KM, Marshall SW, Barr W, Randolph C, Cantu RC, Onate JA, Yang J, Kelly JP (2003) Acute effects and recovery time following concussion in collegiate football players: the NCAA Concussion Study. Jama 290:2556-2563.

McCrory P, Davis G (2005) Paediatric sport related concussion pilot study. Br J Sports Med 39:116.

McCrory P, Meeuwisse WH, Aubry M, Cantu RC, Dvorak J, Echemendia RJ, Engebretsen L, Johnston K, Kutcher JS, Raftery M, Sills A, Benson BW, Davis GA, Ellenbogen R, Guskiewicz KM, Herring SA, Iverson GL, Jordan BD, Kissick J, McCrea M, McIntosh

AS, Maddocks D, Makdissi M, Purcell L, Putukian M, Schneider K, Tator CH, Turner M (2013) Consensus statement on concussion in sport: the 4th International Conference on Concussion in Sport, Zurich, November 2012. J Athl Train 48:554-575.

McKee AC, Cantu RC, Nowinski CJ, Hedley-Whyte ET, Gavett BE, Budson AE, Santini VE, Lee HS, Kubilus CA, Stern RA (2009) Chronic traumatic encephalopathy in athletes: progressive tauopathy after repetitive head injury. J Neuropathol Exp Neurol 68:709-735.

McKee AC, Daneshvar DH, Alvarez VE, Stein TD (2014) The neuropathology of sport. Acta Neuropathol 127:29-51.

McKee AC, Stein TD, Kiernan PT, Alvarez VE (2015) The neuropathology of chronic traumatic encephalopathy. Brain Pathol 25:350-364.

McKee AC, Stern RA, Nowinski CJ, Stein TD, Alvarez VE, Daneshvar DH, Lee HS, Wojtowicz SM, Hall G, Baugh CM, Riley DO, Kubilus CA, Cormier KA, Jacobs MA, Martin BR, Abraham CR, Ikezu T, Reichard RR, Wolozin BL, Budson AE, Goldstein LE, Kowall NW, Cantu RC (2013) The spectrum of disease in chronic traumatic encephalopathy. Brain 136:43-64.

McKenna BS, Theilmann RJ, Sutherland AN, Eyler LT (2015) Fusing Functional MRI and Diffusion Tensor Imaging Measures of Brain Function and Structure to Predict Working Memory and Processing Speed Performance among Inter-episode Bipolar Patients. J Int Neuropsychol Soc 1-12.

Meijer FJ, Bloem BR, Mahlknecht P, Seppi K, Goraj B (2013) Update on diffusion MRI in Parkinson's disease and atypical parkinsonism. J Neurol Sci 332:21-29.

Mielke MM, Savica R, Wiste HJ, Weigand SD, Vemuri P, Knopman DS, Lowe VJ, Roberts RO, Machulda MM, Geda YE, Petersen RC, Jack CR, Jr. (2014) Head trauma and in vivo measures of amyloid and neurodegeneration in a population-based study. Neurology 82:70-76.

Mitra K, Gangopadhaya PK, Das SK (2003) Parkinsonism plus syndrome--a review. Neurol India 51:183-188.

Mitsis EM, Riggio S, Kostakoglu L, Dickstein DL, Machac J, Delman B, Goldstein M, Jennings D, D'Antonio E, Martin J, Naidich TP, Aloysi A, Fernandez C, Seibyl J, DeKosky ST, Elder GA, Marek K, Gordon W, Hof PR, Sano M, Gandy S (2014) Tauopathy PET and amyloid PET in the diagnosis of chronic traumatic encephalopathies: studies of a retired NFL player and of a man with FTD and a severe head injury. Transl Psychiatry 4:e441.

Morales R, Green KM, Soto C (2009) Cross currents in protein misfolding disorders: interactions and therapy. CNS Neurol Disord Drug Targets 8:363-371.

Murugavel M, Cubon V, Putukian M, Echemendia R, Cabrera J, Osherson D, Dettwiler A (2014) A longitudinal diffusion tensor imaging study assessing white matter fiber tracts after sports-related concussion. J Neurotrauma 31:1860-1871.

Nandhagopal R, McKeown MJ, Stoessl AJ (2008) Functional imaging in Parkinson disease. Neurology 70:1478-1488.

Nariai T, Inaji M, Tanaka Y, Hiura M, Hosoda C, Ishii K, Ohno K (2013) PET molecular imaging to investigate higher brain dysfunction in patients with neurotrauma. Acta Neurochir Suppl 118:251-254.

Nath U, Ben-Shlomo Y, Thomson RG, Morris HR, Wood NW, Lees AJ, Burn DJ (2001) The prevalence of progressive supranuclear palsy (Steele-Richardson-Olszewski syndrome) in the UK. Brain 124:1438-1449.

Ng HK, Mahaliyana RD, Poon WS (1994) The pathological spectrum of diffuse axonal injury in blunt head trauma: assessment with axon and myelin strains. Clin Neurol Neurosurg 96:24-31.

Nicholls DG, Budd SL (1998) Mitochondria and neuronal glutamate excitotoxicity. Biochim Biophys Acta 1366:97-112.

Noble JM, Hesdorffer DC (2013) Sport-Related Concussions: A Review of Epidemiology, Challenges in Diagnosis, and Potential Risk Factors. Neuropsychol Rev.

Ohhashi G, Tani S, Murakami S, Kamio M, Abe T, Ohtuki J (2002) Problems in health management of professional boxers in Japan. Br J Sports Med 36:346-352; discussion 353.

Okamura N, Furumoto S, Fodero-Tavoletti MT, Mulligan RS, Harada R, Yates P, Pejoska S, Kudo Y, Masters CL, Yanai K, Rowe CC, Villemagne VL (2014) Non-invasive assessment of Alzheimer's disease neurofibrillary pathology using 18F-THK5105 PET. Brain 137:1762-1771.

Okamura N, Furumoto S, Harada R, Tago T, Yoshikawa T, Fodero-Tavoletti M, Mulligan RS, Villemagne VL, Akatsu H, Yamamoto T, Arai H, Iwata R, Yanai K, Kudo Y (2013) Novel 18F-labeled arylquinoline derivatives for noninvasive imaging of tau pathology in Alzheimer disease. J Nucl Med 54:1420-1427.

Oppenheimer DR (1968) Microscopic lesions in the brain following head injury. J Neurol Neurosurg Psychiatry 31:299-306.

Otte E, Rousseau R (2002) Social network analysis: a powerful strategy, also for the information sciences. Journal of Information Science 28:441-453.

Pandit AS, Expert P, Lambiotte R, Bonnelle V, Leech R, Turkheimer FE, Sharp DJ (2013) Traumatic brain injury impairs small-world topology. Neurology 80:1826-1833.

Papo D, Buldu JM, Boccaletti S, Bullmore ET (2014) Complex network theory and the brain. Philos Trans R Soc Lond B Biol Sci 369.

Parker HL (1934) Traumatic Encephalopathy (`Punch Drunk') of Professional Pugilists. J Neurol Psychopathol 15:20-28.

Peskind ER, Petrie EC, Cross DJ, Pagulayan K, McCraw K, Hoff D, Hart K, Yu CE, Raskind MA, Cook DG, Minoshima S (2011) Cerebrocerebellar hypometabolism associated with repetitive blast exposure mild traumatic brain injury in 12 Iraq war Veterans with persistent post-concussive symptoms. Neuroimage 54 Suppl 1:S76-82.

Pettus EH, Povlishock JT (1996) Characterization of a distinct set of intra-axonal ultrastructural changes associated with traumatically induced alteration in axolemmal permeability. Brain Res 722:1-11.

Phelps ME, Hoffman EJ, Mullani NA, Ter-Pogossian MM (1975) Application of annihilation coincidence detection to transaxial reconstruction tomography. J Nucl Med 16:210-224.

Prins M, Greco T, Alexander D, Giza CC (2013) The pathophysiology of traumatic brain injury at a glance. Dis Model Mech 6:1307-1315.

Provenzano FA, Jordan B, Tikofsky RS, Saxena C, Van Heertum RL, Ichise M (2010) F-18 FDG PET imaging of chronic traumatic brain injury in boxers: a statistical parametric analysis. Nucl Med Commun 31:952-957.

Purcell L, Harvey J, Seabrook JA (2015) Patterns of Recovery Following Sport-Related Concussion in Children and Adolescents. Clin Pediatr (Phila).

Queen SA, Chen MJ, Feeney DM (1997) d-Amphetamine attenuates decreased cerebral glucose utilization after unilateral sensorimotor cortex contusion in rats. Brain Res 777:42-50.

Quintero L, Sayed T, Wahba MM (2013) Safety models incorporating graph theory based transit indicators. Accid Anal Prev 50:635-644.

Raichle ME, MacLeod AM, Snyder AZ, Powers WJ, Gusnard DA, Shulman GL (2001) A default mode of brain function. Proceedings of the National Academy of Sciences 98:676-682.

Raichle ME, Mintun MA (2006) Brain work and brain imaging. Annu Rev Neurosci 29:449-476.

Ravina B, Eidelberg D, Ahlskog JE, Albin RL, Brooks DJ, Carbon M, Dhawan V, Feigin A, Fahn S, Guttman M, Gwinn-Hardy K, McFarland H, Innis R, Katz RG, Kieburtz K, Kish SJ, Lange N, Langston JW, Marek K, Morin L, Moy C, Murphy D, Oertel WH, Oliver G, Palesch Y, Powers W, Seibyl J, Sethi KD, Shults CW, Sheehy P, Stoessl AJ, Holloway R (2005) The role of radiotracer imaging in Parkinson disease. Neurology 64:208-215.

Reeves TM, Phillips LL, Povlishock JT (2005) Myelinated and unmyelinated axons of the corpus callosum differ in vulnerability and functional recovery following traumatic brain injury. Exp Neurol 196:126-137.

Rubinov M, Sporns O (2010) Complex network measures of brain connectivity: uses and interpretations. Neuroimage 52:1059-1069.

Schmahmann JD, Smith EE, Eichler FS, Filley CM (2008) Cerebral white matter: neuroanatomy, clinical neurology, and neurobehavioral correlates. Ann N Y Acad Sci 1142:266-309.

Shah M, Catafau AM (2014) Molecular Imaging Insights into Neurodegeneration: Focus on Tau PET Radiotracers. J Nucl Med 55:871-874.

Shao X, Carpenter GM, Desmond TJ, Sherman P, Quesada CA, Fawaz M, Brooks AF, Kilbourn MR, Albin RL, Frey KA, Scott PJ (2012) Evaluation of [(11)C]N-Methyl Lansoprazole as a Radiopharmaceutical for PET Imaging of Tau Neurofibrillary Tangles. ACS Med Chem Lett 3:936-941.

Sharp DJ, Scott G, Leech R (2014) Network dysfunction after traumatic brain injury. Nat Rev Neurol 10:156-166.

Shin J, Kepe V, Barrio JR, Small GW (2011) The merits of FDDNP-PET imaging in Alzheimer's disease. J Alzheimers Dis 26 Suppl 3:135-145.

Shin SS, Pathak S, Presson N, Bird W, Wagener L, Schneider W, Okonkwo DO, Fernandez-Miranda JC (2014) Detection of white matter injury in concussion using high-definition fiber tractography. Prog Neurol Surg 28:86-93.

Shoghi-Jadid K, Small GW, Agdeppa ED, Kepe V, Ercoli LM, Siddarth P, Read S, Satyamurthy N, Petric A, Huang SC, Barrio JR (2002) Localization of neurofibrillary tangles and beta-amyloid plaques in the brains of living patients with Alzheimer disease. Am J Geriatr Psychiatry 10:24-35.

Shrey DW, Griesbach GS, Giza CC (2011) Physical Medicine and Rehabilitation Clinics of North America 2011 The Pathophysiology of Concussions in Youth. Phys Med Rehabil Clin N Am 22:577-602.

Shukla R, Sinha M, Kumar R, Singh D (2009) ‘Hummingbird’ sign in progressive supranuclear palsy. Ann Indian Acad Neurol 12:133.

Shumskaya E, Andriessen TM, Norris DG, Vos PE (2012) Abnormal whole-brain functional networks in homogeneous acute mild traumatic brain injury. Neurology 79:175-182.

Small GW, Kepe V, Siddarth P, Ercoli LM, Merrill DA, Donoghue N, Bookheimer SY, Martinez J, Omalu B, Bailes J, Barrio JR (2013) PET Scanning of Brain Tau in Retired National Football League Players: Preliminary Findings. The American Journal of Geriatric Psychiatry 21:138-144.

Small GW, Siddarth P, Kepe V, Ercoli LM, Burggren AC, Bookheimer SY, Miller KJ, Kim J, Lavretsky H, Huang SC, Barrio JR (2012) Prediction of cognitive decline by positron emission tomography of brain amyloid and tau. Arch Neurol 69:215-222.

Smith-Forrester J, Sun, J., Kusch, C., Barrable, B., Panenka, W., Virji-Babul, N. (2015) Sports Concussion Assessment Tool 3 (SCAT3): Baseline values in adolescent male ice hockey players. Submitted.

Sporns O, Honey CJ (2006) Small worlds inside big brains. Proc Natl Acad Sci U S A 103:19219-19220.

Stam CJ (2014) Modern network science of neurological disorders. Nat Rev Neurosci 15:683-695.

Stamelou M, Bhatia KP (2015) Atypical parkinsonism: diagnosis and treatment. Neurol Clin 33:39-56.

Steele JC, Richardson JC, Olszewski J (1964) PROGRESSIVE SUPRANUCLEAR PALSY. A HETEROGENEOUS DEGENERATION INVOLVING THE BRAIN STEM, BASAL GANGLIA AND CEREBELLUM WITH VERTICAL GAZE AND PSEUDOBULBAR PALSY, NUCHAL DYSTONIA AND DEMENTIA. Arch Neurol 10:333-359.

Stemper BD, Shah AS, Pintar FA, McCrea M, Kurpad SN, Glavaski-Joksimovic A, Olsen C, Budde MD (2015) Head rotational acceleration characteristics influence behavioral and diffusion tensor imaging outcomes following concussion. Ann Biomed Eng 43:1071-1088.

Stern RA, Daneshvar DH, Baugh CM, Seichepine DR, Montenigro PH, Riley DO, Fritts NG, Stamm JM, Robbins CA, McHale L, Simkin I, Stein TD, Alvarez VE, Goldstein LE, Budson AE, Kowall NW, Nowinski CJ, Cantu RC, McKee AC (2013) Clinical presentation of chronic traumatic encephalopathy. Neurology 81:1122-1129.

Stoessl AJ (2014) Developments in neuroimaging: positron emission tomography. Parkinsonism Relat Disord 20 Suppl 1:S180-183.

Strong MJ, Yang W (2011) The frontotemporal syndromes of ALS. Clinicopathological correlates. J Mol Neurosci 45:648-655.

Sullivan S, Friess SH, Ralston J, Smith C, Propert KJ, Rapp PE, Margulies SS (2013) Behavioral deficits and axonal injury persistence after rotational head injury are direction dependent. J Neurotrauma 30:538-545.

Sundman MH, Hall EE, Chen NK (2014) Examining the relationship between head trauma and neurodegenerative disease: A review of epidemiology, pathology and neuroimaging techniques. J Alzheimers Dis Parkinsonism 4.

Tago T, Furumoto S, Okamura N, Harada R, Ishikawa Y, Arai H, Yanai K, Iwata R, Kudo Y (2014) Synthesis and preliminary evaluation of 2-arylhydroxyquinoline derivatives for tau imaging. J Labelled Comp Radiopharm 57:18-24.

Tang-Schomer MD, Johnson VE, Baas PW, Stewart W, Smith DH (2012) Partial interruption of axonal transport due to microtubule breakage accounts for the formation of periodic varicosities after traumatic axonal injury. Exp Neurol 233:364-372.

Tang CY, Eaves E, Dams-O'Connor K, Ho L, Leung E, Wong E, Carpenter D, Ng J, Gordon W, Pasinetti G (2012) Diffuse Disconnectivity in tBi: a resting state fMri anD Dti stuDy. Transl Neurosci 3:9-14.

Taniguchi T, Kawamata T, Mukai H, Hasegawa H, Isagawa T, Yasuda M, Hashimoto T, Terashima A, Nakai M, Mori H, Ono Y, Tanaka C (2001) Phosphorylation of tau is regulated by PKN. The Journal of biological chemistry 276:10025-10031.

Veeramuthu V, Narayanan NV, Tan LK, Delano-Wood L, Chinna K, Bondi MW, Waran V, Ganesan D, Ramli N (2015) Diffusion Tensor Imaging Parameters in Mild Traumatic Brain Injury and Its Correlation with Early Neuropsychological Impairment: A Longitudinal Study. J Neurotrauma.

Villemagne VL, Furumoto S, Fodero-Tavoletti MT, Mulligan RS, Hodges J, Harada R, Yates P, Piguet O, Pejoska S, Dore V, Yanai K, Masters CL, Kudo Y, Rowe CC, Okamura N (2014) In vivo evaluation of a novel tau imaging tracer for Alzheimer's disease. Eur J Nucl Med Mol Imaging 41:816-826.

Virji-Babul N, Borich MR, Makan N, Moore T, Frew K, Emery CA, Boyd LA (2013) Diffusion tensor imaging of sports-related concussion in adolescents. Pediatr Neurol 48:24-29.

Virji-Babul N, Hilderman C, Makan N, Liu A, Smith-Forrester J, Franks C, Wang JZ (2014) Changes in functional brain networks following sports related concussion in adolescents. J Neurotrauma.

Washington PM, Morffy N, Parsadanian M, Zapple DN, Burns MP (2013) Experimental Traumatic Brain Injury Induces Rapid Aggregation and Oligomerization of Amyloid-Beta in an Alzheimer's Disease Mouse Model. J Neurotrauma.

Watts DJ, Strogatz SH (1998) Collective dynamics of 'small-world' networks. Nature 393:440-442.

Wilde EA, McCauley SR, Hunter JV, Bigler ED, Chu Z, Wang ZJ, Hanten GR, Troyanskaya M, Yallampalli R, Li X, Chia J, Levin HS (2008) Diffusion tensor imaging of acute mild traumatic brain injury in adolescents. Neurology 70:948-955.

Willer B, Leddy JJ (2006) Management of concussion and post-concussion syndrome. Curr Treat Options Neurol 8:415-426.

Williams DR, Holton JL, Strand C, Pittman A, de Silva R, Lees AJ, Revesz T (2007) Pathological tau burden and distribution distinguishes progressive supranuclear palsy-parkinsonism from Richardson's syndrome. Brain 130:1566-1576.

Wils H, Kleinberger G, Janssens J, Pereson S, Joris G, Cuijt I, Smits V, Ceuterick-de Groote C, Van Broeckhoven C, Kumar-Singh S (2010) TDP-43 transgenic mice develop spastic paralysis and neuronal inclusions characteristic of ALS and frontotemporal lobar degeneration. Proc Natl Acad Sci U S A 107:3858-3863.

Wood H (2013) Alzheimer disease: [11C]PBB3--a new PET ligand that identifies tau pathology in the brains of patients with AD. Nat Rev Neurol 9:599.

Xiong Y, Gu Q, Peterson PL, Muizelaar JP, Lee CP (1997) Mitochondrial dysfunction and calcium perturbation induced by traumatic brain injury. J Neurotrauma 14:23-34.

Yagishita A, Oda M (1996) Progressive supranuclear palsy: MRI and pathological findings. Neuroradiology 38 Suppl 1:S60-66.

Yeh PH, Wang B, Oakes TR, French LM, Pan H, Graner J, Liu W, Riedy G (2014) Postconcussional disorder and PTSD symptoms of military-related traumatic brain injury associated with compromised neurocircuitry. Hum Brain Mapp 35:2652-2673.

Yokoyama Y, Toyoshima Y, Shiga A, Tada M, Kitamura H, Hasegawa K, Onodera O, Ikeuchi T, Someya T, Nishizawa M, Kakita A, Takahashi H (2015) Pathological and Clinical Spectrum of Progressive Supranuclear Palsy: With Special Reference to Astrocytic Tau Pathology. Brain Pathol.

Yoshino A, Hovda DA, Kawamata T, Katayama Y, Becker DP (1991) Dynamic changes in local cerebral glucose utilization following cerebral conclusion in rats: evidence of a hyper- and subsequent hypometabolic state. Brain Res 561:106-119.

Zemper ED (2003) Two-year prospective study of relative risk of a second cerebral concussion. Am J Phys Med Rehabil 82:653-659.

Zhang Y, Tartaglia MC, Schuff N, Chiang GC, Ching C, Rosen HJ, Gorno-Tempini ML, Miller BL, Weiner MW (2013) MRI signatures of brain macrostructural atrophy and microstructural degradation in frontotemporal lobar degeneration subtypes. J Alzheimers Dis 33:431-444.

Zhou H, Huang C, Chen H, Wang D, Landel CP, Xia PY, Bowser R, Liu YJ, Xia XG (2010) Transgenic rat model of neurodegeneration caused by mutation in the TDP gene. PLoS Genet 6:e1000887.

Zhu DC, Covassin T, Nogle S, Doyle S, Russell D, Pearson RL, Monroe J, Liszewski CM, DeMarco JK, Kaufman DI (2015) A potential biomarker in sports-related concussion: brain functional connectivity alteration of the default-mode network measured with longitudinal resting-state fMRI over thirty days. J Neurotrauma 32:327-341.

Appendices

Appendix A Summary of Complex Network Analysis Measures

Graph Theory Network Measures from the Brain Connectivity Toolbox

Centrality: identifies the most important constituent nodes and edges within a network. Centrality encompasses both the number of connections to a node (*degree centrality*) as well as physical proximity of other nodes (*closeness centrality*). *Betweenness centrality* represents the fraction of all 'shortest paths' that contain a particular node of interest. This is of particular interest when discussing subnetworks. If the node participates in numerous short paths, the betweenness centrality value will be large.

Modularity: Modularity is calculated from eigenvalues and eigenvectors of the connectivity matrices. Larger values indicate that the network contains tight connections within modules, and the modules are independent of one another.

Density: the fraction of connections to node or group of nodes present to all possible connections.

Degree: the number of edges connected to a particular node. This is one of the most important network measures as it identifies *hubs*, nodes with a large number of associated edges.

Clustering Coefficient: is a measure of segregated network structure. It identifies the extent to which nodes of interest tend to cluster together in a given network, and may be global or locally derived. CC values range between 0 and 1. It is calculated as the fraction of triangle (triplets where three vertices are fully connected by intervening edges) motifs around a node. In the applications to subnetworks, clustering coefficients measure 'local connectivity', where higher values are associated with network resilience to damage (robustness).

Transitivity: may be used in place of clustering coefficient. The ratio of triangles to triplets in the network.

Characteristic Path Length: paths are series of edges that connect nodes, but never return to a node (never visit more than once). The average shortest path length in a network. Path lengths are indicative of global and local integration.

Hub Value/Authority: is related to the structure of a node's neighbours. Larger values indicate that important nodes (hubs) are connected to the node of interest.

Assortativity: a correlation coefficient between the degree of all nodes on opposite ends of an edge. Positive values represent the two nodes in question share a similar degree value (i.e. High degree nodes connect with other high degree nodes).

Efficiency: the average inverse shortest path length in a network. This measure is inversely proportional to the characteristic path length of the same network. It may be computed as *global efficiency* for the whole brain, or *local efficiency* for subnetworks of interest. This describes how information flows within a network.

Appendix B Automated Anatomical Labeling Regions for Subnetworks of Interest

Attention Network		
Region #	**AAL Label**	**Brain Structure**
11	1 Frontal Inf Oper L	Inferior Frontal Gyrus, Opercular Part
12	1 Frontal Inf Oper R	
13	1 Frontal Inf Tri L	Inferior Frontal Gyrus, Triangular Part
14	1 Frontal Inf Tri R	
15	1 Frontal Inf Orb L	Inferior Frontal Gyrus, Orbital Part
16	1 Frontal Inf Orb R	
31	1 Cingulum Ant L	Anterior Cingulate and Paracingulate Gyri
32	1 Cingulum Ant R	
65	1 Angular L	Angular Gyrus
66	1 Angular R	
Executive Function Network		
Region #	**AAL Label**	**Brain Structure**
3	1 Frontal Sup L	Superior Frontal Gyrus, Dorsolateral
4	1 Frontal Sup R	
23	1 Frontal Sup Medial L	Superior Frontal Gyrus, Medial
24	1 Frontal Sup Medial R	
Default Mode Network		
Region #	**AAL Label**	**Brain Structure**
23	1 Frontal Sup Medial L	Superior Frontal Gyrus, Medial
24	1 Frontal Sup Medial R	
25	1 Frontal Med Orb L	Superior Frontal Gyrus, Medial Orbital
26	1 Frontal Med Orb R	
35	1 Cingulum Post L	Posterior Cingulate Gyrus
36	1 Cingulum Post R	
59	1 Parietal Sup L	Superior Parietal Gyrus
60	1 Parietal Sup R	
65	1 Angular L	Angular Gyrus
66	1 Angular R	
67	1 Precuneus L	Precuneus
68	1 Precuneus R	
85	1 Temporal Mid L	Middle Temporal Gyrus
86	1 Temporal Mid R	

Frontal Association Network		
Region #	**AAL Label**	**Brain Structure**
3	1 Frontal Sup L	Superior Frontal Gyrus, Dorsolateral
4	1 Frontal Sup R	
5	1 Frontal Sup Orb L	Superior Frontal Gyrus, Orbital Part
6	1 Frontal Sup Orb R	
7	1 Frontal Mid L	Middle Frontal Gyrus
8	1 Frontal Mid R	
9	1 Frontal Mid Orb L	Middle Frontal Gyrus, Orbital Part
10	1 Frontal Mid Orb R	
11	1 Frontal Inf Oper L	Inferior Frontal Gyrus, Opercular Part
12	1 Frontal Inf Oper R	
13	1 Frontal Inf Tri L	Inferior Frontal Gyrus, Triangular Part
14	1 Frontal Inf Tri R	
15	1 Frontal Inf Orb L	Inferior Frontal Gyrus, Orbital Part
16	1 Frontal Inf Orb R	
23	1 Frontal Sup Medial L	Superior Frontal Gyrus, Medial
24	1 Frontal Sup Medial R	
25	1 Frontal Med Orb L	Superior Frontal Gyrus, Medial Orbital
26	1 Frontal Med Orb R	

Appendix C Beck Depression Inventory

Beck Depression Inventory - II

Subject ID: _____ Date/Time: _____

This questionnaire consists of 21 groups of statements. Please read each group of statements carefully, and then pick out the one statement in each group that best describes the way you have been feeling during the past two weeks, including today. Circle the number beside the statement you have picked. If several statements in the group seem to apply equally well, circle the highest number for that group. Be sure that you do not choose more than one statement for any group.

1. Sadness
0 I do not feel sad.
1 I feel sad much of the time.
2 I am sad all the time.
3 I am so sad or unhappy that I can't stand it.

2. Pessimism
0 I am not discouraged about my future.
1 I feel more discouraged about my future than I used to be.
2 I do not expect things to work out for me.
3 I feel my future is hopeless and will only get worse.

3. Past Failure
0 I do not feel like a failure.
1 I have failed more than I should have.
2 As I look back, I see a lot of failures.
3 I feel I am a total failure as a person.

4. Loss of pleasure
0 I get as much pleasure as I ever did from the things I enjoy.
1 I don't enjoy things as much as I used to.
2 I get very little pleasure from the things I used to enjoy.
3 I can't get any pleasure from the things I sued to enjoy.

5. Guilty Feelings
0 I don't feel particularly guilty.
1 I don't feel guilty over many things I have done or should have done.
2 I feel quite guilty most of the time.
3 I feel guilty all of the time.

6. Punishment Feelings
0 I don't feel I am being punished.
1 I feel I may be punished.
2 I expect to be punished.
3 I feel I am being punished.

7. Self-Dislike
0 I feel the same about myself as ever.
1 I have lost confidence in myself.
2 I am disappointed in myself.
3 I dislike myself.

8. Self-Criticalness
0 I don't criticize or blame myself more than usual.
1 I am more critical of myself than I used to be.
2 I criticize myself for all my faults.
3 I blame myself for everything ad that happens.

9. Suicidal Thoughts or Wishes
0 I don't have any thoughts of killing myself.
1 I have thoughts of killing myself, but I would not carry them out.
2 I would like to kill myself.
3 I would kill myself if I had the chance.

10. Crying
0 I don't cry any more than I used to.
1 I cry more than I used to.
2 I cry over every little thing.
3 I feel like crying, but I can't.

11. Agitation
0 I am not more restless or wound up than usual.
1 I feel more restless or wound up than usual.
2 I am so restless or agitated that it's hard to stay still.
3 I am so restless or agitated that I have to keep moving or doing something.

12. Loss of Interest
0 I have not lost interest in other people or activities.
1 I am less interested in other people or things than before.
2 I have lost most of my interest in other people or things.
3 It's hard to get interested in anything.

13. Indecisiveness

0 I make decisions as well as ever.
1 I find it more difficult to make decision than usual.
2 I have much greater difficulty in making decisions than I used to.
3 I have trouble making any decisions.

14. Worthlessness

0 I do not feel I am worthless.
1 I don't consider myself as worthwhile and useful as I used to do.
2 I feel more worthless as compared to other people.
3 I feel utterly worthless.

15. Loss of Energy

0 I have as much energy as ever.
1 I have less energy than I used to have.
2 I don't have enough energy to do very much.
3 I don't have enough energy to do anything.

16. Changes in Sleeping Pattern

0 I have not experienced any change in my sleeping pattern.
1 I sleep somewhat more/less than usual.
2 I sleep a lot more/less than usual.
3 I sleep most of the day. OR I wake up 1-2 hours early and can't get back to sleep.

17. Irritability

0 I am no more irritable than usual.
1 I am more irritable than usual.
2 I am much more irritable than usual.
3 I am irritable all the time.

18. Changes in Appetite

0 I have not experienced any change in my appetite.
1 My appetite is somewhat less/greater than usual.
2 My appetite is much less/greater than usual.
3 I have no appetite at all. OR I crave food all the time.

19. Concentration Difficulty

0 I can concentrate as well as ever.
1 I can't concentrate as well as usual.
2 It's hard to keep my mind on anything for very long.
3 I find I can't concentrate on anything.

20. Tiredness or Fatigue

0 I am no more tired or fatigued than usual.
1 I get more tired or fatigued more easily than usual.
2 I am too tried or fatigued to do a lot of the things I used to do.
3 I am too tired or fatigued to do most of the things I used to do.

21. Loss of Interest in Sex

0 I have not noticed any recent change in my interest in sex.
1 I am less interested in sex than I sued to be.
2 I am much less interested in sex now.
3 I have lost interest in sex completely.

Total: ____

Appendix D Montreal Cognitive Assessment

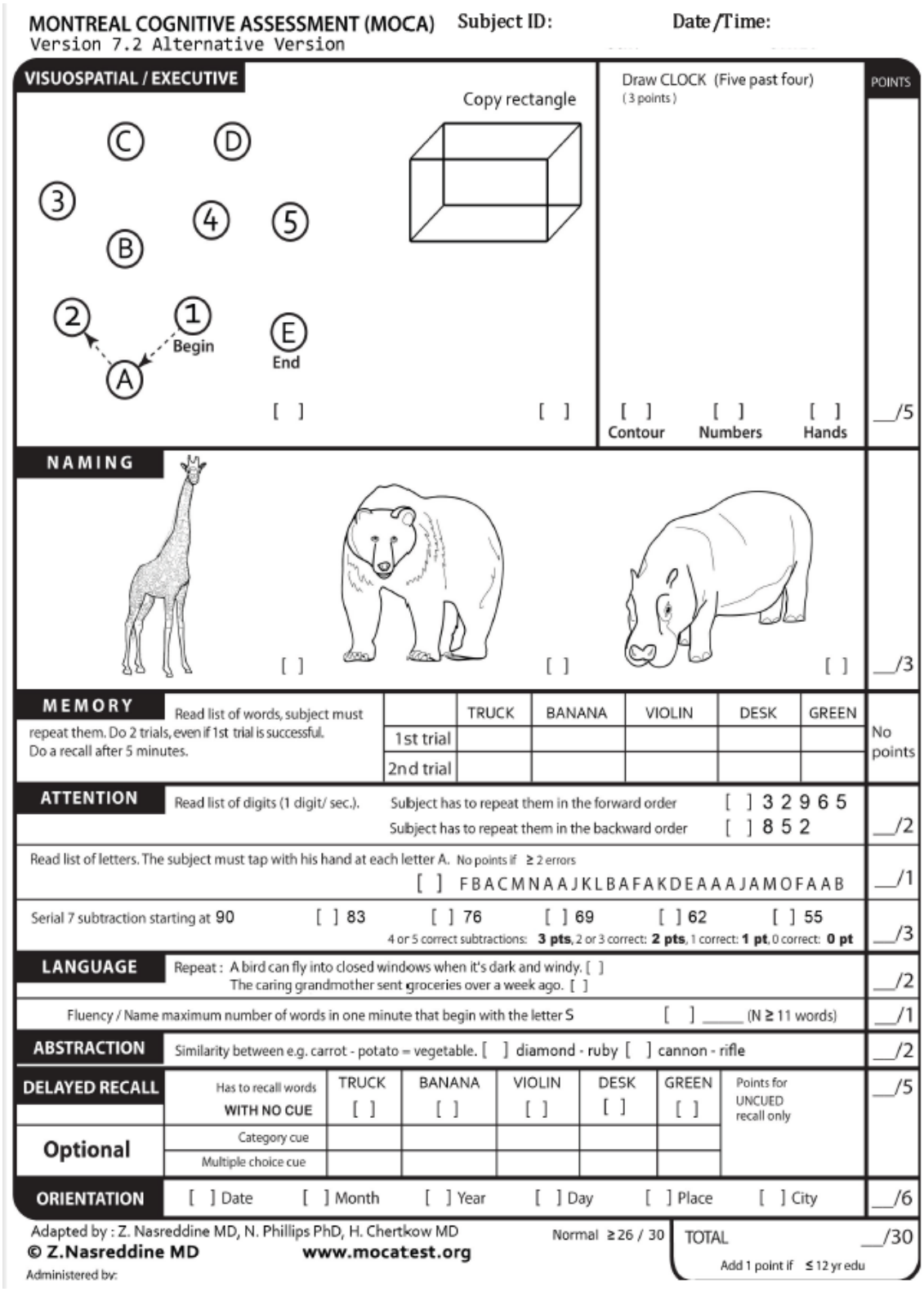

MONTREAL COGNITIVE ASSESSMENT (MOCA) Subject ID: Date /Time:
Version 7.2 Alternative Version

VISUOSPATIAL / EXECUTIVE — POINTS

Copy rectangle

Draw CLOCK (Five past four) (3 points)

[ ] Contour [ ] Numbers [ ] Hands __/5

NAMING __/3

MEMORY Read list of words, subject must repeat them. Do 2 trials, even if 1st trial is successful. Do a recall after 5 minutes.

	TRUCK	BANANA	VIOLIN	DESK	GREEN
1st trial					
2nd trial					

No points

ATTENTION Read list of digits (1 digit/ sec.). Subject has to repeat them in the forward order [ ] 3 2 9 6 5
Subject has to repeat them in the backward order [ ] 8 5 2 __/2

Read list of letters. The subject must tap with his hand at each letter A. No points if ≥ 2 errors
[ ] F B A C M N A A J K L B A F A K D E A A A J A M O F A A B __/1

Serial 7 subtraction starting at 90 [ ] 83 [ ] 76 [ ] 69 [ ] 62 [ ] 55
4 or 5 correct subtractions: **3 pts**, 2 or 3 correct: **2 pts**, 1 correct: **1 pt**, 0 correct: **0 pt** __/3

LANGUAGE Repeat : A bird can fly into closed windows when it's dark and windy. [ ]
The caring grandmother sent groceries over a week ago. [ ] __/2

Fluency / Name maximum number of words in one minute that begin with the letter S [ ] _____ (N ≥ 11 words) __/1

ABSTRACTION Similarity between e.g. carrot - potato = vegetable. [ ] diamond - ruby [ ] cannon - rifle __/2

DELAYED RECALL __/5

	Has to recall words WITH NO CUE	TRUCK	BANANA	VIOLIN	DESK	GREEN	Points for UNCUED recall only
		[ ]	[ ]	[ ]	[ ]	[ ]	
Optional	Category cue						
	Multiple choice cue						

ORIENTATION [ ] Date [ ] Month [ ] Year [ ] Day [ ] Place [ ] City __/6

Adapted by : Z. Nasreddine MD, N. Phillips PhD, H. Chertkow MD
© Z.Nasreddine MD www.mocatest.org
Normal ≥ 26 / 30
TOTAL __/30
Add 1 point if ≤ 12 yr edu
Administered by:

Appendix E MDS-UPDRS III

Subject ID: Time:
Date: Session:

Is the patient on medication for treating the symptoms of PD? No Yes

If the patient is receiving medication for treating the symptoms of PD, mark the patient's clinical state using the following definitions:

On: On is the typical functional state when patients are receiving medication and have a good response

OFF: Off is the typical functional state when patients have a poor response in spite of taking medications

Is the patient on levodopa? No Yes
If yes, minutes since last levodopa dose: _____

Speech

0 = No speech problems
1 = Loss if modulation, diction or volume, but still all words are easy to understand
2 = Loss of modulation, diction, volume with a few words unclear, but the overall sentences easy to follow
3= Speech is difficult to understand to the point that some, but not most, sentences are poorly understood
4= Most speech is difficult to understand or unintelligible

Facial Expression

0 = Normal facial expression
1 = Minimal masked facies manifested only by decreased frequency of blinking
2 = In addtiotion to decreased eye-blink frequency, masked facies present in the lower face as well, namely fewer movements around the mouth, such as less spontaneous smiling, but lips not parted
3= Masked facies with lips parted some of the time when the mouth is at rest
4= Masked facies with lips parted most of the time when the mouth is at rest

Postural Tremor Of Hands R L

0 = No tremor
1 = Tremor is present but less than 1cm in amplitude
2 = Tremor is at least 1 but less than 3cm in amplitude
3= Tremor is at least 3 but less than 10cm in amplitude
4= Tremor is at least 10cm in amplitude

Kinetic Tremor Of Hands R L

0 = No tremor
1 = Tremor is present but less than 1cm in amplitude
2 = Tremor is at least 1 but less than 3cm in amplitude
3= Tremor is at least 3 but less than 10cm in amplitude
4= Tremor at least 10cm in amplitude

Rest Tremor Amplitude

Lip/Jaw

RUE	LUE
RLE	LLE

Extremity ratings

0 = No tremor
1 = < 1 cm in maximal amplitude.
2 = > 1 cm but < 3 cm in maximal amplitude
3 = 3 - 10 cm in maximal amplitude.
4 = > 10 cm in maximal amplitude

Lip and Jaw Ratings:

0 = No tremor
1 = < 1 cm in maximal amplitude
2 = > 1 cm but < 2 cm in maximal amplitude
3= > 2 cm but < 3 cm in maximal amplitude
4= > 3 cm in maximal amplitude.

Constancy of Rest Tremor

0 = No tremor
1 = Tremor at rest is present <25% of the entire examination period
2 = Tremor at rest is present 26-50% of the entire examination period.
3= Tremor at rest is present 51-75% of the entire examination period.
4= Tremor at rest is present > 75% of the entire examination period.

Finger Tapping

R | L

0 = No problems
1 = Any of the following: a) the regular rhythm is broken with one or two interruptions or hesitations; b) slight slowing; c) the amplitude decrements near the end of the 10 taps
2 = a) 3 to 5 interruptions during tapping; b) mild slowing; c) the amplitude decrements midway in the 10-tap sequence
3= a) more than 5 interruptions during tapping or at least one longer arrest in ongoing movement; b) moderate slowing; c) the amplitude decrements starting after 1st tap
4= Cannot or can only barely perform the task

Hand Movements

R | L

0 = No problems
1 = Any of the following: a) the regular rhythm is broken with on e or two interruptions or hesitations of the movement; b) slight slowing; c) the amplitude decrements near the end of the task
2 = a) 3 to 5 interruptions during the movements; b) mild slowing; c) the amplitude decrements midway in the task
3= a) more than 5 interruptions during the movement or at least one longer arrest in ongoing movement; b) moderate slowing; c) the amplitude decrements starting after the 1st open-and close-sequence
4= Cannot or can only barely perform the task because of slowing, interruptions or decrements

Pronation-Supination Movements of Hands

R | L

0 = No problems
1 = Any of the following: a) regular rhythm is broken with one or two interruptions or hesitations of the movements b) slight slowing; c) the amplitude decrements near the end of the sequence
2 = a) 3 to 5 interruptions during the movements; b) mild slowing; c) the amplitude decrements midway in the task
3= a) more than 5 interruptions during the movement or at least one longer arrest in ongoing movement; b) moderate slowing; c) the amplitude decrements starting after the 1st supination-pronation sequence
4= Cannot or can only barely perform the task because of slowing, interruptions or decrements

Toe Tapping

	R	L

0 = No problems
1 = Any of the following: a) 3 to 5 interruptions during the movements; b) slight slowing; c) the amplitude decrements near the end of the sequence
2 = a) 3 to 5 interruptions during the movements; b) mild slowing; c) the amplitude decrements midway in the task
3= a) more than 5 interruptions during the movement or at least one longer arrest in ongoing movement; b) moderate slowing; c) the amplitude decrements starting after the 1st tap
4= Cannot or can only barely perform the task because of slowing, interruptions or decrements

Leg Agility

	R	L

0 = No problems
1 = Any of the following: a) regular rhythm is broken with one or two interruptions or hesitations of the movements; b) slight slowing; c) the amplitude decrements near the end of the sequence
2 = Any of the following: a) 3 to 5 interruptions during the movements; b) mild slowing; c) the amplitude decrements midway in the task
3= Any of the following: a) more than 5 interruptions during the movement or at least one longer arrest in ongoing movement; b) moderate slowing; c) the amplitude decrements starting after 1st tap
4= Cannot or can only barely perform the task because of slowing, interruptions or decrements

Arising From Chair

0 = No problems
1 = Slow; or may need more than one attempt; or may need to move forward in the chair to arise. No need to use the arms of the chair
2 = Pushes self up from arms of seat without difficulty
3= Needs to push off, but tends to fall back and may have to try more than one time, but can get up without help
4= Unable to arise without help

Posture

0 = No problems:
1 = Not quite erect, but posture could be normal for older person
2 = Definite flexion, scoliosis or leaning to one side, but patient can correct posture to normal posture when asked to do so
3= Stooped posture, scoliosis or leaning to one side that cannot be corrected volitionally to a normal posture by the patient
4= Flexion, scoliosis or leaning with extreme abnormally of posture

Freezing of Gait

0 = No freezing
1 = Freezes on starting, turning or walking through doorway with a single halt during any of these events, but then continues smoothly without freezing during straight walking
2 = Freezes on starting, turning or walking through doorway with more than one halt during any of these events, but then continues smoothly without freezing during straight walking
3= Freezes once during straight walking
4= Freezes multiple times during straight walking

Gait

0 = No problems:
1 = Independent walking with minor gait impairment
2 = Independent walking but with substantial gait impairment
3= Requires an assistance device for safe walking but not a person
4= Cannot walk at all or only with another person's assistance

Postural Stability

0 = No problems: Recovers in one or two steps
1 = 3-5 steps, but subject recovers unaided
2 = More than 5 steps, but subject recovers unaided
3= Stands safely, but with absence of postural response; falls if not caught by examiner
4= Very unstable, tends to lose balance spontaneously or with just a gentle pull on the shoulders

MDS-UPDRS: Motor Examination

Global Spontaneity of Movement (Body Bradykinesia)

0 = No problems:
1 = Slight global slowness and poverty of spontaneous movements
2 = Mild global slowness and poverty of spontaneous movements
3= Moderate global slowness and poverty of spontaneous movements
4= Severe global slowness and poverty of spontaneous movements

Rigidity

Neck

Judged on slow passive movement of major joints with patient in sitting position

RUE	LUE
RLE	LLE

0 = Absent
1 = Slight, only detected with activation maneuver
2 = Rigidity detected without the activation maneuver, but full range of motion is easily achieved
3= Rigidity detected without the activation maneuver; full range of motion is achieved with effort
4= Severe, full range of motion not achieved

DYSKINESIA IMPACT ON PART III RATINGS

A. Were dyskinesias (chorea or dystonia) present during examination? No Yes

B. If yes, did these movements interfere with your ratings? No Yes

Hoehn and Yahr Stage

0 Asymptomatic
1 Unilateral involvement only
2 Bilateral involvement without impairment of balance
3 Mild to moderate involvement; some postural instability but physically independent; needs assistance to recover from pull test.
4 Severe disability; still able to walk or stand unassisted
5 Wheelchair bound or bedridden unless aided.